

# **PROCESSING METHODOLOGIES FOR DOPPLER ULTRASOUND SIGNALS**

By

**Sulieman Mohammed Salih Zobly**

A thesis Submitted to the  
Faculty of Engineering at Cairo University  
In Partial Fulfillment of the  
Requirements for the Degree of  
DOCTOR OF PHILOSOPHY

In

**SYSTEMS AND BIOMEDICAL ENGINEERING**

**FACULTY OF ENGINEERING, CAIRO UNIVERSITY**

**GIZA - EGYPT**

**2012**

# **PROCESSING METHODOLOGIES FOR DOPPLER ULTRASOUND SIGNALS**

**By**

**Sulieman Mohammed Salih Zobly**

A Thesis Submitted to the  
Faculty of Engineering at Cairo University  
In Partial Fulfillment of the  
Requirements for the Degree of  
DOCTOR OF PHILOSOPHY

in

**BIOMEDICAL AND SYSTEMS ENGINEERING**

Under The Supervision of

**Prof. Dr Abu-Bakr M. Youssef**

**Prof. Dr. Yasser Mustafa Kadah**

Thesis advisor

Thesis Main advisor

**FACULTY OF ENGINEERING - CAIRO UNIVERSITY**

**GIZA - EGYPT**

2012

# **PROCEEING METHODOLOGIES FOR DOPPLER ULTRASOUND SIGNALS**

By

**Sulieman Mohammed Salih Zobly**

A Thesis Submitted to the  
Faculty of Engineering at Cairo University  
in Partial Fulfillment of the  
Requirements for the Degree of  
DOCTOR OF PHILOSOPHY

in

**BIOMEDICAL AND SYSTEMS ENGINEERING**

Approved by the Examining Committee

Prof. Dr. Mohammed Ibrahim Al-Adawy

---

Prof. Dr. Abd Allah Sayed Ahmed Mohamed

---

Prof. Dr. Abu-Bakr Mohammed Youssef

Thesis advisor

---

Prof. Dr. Yasser Mustafa Kadah

Thesis Main advisor

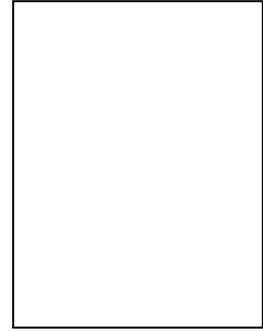
---

FACULTY OF ENGINEERING - CAIRO UNIVERSITY

GIZA - EGYPT

2012

**Engineer:** Sulieman Mohammed Salih Zobly  
**Date of Birth:** 1 / 1 / 1977  
**Nationality:** Sudanese  
**E-mail:** sulieman16@yahoo.com  
**Phone:** 01115131170  
**Address:** Faisal, Giza  
**Registration Date:** 12 / 12 / 2010  
**Awarding Date:** / /  
**Degree:** Doctor of Philosophy  
**Department:** System and Biomedical Engineering  
**Supervisors:** Prof. Dr. Abu-Bakr M. Youssef  
Prof. Dr. Yasser Mustafa Kadah



**Examiners:**

Prof. Dr. Mohammed I. Al-Adawy    Prof. Dr. Helwan University  
Prof. Dr. Abd Alla S. Mohamed    Prof. Dr.  
Prof. Dr. Abu-Bakr. M. Youssef    Prof. Dr.  
Prof. Dr. Yasser M. Kaddah    Prof. Dr.

**Title of Thesis:** Processing Methodologies for Doppler Ultrasound Signals

**Key Words:** (Doppler ultrasound - spectrogram - reconstruction - compressed sensing - clutter rejection)

**Summary:**

The Doppler shift is now commonly used in ultrasound imaging to determine blood flow velocity and direction. During the acquisition of Doppler data a train of pulses transmitted repeatedly to be acquired from selected region of interest. The current data acquisition in Doppler system is limited by bioeffect of ultrasound heating, which is caused by rapid transmission of ultrasound pulses for a long time to the same location increase the average power per unit area beyond the AIUM safety standard. To overcome this limitation we propose a framework of compressed sensing (CS), which state that images and signals can be reconstructed by using a few numbers of measurements. The result shows that the proposed data acquisition alleviates the present data acquisition limitation and successfully demonstrated in real Doppler ultrasound data.

The Doppler signal generated from a moving object contain not only great information about flow, but also backscatter signal contain clutter originated from surrounding tissue or slowly moving vessels. To estimate the flow accurately the clutter has to remove. In this work we proposed new clutter rejection methods to suppress the clutter. The methods validated using real and simulated Doppler data. The methods removed the clutter with high performance.

## Abstract

The difference between the frequencies in Doppler systems is commonly used to determine the blood flow velocity and direction within the body, this phenomenon is known as Doppler effects. Doppler generates either continuous wave (CW) or pulsed wave (PW) ultrasound. During the acquisition of Doppler data a train of pulses transmitted repeatedly to be acquired from selected region of interest. In most case Doppler signal acquisition done in more than one mode, this lead to a limitation in Doppler data acquisition.

The current data acquisition in Doppler system is limited by, bioeffect of ultrasound heating, which is caused by rapid transmission of ultrasound pulses for a long time to the same location lead to increasing in the average power per unit area beyond the AIUM safety standard. Beside the complicated scanning methods when the operator used mixed mode scanning, in other words highlight a specific scan line in a B-mode image and simultaneously generate the real-time Doppler spectrogram for that line on the same display scan. In addition the current acquisition methods use too much data to acquire the image this lead in increasing the process time and limit displaying the Doppler spectrogram in real-time.

To overcome this limitation we propose a framework of compressed sensing (CS) to reduce the number of acquisitions. CS is a new sampling framework; state that images and signals can be reconstructed by using a few numbers of measurements. CS is the process for acquiring and reconstructing a signal that is supposed to be sparse or compressible. CS is useful in applications where one cannot afford to collect or transmit a lot of measurements such as medical imaging, data compression and data acquisition. The result shows that the proposed data acquisition alleviates the present data acquisition limitation and successfully demonstrated in real Doppler ultrasound data.

The reconstruction time can be accelerated so as to achieve optimum reconstruction time by using multiprocessors systems. The algorithm applied to  $\ell_1$ -minimization

algorithms using duo-core CPU. The result shows that combining the CS and Parallel algorithms high quality recovered image within a very low time.

The Doppler signal generated from a moving object contain not only great information about flow, but also backscatter signal contain clutter originated from surrounding tissue or slowly moving vessels. To get a Doppler ultrasound spectrogram image with a good quality, the clutter signals must be removed completely. Without enough clutter rejection, low velocity blood flow cannot be measured, and estimates of higher velocities will have a large bias. In most cases it is very difficult to achieve a complete suppression without affecting the Doppler signal. The current clutter rejections are; finite impulse response FIR, infinite impulse response IIR and polynomial regression PR filters. Due to limitations of current clutter rejection we proposed new cluttering methods to subtract unwanted signal. The proposed clutter based on principal component analysis and independent component analysis. The methods validate using real and simulated Doppler ultrasound data. The result shows that the proposed method gives better cluttering over the present clutter types, when tested with real Doppler spectrogram data.

# TABLE OF CONTENTS

## Table of Contents

<b>ABSTRACT .....</b>	<b>I</b>
<b>TABLE OF CONTENT .....</b>	<b>III</b>
<b>LIST OF FIGURES.....</b>	<b>VII</b>
<b>LIST OF TABLES.....</b>	<b>XI</b>
<b>LIST OF ABBREVIATION .....</b>	<b>XII</b>
<b>DEDICATION .....</b>	<b>XIV</b>
<b>ACKNOWLEDGEMEN.....</b>	<b>XV</b>
<b>CHAPTER 1      Introduction.....</b>	<b>1</b>
1.1 Introduction .....	1
1.2 Problem Statement .....	4
1.3 Overview of Thesis .....	5
<b>CHAPTER 2      Background.....</b>	<b>7</b>
2.1 Ultrasonic Wave.....	7
2.1.1 Intensity and Power .....	8
2.1.2 Scattering.....	9
2.1.3 Reflection and Transmission .....	10
2.1.4 Attenuation .....	11
2.2 The Doppler Effect.....	12
2.2.1 The Doppler Equation .....	13
2.3 Flow and Tissue Motion in Human Body .....	14
2.4 Doppler Ultrasound Systems.....	15
2.4.1 Continuous Wave System .....	16
2.4.2 Pulsed Wave System .....	17
2.4.3 Duplex System .....	19
2.5 Spectral Doppler Acquisition.....	22
2.6 Doppler Display .....	23
2.6.1 Doppler Spectrogram.....	23

2.7 Compressed Sensing .....	24
2.8 Parallel Computation.....	25
2.9 Clutter Rejection .....	26
2.10 Principal Component Analysis.....	27
2.11 Independent Component Analysis .....	27
<b>CHAPTER 3      Compressed Sensing Theory &amp; Parallel Computing .....</b>	<b>29</b>
3.1 Introduction .....	29
3.2 Compressed Sensing .....	30
3.2.1 Sensing Matrices .....	32
3.2.2 Sparsity.....	34
3.2.3 Incoherence .....	36
3.2.4 Restricted Isometries Property .....	37
3.3 Reconstruction Algorithms .....	39
3.3.1 Convex Optimization .....	42
3.3.2 Greedy Algorithms .....	44
3.3.2.1 Matching Pursuit .....	45
3.3.2.2 Orthogonal Matching Pursuit .....	46
3.3.2.3 Stagewise Orthogonal Matching Pursuit .....	48
3.3.2.4 Compressive Sampling Matching Pursuit .....	49
3.3.2.5 Regularized Orthogonal Matching Pursuit.....	50
3.3.3 Combinatorial Optimization Algorithm .....	52
3.3.4 Total Variation Minimization.....	53
3.4 Robust Compressive Sensing.....	54
3.5 Application of Compressed Sensing .....	55
3.5.1 Application of Compressed Sensing in Medical Imaging.....	56
3.5.1.1 Application of Compressed sensing in Computerized Tomography.....	56
3.5.1.2 Application of Compressed Sensing in Magnetic Resonance Imaging.....	57
3.5.1.3 Application of Compressed Sensing in Doppler Ultrasound .....	58
3.6 Parallel Computing.....	60
<b>CHAPTER 4      Application of CS &amp; Parallel in Doppler Signal .....</b>	<b>63</b>
4.1 Doppler Data .....	64

4.2 Doppler Signal Reconstruction .....	64
4.2.1 Reconstruction via $\ell_1$ Minimization .....	64
4.2.2 Reconstruction via Orthogonal Matching Pursuit .....	66
4.2.3 Reconstruction via Compressive sampling Matching Pursuit.....	66
4.2.4 Reconstruction via Regularized Orthogonal Matching Pursuit.....	68
4.3 Reconstruction Time .....	68
4.4 Reconstructed Image Evaluation.....	68
4.4.1 Root Mean Square Error.....	69
4.4.2 Peak Signal-to-Noise Ratio .....	69
4.5 Parallel Computation.....	70
<b>CHAPTER 5      Clutter Rejection Filters (Wall Filters).....</b>	<b>72</b>
5.1 Motivation.....	72
5.2 Clutter Rejection Filters .....	73
5.2.1 Finite Impulse Response Filters .....	75
5.2.1.1 Linear Phase Filter.....	78
5.2.1.2 Minimum Phase Filter .....	80
5.2.1.3 Equiripple Filter.....	82
5.2.1.4 FIR Filters Comparison .....	84
5.2.2 Infinite Impulse Response Filters.....	86
5.2.2.1 IIR Filters Comparison.....	88
5.2.3 Polynomial Regression Filter .....	89
5.2.4 Filters Comparison .....	93
5.2.5 Principle Component Analysis.....	95
5.2.6 Independent Component analysis.....	97
<b>CHAPTER 6      Cluttering Doppler Data.....</b>	<b>101</b>
6.1 The Data .....	101
5.2.1 Real Data .....	101
5.2.2 Simulation Data.....	101
6.2 Signal Model .....	103
6.3 Cluttering with PCA.....	106
6.4 Cluttering with ICA.....	108

6.5 Cluttering with Non-Adaptive Clutters .....	109
6.6 Clutters Evaluation .....	110
<b>CHAPTER 7      Experimental Result &amp; Discussion .....</b>	<b>112</b>
7.1 Reconstruction Results .....	112
7.1.1 $\ell_1$ Minimization .....	112
7.1.2 Orthogonal Matching Pursuit .....	117
7.1.3 Compressive Sampling Matching Pursuit .....	122
7.1.4 Regularized Orthogonal Matching Pursuit .....	126
7.2 Parallel Computing Results .....	134
7.3 Clutter Rejection Results .....	135
7.3.1 Simulation Results .....	135
7.3.2 Real Doppler Data Results .....	141
<b>CHAPTER 8      Conclusion &amp; Recommendation for Future Work .....</b>	<b>144</b>
8.1 Conclusion .....	144
8.2 Recommendation for Future Work .....	146
<b>REFERENCES .....</b>	<b>147</b>

## LIST OF FIGURES

2-1	Reflection and Transmission of Ultrasound Wave .....	11
2-2	Continuous wave Doppler Transducer.....	16
2-3	Pulsed wave Doppler Transducer .....	18
2-4	Transmitted Pulse by PW System.....	18
2-5	Placement of Sampling Volume (left) and the Record of Blood Flow Velocity Spectrum (right).....	21
2-6	Mixed M-mode and B-mode Scanning.....	21
2-7	The Sample Volume, Gate Depth and Sensitive Region .....	22
2-8	Doppler Spectrogram .....	24
3-1	Schematic Description of Matrix Dimension With a 3-Sparse Vector $\hat{x}$ .....	32
3-2	Signal Represented in Time Domain and Frequency Domain.....	35
3-3	Natural Picture and its Wavelet Coefficients.....	36
3-4	Plot of $rect(t)$ (Blue) and Corresponding Frequency Representation $sinc(f)$ (Red).....	37
3-5	Reconstructed Signal via Convex Optimization.....	44
3-6	Reconstructed Signals via OMP .....	48
3-7	Reconstructed Signals via Combinatorial Algorithm .....	53
3-8	(a) Sampling Data of MR Image in the Fourier Domain which Correspond to Only of All Samples. (b) Reconstructed by Backprojection. (c) Intermediate Iteration of an Efficient Algorithm for Large Scale Total Variation Minimization. (d) The Final Reconstruction is Exact.....	58
3-9	Reconstructed Doppler Sonograms using two Different Numbers of Measurements .....	60
3-10	The PCT and MDCS.....	61
3-11	Multicore System and PCT.....	62
4-1	Comparison of Present Method vs New Methods .....	63
4-2	Serial and Parallel Methods for CS Reconstruction.....	70

5-1	The Clutter Filter and Spectrum of Clutter and Flow Signals .....	73
5-2	General Clutter Rejection Filter .....	74
5-3	The Frequency Response of FIR Filters Designed using Same Parameters and Three Different Orders (a) Constrained Equiripple (b) Least-Square FIR (c) Window (Kaiser) (d) Window (Hanning) (e) Linear-phase (f) Minimum-phase .....	77
5-4	The Frequency Response of the Linear-Phase FIR Filters using Different Orders (a) Using Order 4 (b) Using Order 6 (c) Using Order 8 (d) Using Order 10 .....	79
5-5	Linear Phase FIR Filter Designed using Different Orders.....	80
5-6	The Frequency Response of the Minimum-Phase FIR Filters using Different Orders Using Order 4 (b) Using Order 6 (c) Using Order 8 (d) Using Order 10.....	81
5-7	Min. phase FIR Filter Designed Using Different Orders .....	82
5-8	The Frequency Response of the Equiripple FIR Filters using Different Orders (a) Using Order 4 (b) Using Order 6 (c) Using Order 8 (d) Using Order 10 .....	83
5-9	Frequency Response of Different Orders Equiripple Filters .....	84
5-10	Frequency Response of Minimum Phase, Linear Phase & Equiripple FIR Filters.....	85
5-11	The Frequency Response of Different IIR Filters using Four Different Orders.....	87
5-12	IIR Filter Comparison Designed with Order 3 .....	88
5-13	The Frequency Response for Chebyshev IIR with Different Initialization .....	89
5-14	Polynomial Regression Filter Block Diagram .....	91
5-15	Frequency Response of PR Filters using Different Clutter Space Dimension .....	91
5-16	Frequency Response for PR Filters with Different Package Size and Order $P = 1$ . (a) Package Size 8. (b) Package Size 16 .....	92
5-17	Frequency Responses of Conventional PR Filters and Filter from Relation 5.6 using Package Size 8 .....	93
5-18	Frequency Response of Cheby. IIR and Min. Phase FIR (left), and PR (right) .....	94
5-19	Block Diagram of Signal Separation Process in ICA .....	98
6-1	Doppler Signal Spectrogram.....	104
6-2	The Generated Doppler IQ Signal for Simulation .....	105
6-3	Pre-preparation and Cluttering Process with Different Filters .....	105

7-1	Reconstructed Doppler Spectrogram via $\ell_1$ -norm using Different Number of Measurements (a) Using 5% Points (b) Using 20% Points (c) Using 40% Points (d) Using 60% Points (e) Using 80% Points .....	113
7-2	The Error of the Reconstructed Image via $\ell_1$ -norm (a) Using 80% (b) Using 40% (c) Using 5% .....	114
7-3	Number of Measurements Versus Reconstruction Time .....	115
7-4	Number of Measurements Versus PSNR .....	116
7-5	Number of Measurements Versus RMSE .....	117
7-6	Reconstructed Doppler Spectrogram via OMP Algorithm using Different Number of Points (a) Using 5% Points (b) Using 20% Points (c) Using 40% Points (d) Using 60% Points (e) using 80% points .....	118
7-7	The Error of the Reconstructed Image via OMP Algorithm (a) Using 80% (b) Using 40% (c) Using 5% .....	119
7-8	Number of Measurements Versus Reconstruction Time .....	120
7-9	Number of Measurements Versus PSNR.....	120
7-10	Number of Measurements Versus RMSE.....	121
7-11	Reconstructed Doppler Spectrogram via CoSaMP Algorithm using Different Number of Points (a) Using 5% Points (b) Using 20% Points (c) Using 40% Points (d) Using 60% Points (e) Using 80% Points .....	123
7-12	The Error of the Reconstructed Image via CoSaMP Algorithm (a) Using 80% (b) Using 40% (c) Using 5% .....	124
7-13	Number of Measurements Versus Reconstruction Time .....	124
7-14	Number of Measurements Versus RMSE.....	125
7-15	Number of Measurements Versus PSNR.....	126
7-16	Reconstructed Doppler Spectrogram via ROMP Algorithm using Different Number of Points (a) Using 5% Points (b) Using 20% Points (c) Using 40% Points (d) Using 60% Points (e) Using 80% Points .....	127
7-17	The Error of the Reconstructed Image via ROMP Algorithm (a) Using 80% (b) Using 40% (c) Using 5% .....	128
7-18	Number of Measurements Versus Reconstruction Time .....	129
7-19	Number of Measurements Versus RMSE.....	129

7-20	Number of Measurements Versus PSNR.....	130
7-21	Number of Measurements vs Recovery Time for Different Algorithms.....	132
7-22	Number of Measurements vs RMSE for Different Algorithms.....	133
7-23	Number of Measurements vs PSNR for Different Algorithms.....	134
7-24	The Filtered Signal via ICA, in Time Domain.....	135
7-25	The Filtered Signal via ICA, in Time Domain.....	136
7-26	The Filtered Signal via PCA, in Time Domain.....	136
7-27	The Spectrum of the Signal Filtered using ICA.....	137
7-28	The Spectrum of the Signal Filtered using PCA.....	137
7-29	The Filtered Signal via FIR, in Time Domain.....	138
7-30	The Filtered Signal via IIR, in Time Domain.....	138
7-31	The Filtered Signal via PR, in Time Domain.....	138
7-32	The Spectrum of Filtered Signal Using (a) FIR and (b) PR.....	139
7-33	Doppler Signal Contaminated with Clutter.....	139
7-34	The Performance of Different Clutter Rejection.....	141
7-35	The Resulting Doppler Sonogram Images of Heart for Different Types of Clutter Rejection Filters (a) Using FIR Clutter (b) Using IIR Clutter (c) Using PR Clutter (d) Using PCA Clutter (e) Using ICA Clutter.....	142
7-36	Cluttering Time for Different Filters.....	143

## LIST OF TABLES

2.1	Attenuation Values for Different Human Tissue .....	12
5.1	FIR and IIR Filters design Parameters .....	76
5.2	Passband Cutoff Frequency & Minimum $d_s$ for Filters Design using Different Orders ...	84
5.3	Filters design Parameters .....	94
6.1	Parameters used to Generate Doppler IQ .....	102
6.2	FIR, IIR and PR Filters Design Parameters .....	110
7.1	Number of Points, Recovery Time, MSE, Iteration, RMSE and PSNR using $\ell_1$ -norm ..	117
7.2	Number of Points, Recovery Time, MSE, RMSE and PSNR using OMP .....	121
7.3	Number of Points, Recovery Time, MSE, RMSE and PSNR using CoSaMP .....	126
7.4	Number of Points, Recovery Time, MSE, RMSE and PSNR using ROMP .....	130
7.5	The Parallel Reconstruction Time and Speed up for Different Number of Measurements .....	135
7.6	The Error and RMSE for Different Types of Clutters .....	140
7.7	The Filtering process time for Different Clutters Type .....	143

## LIST OF ABBREVIATIONS

AIUM	American Institute of Ultrasound in Medicine
BSS	Blind Source Separation
$c$	Speed of Sound
CoSaMP	Compressive Sampling Matching Pursuit
CPU	Central Processing Unit
CS	Compressed Sensing
CT	Computerized Tomography
CW	Continuous Wave
EEG	Electroencephalography
EEG	Electroencephalography
$f_d$	Doppler Shift
$f_t$	Transmitted Frequency
$f_r$	Received Frequency
FIR	Finite Impulse Response
I	Intensity
ICA	Independent Component Analysis
IIR	Infinite Impulse Response
$I_{sa}$	Spatial Average Intensity
$I_{sp}$	Spatial Peak Intensity
$I_{spta}$	Spatial Peak Temporal Average Intensity
$I_{sppa}$	Spatial Peak Pulse Average Intensity
$I_{sapa}$	Spatial Average Pulse Average Intensity
$I_{sata}$	Spatial Average Temporal Average Intensity
IQ	Inface Quadrature
MDCS	Matlab Distributed Computing Server

MPI	Message Passing Interface
MP	Matching Pursuit
MRI	Magnetic Resonance Imaging
MSE	Mean Square Error
OMP	Orthogonal Matching Pursuit
PC	Principal Component
PCA	Principal Component Analysis
PCT	Parallel Computing Toolbox
$\rho_0$	Average Density
PSNR	Peak Signal-to-Noise Ratio
PR	Polynomial Regression
PW	Pulsed Wave
ROMP	Regularized Orthogonal Matching Pursuit
RIP	Restricted Isometry Property
RF	Radio Frequency
RMSE	Root Mean Square Error
RMSD	Root Mean Square Deviation
StOMP	Stagewise Orthogonal Matching Pursuit
TV	Total Variation
URI	Ultrasound Research Interface
URI-OPT	Ultrasound Research Interface-Offline Processing Tool

## **DEDECATION**

This thesis is dedicated to my beloved family ...  
All I have and will accomplish are only possible due to their  
endless love, supports and encouragement

## ACKNOWLEDGEMEN

First and foremost I would like to thank my advisor prof. Yasser M. Kadah, for his guidance during my research and study at Cairo University. Without his patient guidance, teaching, insightful ideas and long times of work, this dissertation could not have been completed. I cannot adequately express my thanks for his help and interest in seeing me obtain not only my degree, but succeed in all my endeavors. For all his help and mentoring, I am very grateful. I would like to extend my thanks to my advisor prof. Abu Bakr M. Youssef.

My deepest gratitude goes to my family for their unflagging love and support throughout my life; this dissertation is simply impossible without them. I am indebted to my father, for his care and love. He had never complained in spite of all the hardships in his life. I cannot ask for more from my mother, as she is simply perfect. I have no suitable word that can fully describe her everlasting love for me. I have to give a special mention for the unlimited support given by my brothers, Adam, Ahmed and Awad.

# Chapter 1

## Introduction

### 1.1 Introduction

The difference between transmitted wave frequencies and reflected wave frequencies due to relative motion occurring between the source and the object, this phenomenon known as Doppler effects. In Doppler effects the frequency shift is proportional to the movement speed between the transducer and the object. This effect is now frequently used in ultrasound imaging to determine blood flow velocity and direction.

Ultrasound imaging application in medical fields has several advantages over other medical imaging modalities. It's used non invasive technique, its cheap, less examination time, movable, the investigation done without any ionizing radiation, capable of forming real time imaging and continuing improvement in image quality [1]. These advantages made ultrasound imaging system is the most widely imaging systems used among others medical imaging equipments.

Doppler instruments generate either continuous wave (CW) or pulsed wave (PW) ultrasound [1, 2]. In CW units continuously transmit and received ultrasound wave, thus two element transducers were used for transmitting and receiving housed in one probe for easy handling and guarantee ultrasound beam overlap over a long distance. In PW units a single-element transducer used for transmitting and receiving the ultrasound energy pulses. The depth from where the echoes arise can be calculated by using a time interval between transmitting and then receiving the echoing sound. From the point of view of Doppler techniques, the parameters that describe a wave [2], i.e. amplitude, frequency and phase, are important. Frequency and phase are more important for Doppler methods since the velocity of blood is obtained from the shifts in the frequency and changes in

phase of scattered wave. The developments in Doppler technology have led to a vast increase in the number of non-invasive blood velocity investigation carried out in all areas of medicine.

Doppler systems were used to obtain Doppler information at a specific organ. The master oscillator operates at a constant frequency and drives the transmitting crystal of the probe via transmitting amplifier. The returning ultrasound signal received by receiving crystal, containing echoes from both stationary and moving targets, is fed to the radio frequency (RF) amplifier. This amplified signal is then demodulated and filtered to produce audio frequency signals whose frequencies and amplitudes provide information about motion within the ultrasound beam. Demodulated and filtered Doppler frequency shift signals used to calculate the Doppler spectrogram. The acquisition of Doppler ultrasound data relies on the repeatedly transmitting ultrasound pulses to acquire data from a particular region of interest selected by the sonographer. Transmitting pulses to the same place continuously increased the heat per unit in the body.

Image compression in Doppler ultrasound is needed in order to reduce the data volume and achieve a low rat bit, ideally without losses of image quality. The need for transmission bandwidth and storage space in the medical field, telemedicine applications and continuous development of ultrasound technologies, encourage the development of effective data reduction.

In this thesis, we use the framework of compressed sensing for Doppler ultrasound signal dimensional reduction (compression) and reconstruction. Data reduction in Doppler will reduce the number of acquisitions, increased the patient safety and speed up the processing time. We apply the CS framework to Doppler signal using a few numbers of data to overcome the present Doppler data acquisition limitation. The reconstruction of Doppler signal from these projections achieved using one of the reconstruction algorithms such as convex optimization, which is lead to  $\ell_1$ -norm minimization proposed in [5].  $\ell_1$ -norm can exactly recover  $k$ -sparse signals and closely approximate compressible signals with high probability. The recovered signals were displayed as Doppler spectrogram. To perform the reconstruction four types of reconstruction

algorithms and five different numbers of measurements were used. The recovered images were evaluated by using Root mean Square Error (RMSE), Peak Signal-to-Noise Ratio (PSNR) expressed in dB and reconstruction time. RMSE, PSNR and the process time compared between the algorithms.

The reconstruction time can be accelerated so as to achieve optimum reconstruction time by using multiprocessor systems. The algorithm applied to  $\ell_1$ -minimization algorithms using duo-core central processing unit. The result shows that combining the CS and Parallel computing algorithms gives high quality recovered image within a very low time.

The Doppler signal generated from a moving object contain not only great information about flow, but also backscatter signal contain clutter originated from surrounding tissue or slowly moving vessels. This clutter signal is typically 40 to 80 dB stronger than the Doppler shift signal originated from blood [6-10]. Thus an accurate clutter rejection is needed to estimate the flow accurately, by decreasing the bias in flow estimation. Clutter suppression is very important step in the processing of Doppler signal. A high pass filter is commonly used to remove the clutter signal from the Doppler shift signal. A high pass filter is used to suppress signal from stationary or slow moving tissue or any other organs. Signals originated from a slow moving object and tissues are low-frequency signals, generally they may have amplitude much stronger than high frequency signals generated from the faster blood flow. Thus, for separating the signals from blood and tissue, high pass filter with a sharp transition band is necessary.

Various types of static filter have been proposed to remove the clutter from the backscattered signals originated from moving object or surrounding tissue, such as finite impulse response (FIR) filter with a short impulse response, infinite impulse response (IIR) filter with special initialization so as to reduce the ring-down time and polynomial regression (PR) filter [11 - 16]. The clutter from tissue often changes through space and time due to changes in physiology and tissue structure [17], and due to a limited number of data samples available (less than 20 sample volume [7]), in addition, if the clutter filter not appropriate selected the signal-to-noise ratio would be corrupted [9]. Due to all this,

high pass filter can't effectively suppress the clutter without affecting the desired flow signal [18]. To remove the clutter with high performance we proposed more advance clutter methods that can overcome these drawbacks of the high pass filter.

In this thesis a new method for clutter suppression have been proposed, to remove the clutter originated from moving objects and surrounding tissue. The proposed method analyzes the Doppler data using blind source separation techniques within the framework of principal component analysis (PCA) and independent component analysis (ICA). PCA and ICA proposed in [19 - 21]. ICA and PCA have been proposed for different applications in biomedical field such as, their application in analysis of electroencephalographic (EEG) data and event-related potential (ERP) data [22-23], in the analysis of functional magnetic resonance imaging [24], in Doppler ultrasound [25] and in clutter rejection in color flow mapping [26]. The RF Doppler data is the sum of the signals from blood flow and backscatter signal originated from surrounding tissue or slowly moving vessels. The data prepared to satisfy ICA and PCA by doing some preprocess steps, then small window was considered. Both PCA and ICA applied to the original data set (the data after windowing), so as to re-expressed the data into a new coordinate system such that the clutter and echo signal separated along different bases. Filtering is then achieved by rejecting the bases describing the clutter signal from moving tissue and returning the signal containing information regarding blood flow. The output can be used to generate Doppler spectrogram with high performance. The performance of the techniques is quantified by using a simulated data and real Doppler data (heart data) [27]. In addition, the performance of the proposed method compared with present cluttering filters.

## **1.2 Problem Statement**

The acquisition of Doppler ultrasound data relies on the repeatedly transmitting ultrasound pulses to acquire data from a particular region of interest. Such acquisition must be extremely precise in its periodicity to ensure that the Doppler signal is uniformly

sampled for further spectrogram processing. This can be a major constraint to ultrasound imaging systems when this Doppler signal acquisition is done in such modes as Duplex or Triplex imaging where B-mode or color flow signals are acquired concurrently. This constraint reduces the frame rates for other modes and hence limit the ability of the sonographer to follow events in real-time. Moreover, the rapid periodic transmission of ultrasound pulses to the same location increase the average power per unit area beyond the AIUM safety standards and therefore limitation on the sampling will be imposed reducing the ability to acquire more data.

In this thesis, a new framework is proposed to alleviate such limitations through the use of compressed sensing theory to reduce the number of acquisitions and eliminating the sampling uniformity constraints. The new methodology is presented and demonstrated in real Doppler ultrasound data. Also we proposed combining the compressed sensing theory with parallel computing to accelerate the reconstruction time.

The Doppler signal generated from a moving object contaminated with the clutter signals. Due to the limitations stated in the previous section it's very difficult to remove the clutter with present cluttering methods. Thus a new cluttering method is needed to overcome the current clutters limitation.

New cluttering methods proposed for cluttering rejection so as to overcome the current clutters limitation. The proposed methods base on PCA and ICA. We want to make use of the proposed techniques to improve the image quality in a Doppler ultrasound spectrogram by removing the clutter signal with high performance without affecting the blood flow signal.

### **1.3 Overview of Thesis**

This thesis organized as follows: Chapter 2 gives an overview of the Doppler ultrasound system and the limitation of the Doppler data acquisition. The compressed sensing theory reviewed beside a review of principal component analysis and independent component analysis. Overview of clutter rejection is given. Parallel

computing also reviewed. In chapter 3 we discuss the theory of compressed sensing in more details and its application in different areas. The parallel computing also discussed in the chapter in details. In chapter 4 we discuss our proposed data acquisition and application of compressed sensing for Doppler spectrogram reconstruction. Also the application of parallel methods for reconstruction time reduction was discussed. In chapter 5 methods used to separate the blood flow from stationary or slow moving tissue discussed in detail and the proposed methods for cluttering also discussed in deep. In chapter 6 the application of clutter to the Doppler data was discussed and also the types of the data used for experimental perfection were discussed. The result and discussion of the works was illustrated in chapter 7. In chapter 8 the conclusion and recommendations for future work were given.

# Chapter 2

## Background

This chapter gives the unfamiliar reader a short introductory to Doppler ultrasound and Doppler Effect and terms used in this context. It also gives more indepth information about Doppler ultrasound systems, the model investigated in this thesis work. An overview of a continuous wave, pulsed wave and duplex Doppler systems are given and current data acquisition limitations are reviewed. A review of the compressed sensing theory of the main topics of this thesis is given. A review of parallel computation also was given. The clutter rejection for Doppler signal reviewed, and the proposed methods used for cluttering also were reviewed.

### 2.1- Ultrasonic Wave

Ultrasonic wave is same as audible sound waves produced by the push pull action of the source in the propagating medium. The source is normally a transducer in which the vibrating element is a piece of piezoelectric ceramic or plastic driven by an appropriate voltage signal [1, 2].

The Doppler instrument generates either pulsed wave (PW) or continuous wave (CW) ultrasound; more details will be given later. Beside PW and CW, other types of ultrasonic wave such as shear or surface waves are available but are rarely applied in medical ultrasonic because of their attenuation in soft tissue [1].

From the point of view of Doppler techniques, the parameters that describe a wave, such as amplitude, frequency and phase, are important. The frequency and phase are more important for Doppler methods since the velocity of blood is obtained from the shifts in the frequency and changes in phase of scattered waves.

### 2.1.1 Intensity and Power

The acoustic intensity of a wave is the average flow of energy through a unit area normal to the propagation direction in unit time. The intensity is the average of the rate of work done per unit area by one element of fluid in an adjacent element. The intensity is related to the pressure amplitude  $P_A$ , the particle velocity amplitude  $U_A$  and the displacement amplitude  $X_A$ , by the following relation:

$$I = \frac{1}{2}(P_A^2/\rho_0 c) = \frac{1}{2} \rho_0 c U_A^2 = \frac{1}{2} \rho_0 c (2\pi f)^2 X_A^2 \quad (2.1)$$

Where  $c$  is speed of sound in soft tissue and  $\rho_0$  is the density.

The intensity measured at the focus of the beam or within 1 - 2 cm of the transducer face. The intensity of a continuous wave ultrasound beam measured at spatial peak  $I_{sp}$  or averaged across the beam to give spatial average  $I_{sa}$ . For pulsed wave ultrasound the intensity measured with either temporal average or spatial average. When temporal and average peak combined, they give intensity parameters, which are useful in characterizing the acoustic output of ultrasound systems [1, 2]. The widespread combinations proposed are, spatial peak - temporal average  $I_{spta}$ , spatial peak-pulse average  $I_{sppa}$ , spatial peak - temporal peak  $I_{sptp}$  and spatial average - temporal average  $I_{sata}$ . The intensity is normally measured with a hydrophone, which takes the form of a small probe with a piezoelectric element on it.

The power of an ultrasonic beam is the rate of flow of energy through the cross-sectional area of the beam. When the ultrasonic wave passes through the body, it transports energy from the source (transducers) into the medium (body). The ultrasound power measured with a radiation balance [1]. When the ultrasonic beam is completely absorbed by a target, it applies a force of  $W/c$  on the target. If the target reflected all the ultrasound, the force on it is given by:

$$\text{Radiation force} = 2W/c \quad (2.2)$$

Where  $W$  is the power of the beam and  $c$  is the velocity of sound in the propagating medium

In Doppler ultrasound the intensity and power are very important from safety point of view.

### 2.1.2 Scattering

When an ultrasound wave travelling through a medium strikes a discontinuity of dimensions similar to or less than a wavelength, some of the energy of the wave is scattered in many directions. Scattering is the process of central importance in diagnostic ultrasonics, since it provides most of the signals for both echo imaging and Doppler techniques. The discontinuities may be changes in density or compressibility or both. The red cells in blood, act as scattering centers which produce the signals used in Doppler techniques [1].

The total scattering cross-section,  $\sigma_t$ , of the target represented by the ratio of the total power,  $S$ , scattered by a target to the incident intensity,  $I$ . This ratio is used to compare the scattering power of different structures. The total scattering cross-section given by:

$$\sigma_t = \frac{S}{I} \quad (2.3)$$

From the point of view of Doppler techniques, the study of scattering is important since it improves our understanding of continuous wave and pulsed wave systems. The operator need not be concerned with scattered except to note that the signals from blood is very much weaker than from soft tissue. The sample volume of soft tissue is therefore is much larger than that for blood. Clutter filters normally included in Doppler device to

reduce low frequency signals from moving tissue, the clutter rejection will be discussed in details in chapter 5.

### 2.1.3 Reflection and transmission

When ultrasound waves travelling through one medium to another medium with different acoustic impedance, some of the waves reflected back toward the source of the wave and some are transmitted into the new medium. There are two items must be considered when studying the reflection and transmission of the ultrasonic waves. The first one is the angle that the reflected wave has as it leaves the interface and the angle that the transmitted wave takes as it propagate into the new region. The second is the percentage of intensity power that is reflected at the boundary. The amplitude of the reflected and transmitted waves depends on the change in acoustic impedance. The reflection can be considered as a special case of scattering which occurs on smooth surfaces on which the irregularities are very much smaller than a wavelength [1, 28]. The acoustic impedance  $z$  of the tissue can be defined as the ratio of the wave pressure over the particles velocity  $p_A/v_A$ . The acoustic impedance of the medium represented by the following equation:

$$z = \rho_0 c \quad (2.4)$$

Where  $\rho_0$  is the average density and  $c$  is the velocity.

The acoustic impedance of the tissue differs from each other according to the density. The higher the density or stiffness of a tissue, the higher is its acoustic impedance.

For normal incidence the pressure reflection coefficient given by:

$$R_a = \frac{z_2 - z_1}{z_1 + z_2} \quad (2.5)$$

$z_1$  and  $z_2$  are the acoustic impedance of the first and second medium respectively. In case of oblique incidence as shown in figure 2-1, the reflection coefficient represented as:

$$R_a = \frac{z_2 \cos \theta_i - z_1 \cos \theta_t}{z_1 \cos \theta_t + z_2 \cos \theta_i} = \frac{p_r}{p_i} \quad (2.6)$$

Where  $\theta_i$  and  $\theta_t$  are the angles of incidence and transmitted waves respectively. The angle of the reflected wave is equal to the angle of incidence wave.

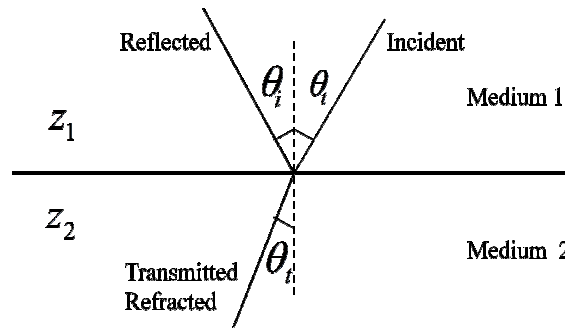


Figure 2-1. Reflection and transmission of ultrasound wave

### 2.1.4 Attenuation

When an ultrasound propagates through soft tissue, the energy associated with the wave is gradually lost so that its intensity reduces with distance travelled, an effect known as attenuation. Because of the absorption and scattering the ultrasound waves propagate tissue will attenuate. The attenuation in the tissue depends on the frequency, and is increased by increasing frequency [2]. The attenuation of ultrasound wave measured in  $\text{dB cm}^{-1} \text{MHz}^{-1}$  when Doppler techniques considered. The attenuation in the blood is lower compared to other human tissues, the attenuation of different human tissue illustrated in table 2.1. Since the Doppler ultrasound wave contains more than one specific frequency, the mean frequency of the received echo is lower than the mean frequency of the emitted ultrasound pulses. As the mean frequency is proportional to the velocity, then the blood velocity can be estimated by considering the frequency shift.

There are numbers of phenomena cause attenuation of ultrasound in tissue. The most important phenomena are absorption, in which the ultrasound energy is converted into heat [29]. The attenuation of practical interest is the rate at which ultrasound intensity in the beam decreases with distance. As well as absorption, the intensity of the beam may be reduced due to scattering of ultrasound out of the beam and to divergence or spreading of the beam with distance. Both frequency and magnitude were changed according to the spectrum of the emitted pulse when travelling through human tissue. These effects depend on the bandwidth of the emitted signal, the transducer center frequency and type of tissue investigated.

Table 2.1 attenuation values for different human tissue [1]

Tissue	Attenuation dB/MHz cm
Liver	0.6 – 0.9
Kidney	0.8 – 1.0
Spleen	0.5 – 1.0
Fat	1.0 – 2.0
<b>Blood</b>	<b>0.17 – 0.24</b>
Plasma	0.01
Bone	16.0 – 23.0

## 2.2 The Doppler Effect

The Doppler Effect is the change observed in the wavelength of ultrasound wave due to relative motion between a wave source and wave reflected. The wave received from moving target (reflected wave) has a frequency differ from that transmitted from the source. The difference between received and transmitted frequency is known as Doppler shift. The frequency increased and decreased according to the speed of motion, the frequency of waves emitted by the source and the angle between the wave direction and

the motion direction. The Doppler Effect enables ultrasound system to be used to detect the motion of blood and tissue. Most Doppler ultrasound systems provide both Doppler spectrogram and color Doppler image [1, 29].

### 2.2.1 The Doppler Equation

When an ultrasound wave transmitted into a human body containing blood vessels, the emitted energy will be received by either same transducer used for transmitting the wave in case of pulsed wave or by another transducer in case of continuous wave. The frequency shift occurs due to the motion of either the source or observer. The resulting Doppler shift used to calculate the velocity of the scatterers. When the observer moves towards the source, the increased frequency,  $f_r$ , due to passing more wave cycles per seconds, is given by:

$$f_r = f_t \frac{c+v}{c} \quad (2.7)$$

Where  $f_t$  is the transmitted frequency,  $c$  is the velocity of sound in tissue and  $v$  is the velocity of the observer (blood).

The velocity is replaced by the component of velocity in the wave direction,  $v \cos\theta$ , if the velocity of the observer is at an angle  $\theta$  to the direction of the wave propagation.

$$f_r = f_t \frac{c+v \cos\theta}{c} \quad (2.8)$$

If the observer is at rest and the source move with the velocity in the direction of wave travel, the wavelengths are compressed. The resulting observed frequency is:

$$f_r = f_t \frac{c}{c-v} \quad (2.9)$$

Taking the angle into account:

$$f_r = f_t \frac{c}{c-v \cos\theta} \quad (2.10)$$

In application of ultrasound, an ultrasonic beam is backscattered from the moving blood cells and tissue. Both of the above effects combine to give the transmitted Doppler shift in frequency. The observed frequency is then given by:

$$f_r = f_t \frac{c+v \cos\theta}{c} \cdot \frac{c}{c-v \cos\theta} = f_t \frac{c+v \cos\theta}{c-v \cos\theta} \quad (2.11)$$

As mentioned the Doppler shift frequency is the difference between incident frequency  $f_t$  and reflected frequency  $f_r$ , is therefore given by:

$$f_d = f_r - f_t \quad (2.12)$$

$$f_d = f_t \frac{c+v \cos\theta}{c-v \cos\theta} - f_t \quad (2.13)$$

Since  $c \gg v$

$$f_d = \frac{2 \cdot f_t \cdot v}{c} \cos\theta \quad (2.14)$$

From the relation (2.14), the Doppler shift depends on the angle  $\theta$  to the direction of the wave propagation and the transmitted frequency. The best reflection takes place when the transducer position at  $90^\circ$  to the surface [30].

## 2.3 Flow and tissue motion in the human body

The human circulatory system is very complicated, where non-stationary flow patterns arise. The human circulatory system is responsible for carrying oxygen and nourishment to the organs and also for the disposal of the waste products resulting from metabolism [31]. The pumping action is carried out by the heart. Basically two different systems can

be distinguished: the arterial and the venous systems. Flow towards the heart is referred to as being venous flow and flow away from the heart as arterial flow. The arterial walls are very flexible and contract and expand in response to the pulsation of the blood. The veins have thinner and less elastic walls, but also have a larger diameter than the corresponding arteries [31]. Therefore the veins function as a blood reservoir. It must be stressed that the flow is pulsating, so very complex flow patterns are encountered. A very common effect that arises with age in humans is the formation of plaque within the vessels. Atherosclerotic plaque hardens the arterial walls which lead to less wall-flexibility and different sometimes harmful flow profiles [2]. This is one of many conditions which influence the flow profiles and the wall-motion properties of the vessels. Since the human body is a very complex system with many different types of tissue, motion can arise due to various sources, e.g: breathing, muscle contraction, etc. As long as the tissue motion velocity is slow compared to the blood flow velocity, it is possible to separate both components. Measuring venous blood flow under slow-flow conditions reduces the possibility of separate tissue motion from blood flow because the blood flow velocity and the tissue motion velocity overlap in the Doppler frequency bands [10]. To measure this low blood velocity, clutter rejection filters are necessary.

## **2.4 Doppler Ultrasound Systems**

Increasing in the number of non-invasive blood velocity investigation in all areas of medicine carried out because of development in Doppler ultrasound technology. Doppler ultrasound used for detecting, measuring and imaging blood flow and other movement within the body. The simplest Doppler systems are stand-alone systems that produce and output signal related to the velocity of the targets in a single sample volume [1]. The transducers in the systems are hand-held. Such system may be very basic and produce a non-directional audio output or may be quite sophisticated, producing directional signals sampled from predetermined depth in the tissue; they may also derive various types of information from the Doppler signal and output one or more Doppler envelope signals.

The non-invasive measurements of blood flow, is a very useful investigation and quite a large number of systems have been developed to perform these measurements, the most common Doppler systems used, continuous wave system (CW) and pulse wave system (PW). They differ in transducer design and operational features, signal processing procedure and in the types of information provided and also duplex ultrasound Doppler has been used.

### 2.4.1 Continuous wave system

Continuous Wave Doppler system is the system that sends and received a continuous ultrasound wave, by using two separate transducer crystal, housed in the same probe. Because transmission and reception are continuous, the system has no depth resolution, except in the sense that signals originating from close to the transducer experience less attenuation than those from distance target. The transmitted and received beams overlap in a Doppler sample volume some distance from the transducer face [2], as shown in the figure 2-2.

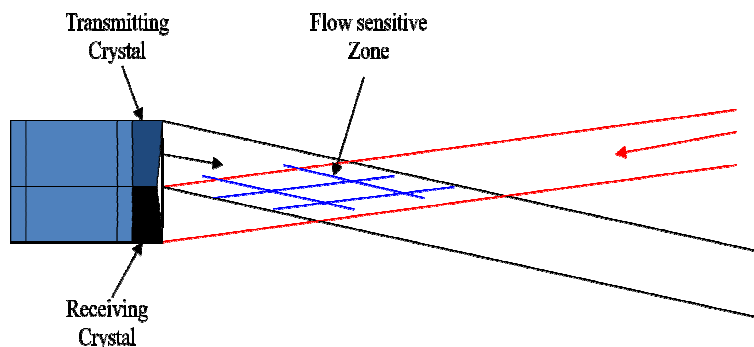


Figure 2-2. Continuous wave Doppler transducer

The region over which Doppler information can be acquired (sample volume) is the region of transmitting and receiving beam overlap. Because there is a continuous transducer transmission and reception, echoes from all depths within the area arrive at the transducer simultaneously [32].

In Doppler system the master Oscillator generates a frequency between 2 – 10 MHz. The frequency chosen depend on the depth of interest; since the ultrasonic attenuation highly depends on the frequency. The oscillation amplified by transmitting amplifier and the output used to drive the transmitting crystal. The electrical energy converted into acoustic energy by crystal, which propagates as a longitudinal wave into the body. The ultrasound energy is reflected and scattered by both moving and stationary particles within the ultrasound beam, and small portion finds its way back to the receiving crystal, which re-converts the acoustic energy into electric energy. The signal amplified by the radio frequency amplifier and mixed with a reference signal from master oscillator. The process of mixing produces both the sum of the transmitted and received frequency, and required the difference frequency or Doppler shift frequency. Low and high pass filter applied to the signal, with low pass filter to remove all signals outside the audio range and live Doppler difference frequency, and high pass filter to remove high-amplitude low-frequency signals from stationary and nearly stationary target, and then amplified signal is processed. The process of the Doppler shift signal is known as demodulation.

The CW Doppler system can determine the direction of follow, it cannot discriminate the difference depths where the motion originates [1]. The usefulness of CW Doppler devices is limited, but they are used clinically to confirm blood flow in superficial vessels, as they are good at detecting low velocities.

### **2.4.2 Pulsed wave system**

Since CW Doppler system cannot be used to study deep structure, particularly the heart and vascular organs. Even for superficial vessel it is sometimes difficult to separate the signal from arteries and veins with CW Doppler. Pulse wave Doppler system overcomes these problems by transmitting a short burst of ultrasound at regular intervals, and receiving only for a short period of time following an operator adjustable delay. The time interval between transmitted and received echo can be used to determine the depth from where the echo arises. The emitted pulse typically consists of bursts of sinusoidal oscillations, as given in complex form by

$$S(t) = g(t)e^{i2\pi f_0 t} \quad (2.15)$$

Figure 2-3 shows the PW Doppler transducer and the depth from where the echo signal generated.

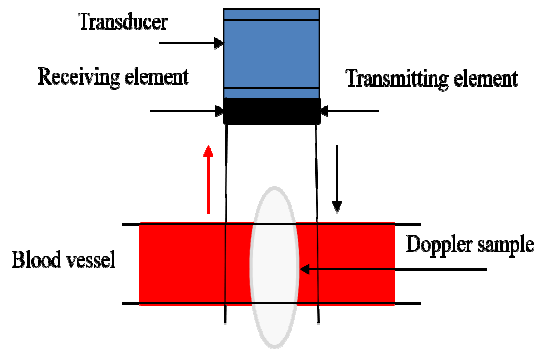


Figure 2-3. Pulsed wave Doppler transducer

The transmitted pulse from single element illustrated in figure 2-4, the pulse signal generated using Field II simulation package.

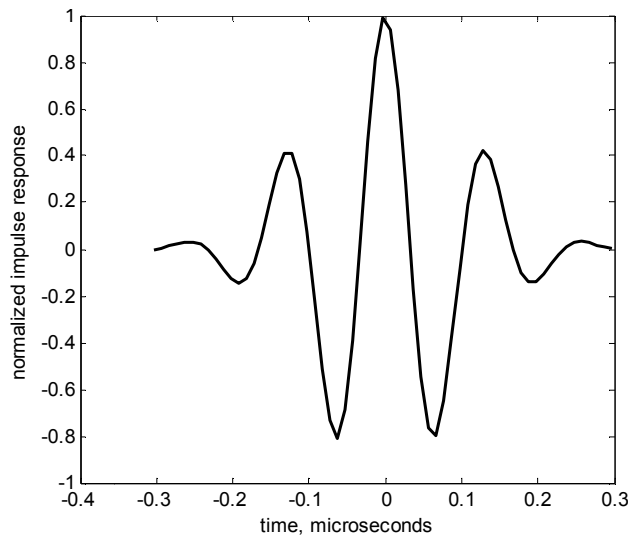


Figure 2-4. Transmitted pulse by PW system (generate using Field II simulation package)

PW Doppler system emits a short burst of ultrasound several times every second, usually at regular intervals. After each pulse has been transmitted, there is a delay before one or more gates in the receiving circuit are opened for a short period of time to admit

signals returning from a small volume of tissue [2]. The time for which the gate is left open, taken together with the length of transmitted pulse, determine the length the sample volume. Specifically, the distances from the transducer to the beginning of the range cell,  $Z_1$ , given by

$$Z_1 = c(t_d - t_p)/2 \quad (2.16)$$

Where  $c$  is the velocity of ultrasound in tissue,  $t_p$  is the pulse length and  $t_d$  is the time delay between the start of transmission and the moment at which the receiver gate opens. The distance from the transducer to the end of the range cell,  $Z_2$ , given by

$$Z_2 = c(t_d + t_g)/2 \quad (2.17)$$

Where  $t_g$  is the period for which the gate is open. The length of the range cell may therefore be written as

$$Z_t = Z_2 - Z_1 = c(t_g + t_p)/2 \quad (2.18)$$

The number of pulses transmitted by the system within a second is referred to as the pulse repetition frequency (PRF). The greater the sample-volume depth, the longer the time before the echoes are returned, and the longer the delay between pulse transmission.

### 2.4.3 Duplex System

Duplex systems are devices that combine a pulse echo B-mode and a Doppler system so that the Doppler shift signal can be recorded from known anatomical locations. The combination of the two modalities can be made in different ways, they all share certain characteristics; direction of obtaining Doppler information all lie within the scan of the

pulse-echo Imager, and the direction of the Doppler beam at any instant is indicated by cursor superimposed on the image.

The early duplex system combined mechanical sector scanners for imaging with a separate Doppler transducer, but now all the duplex systems use same array transducers for both imaging and Doppler measurements. Using the same transducer for imaging and Doppler purpose has advantages, but it has a number of drawbacks which stem from the compromises necessary in order to use the same element for two purposes. Firstly, it is necessary to use very short pulse to achieve good axial resolution with pulse-echo system which generated by heavily damped transducer element. A second area of compromise with dual purpose transducer is that is the out-of-plane width of the ultrasound beam. For imaging purpose a narrow beam was produce to get the best resolution; in Doppler applications it is often advantaged to insonate an entire blood vessel.

To operate the duplex system, the operator first find the blood vessel in the region of interest using the imaging facilities, and then place the Doppler sample volume at the required anatomical location. The scanner then switch to duplex mode to make the require measurement. The duplex Doppler ultrasound enables precise location of Doppler sample volume. To get an accurate estimation of flow it's required repeatedly transmitting of ultrasound pulses to acquire data from a region of interest [33]. Transmitting pulses to the same location for a long time to collect much data may cause increasing the heat in the body beyond the safety limit. Figure 2-5 show the placement of sample volume and the record of the blood flow velocity spectrum.

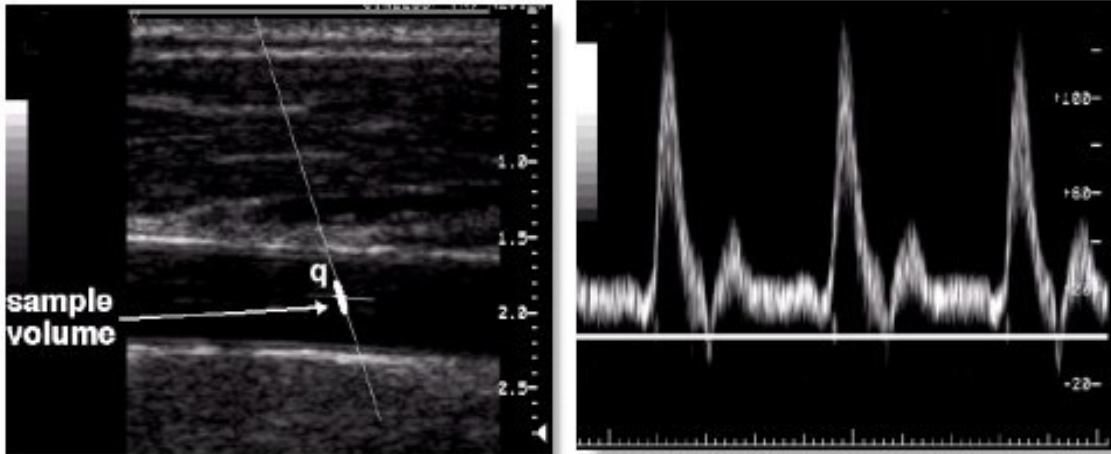


Figure 2-5. Placement of sampling volume (left) and the record of blood flow velocity spectrum (right) [29]

For example if we consider mixed B-mode and M-mode, the beam former rapidly switches back and forth between B-mode and M-mode integration. After every two lines of B-mode integration the beam is made to jump to select M-mode scan line for one transmission and echo acquisition sequence. It then jumps back to continue the B-mode scan for another two lines; then jumps back to M-mode line, ect [29]. This process illustrated in figure 2-6.

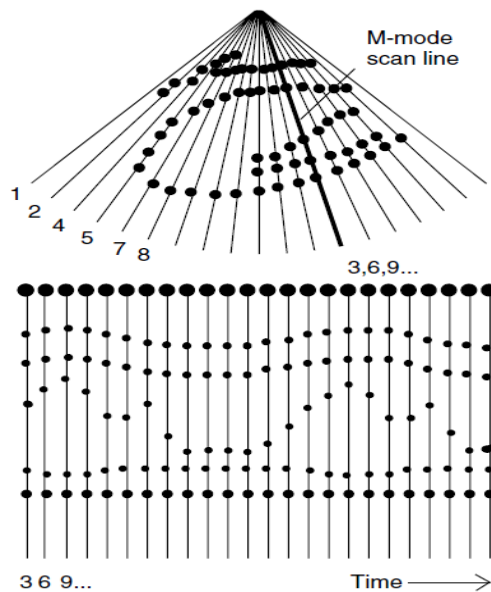


Figure 2-6. Mixed M-mode and B-mode scanning [29]

## 2.5 Spectral Doppler acquisition

Doppler data acquisition relies on repeatedly transmitting of ultrasound pulses to acquire data from a region of interest. Such acquisition must be extremely precise in its periodicity to ensure that the Doppler signal is uniformly sampled for further spectrogram processing. The speed is essential in Doppler systems in both acquisitions the echo data and in processing and displays it. Fast acquisition of data achieved by using either small number of pulses for each line of signal or collecting echo information from many range gate at the same samples.

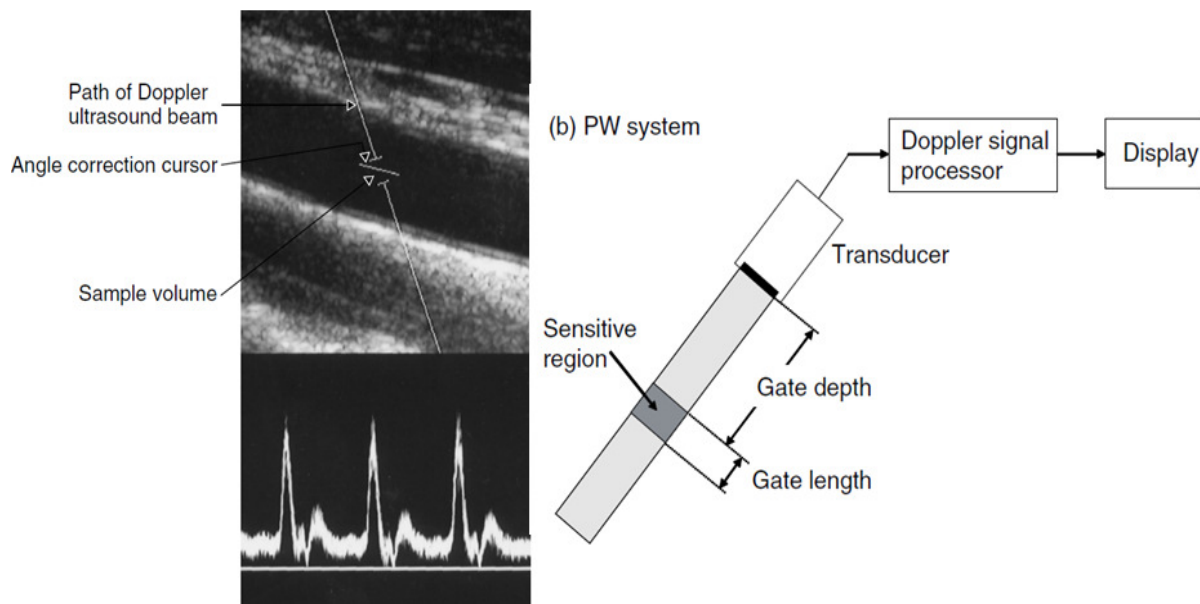


Figure 2-7. The sample volume, gate depth and sensitive region [29]

In order to detect the signal from a specific depth in the tissue, a range gate is used. This enables the system to only receive the returning signal at a given time after the pulse has been transmitted, and then for limited time. The Doppler signal is, therefore, detected from a specific volume within the body, known as the sample volume, at an identified range, as shown in figure 2-7. The length of time over which the range gate is open is known as the gate length or sampling volume length. The depth and the length of sample volume can be controlled by varying the gate range and length.

Transmitting short pulses for a long time in the same region of interest may cause a problem to the patient during the examination.

## **2.6 Doppler display**

Doppler signal can be displayed either as spectral Doppler or 2 D color flow imaging. In this work we will consider only the spectral Doppler. In a real time spectral Doppler all the velocity information detected from a single location within the blood vessel is displayed in the form of frequency shift-time plot. This displays time along the horizontal axis and Doppler frequency shift or calculated velocity along the vertical axis. The flow toward the transducer is displayed as information above the baseline [30].

The most important clinical information is the maximum Doppler shift, which correspond to a spatial maximum in the velocity field. When the ultrasonic beam is directed along the jet stream, the maximum Doppler shift gives the central velocity in the jet, which is related to the pressure drop along the blood stream line [2, 34]. The maximum Doppler shift as a function of time is known as spectrum envelope.

### **2.6.1 Doppler Spectrogram**

The Doppler shift frequency is proportional to velocity, and under ideal uniform sampling conditions the power in a particular frequency band of the Doppler spectrum is proportional to the volume of blood moving with velocities that produce frequencies in that band, and therefore the power Doppler spectrum should have the same shape as the velocity distribution plot for the flow in the vessel. The variation in the shape of the Doppler power spectrum as a function of time is usually presented in the form of sonograms shown in figure 2-8 [1, 35]. Spectral Doppler ultrasound velocimetry involves systematic analysis of the spectrum of frequencies that constitute the Doppler signal. The Doppler frequency shift signal represents the summation of multiple Doppler frequency shifts backscattered by millions of red blood cells. The Doppler signal is processed in sequential steps, consisting of reception and amplification, demodulation and

determination of directionality of flow, and spectral processing [1, 36, 37]. The returning signals are first received and amplified by radio frequency (RF) receiving device. The amplified signals contain of Doppler-shifted frequencies and carrier frequency, extracting carrier frequency from Doppler-shifted frequencies known as demodulation. There are various methods of demodulation [1, 36]. Quadrature sampling is needed to differentiate between flow toward the transducers (positive Doppler shift) and flow away from transducers (negative Doppler shift). The resulting signal consists of not only Doppler frequency shift, but also low-frequency/high-amplitude signal and high-frequency noise. Applying high-pass filter will eliminate the extrinsic low-frequency component of Doppler signals, and low-pass filter allows frequencies only below a certain threshold to pass, thereby removing any frequencies higher than that level. A spectral analysis applied to the resulting data. A full spectral processing that provides comprehensive information on both the frequency and its average power content is called then power-spectrum analysis. Various approaches are used for spectral processing proposed in [38, 39].

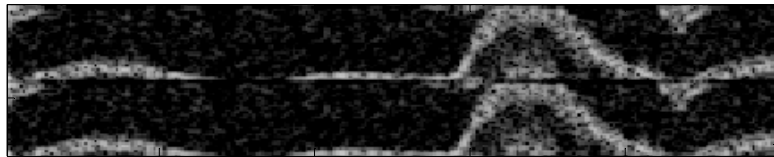


Figure 2-8 Doppler sonogram (generated using MATLAB)

## 2.7 Compressed Sensing

Compressed sensing is a new technique for signals and images compression and reconstruction. The novel theory of compressed sensing provides a fundamentally new approach to data acquisition, which is overcome all the problems of signals and images reconstruction and compression. Compressed sensing (CS) also known as compressive sensing, compressive sampling and sparse sampling. Is a technique for finding sparse solution to the sampled signal and present compressible signals and images at a rate significantly below the Nyquist sampling. This new sampling theory goes against the

wisdom in data acquisition, and states that one can reconstruct certain signals and images from far fewer samples or measurements than what is usually used in traditional methods. CS has played and continues to play a fundamental role in many fields of science. Sparsity leads to efficient estimations, efficient compression and dimensionality reduction and efficient modeling.

CS first was introduced in mathematics by B. Kashin and E. Gluskin in 1970s, then its potential in signal processing brought into focus after 2004, the revolution of this theory start when [5, 40, 41] introduced that, it is possible to reconstruct the signal or image with the minimum number of data, even though the number of data would be insufficient for reconstruct the signal by the Nyquist sampling theory.

CS uses the basic principle that almost every signal is sparse when linearly transformed to some mathematical space. A number of transformations can be used to obtain these sparse representations, such as wavelets or curvelets. The sparse signals themselves have the property that when multiplied by a random matrix, the resulting set of data can later be reconstructed via one of the recovering algorithms to obtain the original data of length  $N$ . This random matrix is called measurement sampling matrix which has to hold to mathematical properties like incoherence or restricted isometry, it has been proven that these properties are present in random matrices, which can vary depending on the application [5].

## **2.8 Parallel Computation**

Parallel computing is a form, which enable users to carry out many calculations at the same time. The large problems in parallel algorithms can be divided into smaller ones, which can be solved in parallel. Distributing the tasks in parallel computation leads to shorten the process time [42, 43].

MATLAB is a programming language that's used in different research area. With Matlab it is possible to achieve high efficiency because one line of Matlab code can typically replace multiple lines of C or FORTRAN code. In addition, Matlab supports a

range of operating systems and processor structural design, providing probability and flexibility [44]. Thus Matlab allows users to create an accessible parallel computing framework. There are several matlab libraries have been developed to allow the user to run multiple instance of matlab to speed up their program. The most common used programs are parallel Matlab (pMatlab) and Matlab message passing interface (MatlabMPI). Parallelize achieved by using either different computers connected with the network or mutlicore CPUs, the most common used is multicore CPU. Using multiprocessors to accelerate the reconstruction proposed in [45 - 48]. We want to make use of this algorithm so as to accelerate the reconstruction of Doppler ultrasound spectrogram, especially when reconstruction performed using  $\ell_1$ -minimization.

## 2.9 Clutter Rejection

Blood flow signal separation is an important topic in Doppler ultrasound systems. The signals from surrounding tissue and slowly moving target vessels walls and other tissue structure gives an additive low frequency noise (clutter noise) which is much stronger than the signals from blood flow. The signal-to-clutter level can be as low as 100 dB [10]. Clutter signals are normally suppressed using high pass filter, which is designed with sufficient stop-band so as to minimize the error in the velocity parameter estimator. Without sufficient cluttering it not possible to estimates the flow within the human body. The most common used filters for separation are standard linear time invariant filters; finite impulse response (FIR) and infinite impulse response (IIR), and also polynomial regression (PR) filter have been used [10].

A FIR filter with narrower bandwidth, narrower stop-band and the narrower transition band is a possible solution; the number of output sample is then reduced according to the filter order. IIR filter also be used, if special precaution is taken to initialize the filter, in order to reduce the ring down time. The IIR filter initialization described in [15]. PR filter proposed in [49], where the clutter signal estimated by linear regression, and then

subtracted from the input signal. The advantage of this technique is that the number of output samples is not reduced.

The FIR, IIR and PR filters were considered as non-adaptive filters. When the non-adaptive filter is used to remove unwanted signals, it is required to select design parameters that allow us to remove the clutter signal without affecting the blood flow signal, which is not possible sometimes. Also, these filters reduce the length of the signal. We proposed adaptive filters that can remove the clutter with high performance, principal component analysis (PCA) and independent component analysis (ICA).

## **2.10 Principal Component Analysis**

Principal component analysis (PCA) is a mathematical tool from applied linear algebra, which transforms a number of correlated variables into a smaller number of uncorrelated variables known as principal components (PC). PCA is a simple method of extracting relevant information from confusing data sets [19]. PCA is a very important tool for data analysis and identifying the most meaningful basis to re-express the data set. The main advantages of PCA can be used to find patterns in high-dimensional data, where the luxury of graphical representation is not available. Once PCA finds the patterns in the data, the data can be compressed by reducing the dimension without much loss of information [50]. Since the Doppler signal originates from different sources, it is possible to use PCA to subtract the clutter from the Doppler signal.

## **2.11 Independent Component Analysis**

Independent component analysis (ICA) is a signal processing technique whose goal is to express a set of random variables as a linear combination of statistically independent component variables. ICA belongs to a class of techniques that are commonly termed blind source separation. ICA is considered as an extension of PCA where higher-order statistical order is used to determine the basis vectors that are statistically independent as

possible rather than second order [20]. This is a reason some are selecting the ICA rather than PCA for data analysis.

## Chapter 3

### Compressed Sensing Theory & Parallel Computation

In this chapter we intended to address the novel theory of signals and image reconstruction, compressed sensing theory (CS), which is providing a fundamentally new approach to data acquisitions. First we will give a general introduction about the novel theory, its application in different fields and show how this new sampling theory will probably lead to a revolution in signal and image processing theory. This lead us to discuss compressed sensing theory, then go through the reconstruction algorithm and discuss the application of CS in signals and image reconstruction, especially in the field of biomedical engineering (medical imaging), then I will conclude with application of CS in Medical Doppler Ultrasound. The parallel computing algorithm, which is used for parallelizing computation so as to reduce the reconstruction time also discussed.

#### 3.1 Introduction to CS

To convert a signal from a continuous time to discrete time, a process called sampling is used. Sampling theorem also known as Shannon's / Nyquist sampling theorem [51 - 53], states that if a continuous time signal  $f(t)$  is band-limited with its highest frequency component less than  $\omega$ , then  $f(t)$  can be completely recovered from its sample values if the sampling frequency is equal to or greater than  $2\omega$  [52, 53]. This principle underlies nearly all signal acquisition protocols used in medical imaging devices, radio receivers and analog to digital conversion. Although there are some systems and devices that are not naturally band-limited, their construction usually involves using band-limiting filters before sampling, and so can also be dictated by Shannon's theorem [51]. Sampling at rates below the highest frequency component causes a phenomenon known as aliasing. In applications of imaging and video recording for example, the Nyquist rate is set so high that too many samples or measurement result, making compression necessary prior to

storage or transmission. In medical imaging (MRI, CT,..., ect), in order to get a good image, which translates to keeping the patient in the machine for a long time [54]. The above limitation of Shannon sampling theory has triggered researchers to think about new methods to overcome these problems. In the last few years, an alternative theory of “Compressive Sensing (CS)” also known as compressive sampling, compressed sampling or sparse reconstruction, offers an essentially new approach to data acquisition which transcends the common wisdom. CS theory shows that certain signals and images can be recovered from what was in the past supposed to be highly incomplete measurements [5, 55 - 59]. In CS, sampling and compression now performed in one step.

CS was first introduced by Donoho in 2006, when he published his first paper [5] with an explanation of its properties. He stated that CS reduced the measurement time, the sampling rate and reduced the use of Analog-to-Digital Converter resources. Then in 2008, Candes [57] stated that CS relies on two principles: **sparsity**, which pertains to the signal of interest, and **incoherence**, which pertains to the sensing modality. These principles will be discussed later.

## 3.2 Compressed Sensing

Compressed sensing is a technique for finding sparse solution to the underdetermined linear system. In signal processing, CS defined as the process for acquiring and reconstructing a signal that is supposed to be sparse or compressible.

CS potentially is useful in applications where one cannot afford to collect or transmit a lot of measurements such as medical imaging, data compression and data acquisition (for more detail view [57, 60]). There are rapidly growing in application of CS in the field of medical imaging and image processing.

CS methods provide a robust framework for reducing the numbers of measurements require to summarize the sparse signals [55, 61]. For this reason CS methods are useful in areas where analog-to-digital costs are high.

Research in this area has two major components [62].

- 1- Sampling: how many samples are necessary to reconstruct signals to a specified precision? What type of sample? How can these sample schemes to be implemented in practices?
- 2- Reconstruction: given the compressive samples, what an algorithm can efficiently construct a signal approximation?

CS uses the basic principle that almost every signal is sparse (or nearly sparse) when linearly transformed to some mathematical space. A number of transformations can be used to obtain sparse representations, such as wavelets [56, 57]. The sparse signals themselves have the property that when multiplied by a random matrix the resulting set of data can later be reconstructed via one of the recovering algorithms to obtain the original data of length  $N$ . This random matrix is known as a measurement sampling matrix, which have to hold to mathematical properties like incoherence or restricted isometry, it has been proven that these properties are present in random matrices, which can vary depending on the application [5]. The whole theory can be described as:

$$y = \Phi f = \Phi\Psi \hat{x} \quad (3.1)$$

This means that the sample  $y$  of the signal  $f$  is a linear function of  $f$ . The sensing matrix  $\Phi$  is in term of  $M \times N$  where  $M \ll N$ , implying that sampling and compression are now performed in one step. So,  $y$  represented in term of  $M \times 1$  vector, while  $f$  is in  $N \times 1$ . Due to sparsity-inducing matrix  $\Psi$  the vector  $\hat{x}$  is  $k$ -sparse, meaning that it has at most  $k$  non-zero entries. Figure 3-1 schematically shows the matrix and vector dimensions that is dimension reduction and so the compression after the sampling process.

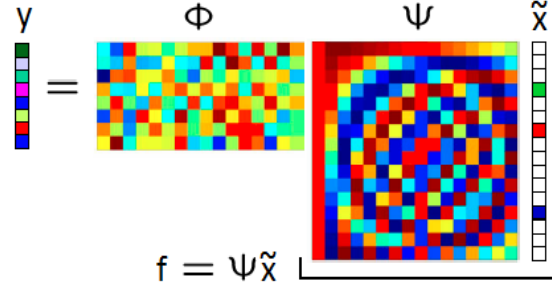


Figure 3-1: Schematic description of matrix dimension with a 3-sparse vector  $\hat{x}$  [63]

The standard procedure for compressive sparse signals, known as transform coding (as indicated in [66]) is to (i) acquire the full  $N$ -samples of signal  $y$ ; (ii) compute the complete set of transform coefficients  $x$ ; (iii) locate the  $k$  largest, significant and discard the small coefficients; (iv) encode the values and locations of the largest coefficients. The important features of compressive sampling are that many types of signals and images can be well-approximated by a sparse expansion in term of a appropriate basis that is by only a small number of non-zero coefficients. Another feature is that useful reconstruction can be achieved by using efficient algorithms [56, 65]. In this part we will discuss the sensing matrices (compressive sensing problem), principles of CS (Sparsity and incoherence) and restricted isometry properties (RIP).

### 3.2.1 Sensing Matrices

In CS signals acquired directly without going through the transitional stage of acquiring  $N$  samples. Considering a general linear measurement process that computes  $M < N$  inner products between  $x$  and a collection of vectors  $\{\Phi_j\}_j^M = I$  as in  $y_j = (x, \Phi_j)$ . Arrange measurements  $y_j$  in an  $M \times 1$  vector  $y$  and the measurement vectors  $\Phi_j^T$  as rows in term of  $M \times N$  matrix  $\Phi$ . Then, by substituting  $\Psi$  from  $x = \Psi s$ ,  $y$  can be written as:

$$y = \Phi x = \Phi \Psi s = \theta s \quad (3.2)$$

Where  $\theta = \Phi \Psi$  is a matrix in term of  $M \times N$ . The measurement process is not adaptive, meaning that  $\Phi$  is fixed and does not depend on the signal  $x$ .

There are two main theoretical questions in CS, first, how should we design the sensing matrix  $\Phi$  to ensure that it preserves the information in the signal  $x$ ? Second, how can we recover the original signal  $x$  from measurements  $y$  [63, 65]? In the case where our data are sparse or compressible, we will see that we can design matrices  $\Phi$  with  $M \ll N$  that ensure that we will be able to recover the original signal accurately and efficiently using a variety of practical algorithms.

We begin establishing conditions on  $\Phi$  in the context of designing a sensing matrix by considering the null space property (NSP) of  $\Phi$ , denoted in [66].

$$N(\Phi) = \{z: \Phi z = 0\} \tag{3.3}$$

If we wish to be able to recover all sparse signals  $x$  from the measurements  $\Phi x$ , then it is immediately clear that for any pair of vectors  $x, x' \in \Sigma k$ , we must have  $\Phi x = \Phi x'$ , since it would be impossible to distinguish  $x$  from  $x'$  based on the measurements  $y$ . More formally, by observing that if  $\Phi x = \Phi x'$  then  $\Phi(x - x') = 0$  with  $x - x' \in \Sigma 2k$ , we see that  $\Phi$  uniquely represents all  $x \in \Sigma k$  if and only if  $N(\Phi)$  contains no vectors in  $\Sigma k$ . There are many equivalent ways of characterizing this property; one of the most common is known as the spark. The spark of a given matrix  $\Phi$  is the smallest number of columns of  $\Phi$  that are linearly dependent.

When dealing with exactly sparse vectors, the spark provides a complete characterization when sparse recovery is possible. However, when dealing with approximately sparse signals we must introduce somewhat more restrictive conditions on the null space of  $\Phi$  [67]. We must also ensure that  $N(\Phi)$  does not contain any vectors that are too compressible in addition to vectors that are sparse.

### 3.2.2 Sparsity (Compressible Signal)

Signals can often be well-approximated as a linear combination of just a few elements from a known basis or dictionary. When this representation is exact we say that the signal is sparse. Sparse signal models provide a mathematical framework for capturing the fact that in many cases these high-dimensional signals contain relatively little information compared to their ambient dimension [59, 65, 68, 69].

Compressive sampling based on the experiential observation that many types of real-world signals and images have a sparse expansion in terms of a suitable basis or frame, for instance a wavelet expansion. If the expansion of the original signal or image as a linear combination of the selected basis functions has many zero coefficients, then it's often possible to reconstruct the signal or image exactly.

Let us consider a finite-length, one-dimensional, discrete-time signal  $f$ , which can be viewed in term of  $N \times 1$  column vector in  $\mathbb{R}^N$  with elements  $f[n]$ ,  $n = 1, 2, \dots, N$ . Any signal in  $\mathbb{R}^N$  can be represented in terms of a basis of  $N \times 1$  vectors  $(\Psi_i)_i^N = 1$ . Using  $N \times N$  basis matrix  $\Psi = [\Psi_1 | \Psi_2 | \dots | \Psi_N]$  with the vector  $(\Psi_i)$  as a column, a signal  $f$  can be expressed as:  $f = \Psi x$  where,  $x$  is  $N \times 1$  column vector of weighting coefficients  $x_i = (f, \Psi_i) = \Psi_i^T x$ . Clearly  $f$  and  $x$  are equivalent representations of the signal, with  $f$  in the time or space domain and  $x$  in the  $\Psi$  domain. The signal  $f$  is  $k$ -sparse if it is a linear combination of only  $k$  of the  $x_i$  coefficient in  $f = \Psi x$  are nonzero and  $(N - k)$  are zero. The case of interest is when  $k \ll N$ . The signal  $f$  is sparse (compressible) if the representation  $f = \Psi x$  has just a few large coefficients and many small coefficients. The signal  $f$  can be efficiently approximated from only a few significant coefficients. Sparsity is important in compressive sensing as it determines how efficiently one can acquire signals non-adaptively.

Figure 3-2 shows a typical transformation of the signal from time domain to frequency domain. The signal is a combination of sinusoids with 18 Hz and 36 Hz frequency. In the time domain, the representation of the signal reached a high density. After Fourier

transformation, the signal can be represented by two Fourier transform coefficients, which is obviously in a sparse way.

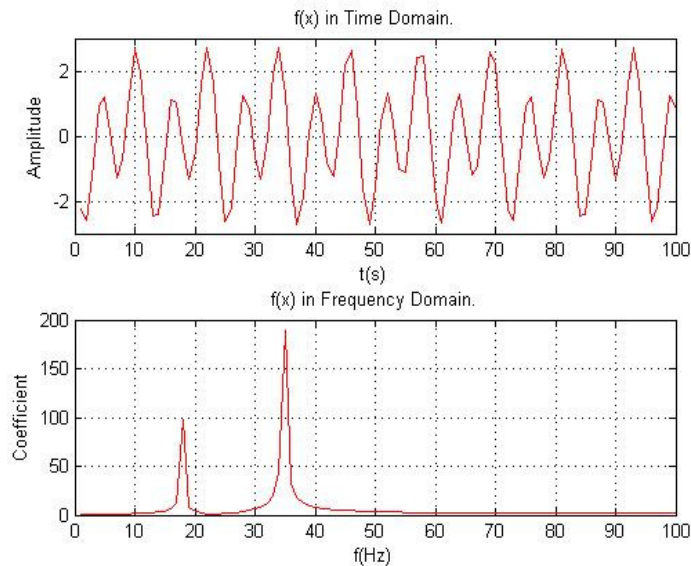


Figure 3-2: Signal represented in time domain and frequency domain [generated with Matlab]

Megapixel photo also has a concise representation. Signals with this structure are known to be very nearly sparse when represented using a wavelet transform. The wavelet transform consists of recursively dividing the image into its low and high-frequency components. The lowest frequency components provide a coarse scale approximation of the image, while the higher frequency components fill in the detail and resolve edges. Figure 3-3 shows the natural image and its wavelet transform, which shows that the most coefficients are very small. Hence, we can obtain a good approximation of the signal by setting the small coefficients to zero, to obtain a  $k$ -sparse representation.

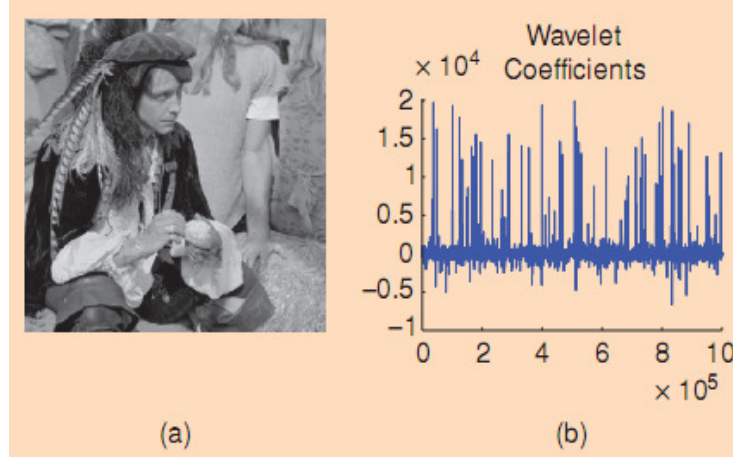


Figure 3-3: Natural picture and its wavelet coefficients [59]

### 3.2.3 Incoherence

Incoherence is an important feature in compressive sampling, and was defined in [55 – 57, 59, 62, 65, 67]. By considering the pair of orthobasis  $(\Phi, \Psi)$  of  $\mathbb{R}^N$ , the coherence between the sensing basis  $\Phi$  and the representation basis  $\Psi$  is

$$\mu(\Phi, \Psi) = \sqrt{n} \cdot \max_{1 \leq k, j \leq n} |\langle \Phi_k, \Psi_j \rangle| \quad (3.4)$$

From the linear algebra,  $\mu(\Phi, \Psi) \in [1, \sqrt{n}]$

The coherence measures the largest correlation between any two elements  $\Phi$  and  $\Psi$ . If  $\Phi$  and  $\Psi$  contain correlated elements, the coherence is large, otherwise, is small. From an experimental point of view, the incoherence of  $\Phi$  and  $\Psi$  means that the information carried by a few entries of  $S$  is spread all over the  $M$  entries of  $y = \Phi \Psi S$ . Each sample  $y_k$  is likely to contain a piece of information about each significant entry of  $x$ .

CS is mainly concerned with low coherence pairs. The incoherence properties hold for many pairs of bases, including for example, delta spikes and the sin waves of a Fourier basis, or the Fourier basis and wavelets significantly, this incoherence also holds with high probability between an arbitrary fixed bases and randomly generated one.

Figure 3-4 shows a narrow  $rect(t)$  function in the time domain corresponds to the wide-

spared  $\text{sinc}(t)$  function in the frequency domain. Sampling in the time domain can be done with spike basis, say  $\varphi_k(t) = \delta(t - k)$ . Representing the signal of interest in the Fourier domain with  $\Psi_j(t) = n^{-1/2} e^{i2\pi jt/n}$  lead to coherence of  $\mu(\varphi, \Psi) = 1$ .

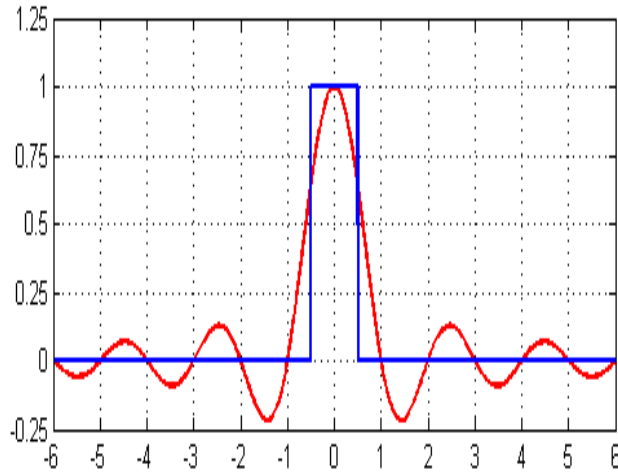


Figure 3-4 plot of  $\text{rect}(t)$  (blue) and corresponding frequency representation  $\text{sinc}(f)$  (red)

The incoherence between  $\Phi$  and  $\Psi$  also indicates how many samples we will need at least in order to be able to reconstruct our signal from our measurements [57].

$$m \geq C \cdot \mu^2(\phi, \Psi) \cdot k \cdot \log n \quad (3.5)$$

Where  $m$  is the number of samples,  $k$  the number of nonzero entries of our signal in  $\Psi$  and  $C$  is some positive constant. If our signal is truly sparse ( $k \ll n$ ) and the coherence value is close to one, we need far less samples than that in the time domain.

### 3.2.4 Restricted Isometries Property

When the size of data infected with noise or have been corrupted by some error, it will be valuable to consider somewhat stronger conditions. In [40, 70, 71], Candes, Tao and others introduced the isometry condition on matrices  $\Phi$  and established its important role in CS theory. It says that “if a sampling matrix satisfies the RIP of a certain order

proportional to the sparsity of the signal, then the original signal can be reconstructed even if the sampling matrix provides a sample vector, which is much smaller in size than the original signal”.

**Definition 3.1:** A matrix  $\Phi$  satisfies the restricted isometry property (RIP) of the order  $k$  if there exists a  $\delta_k \in (0, 1)$  such that

$$(1 - \delta_k)\|x\|_2^2 \leq \|\Phi x\|_2^2 \leq (1 + \delta_k)\|x\|_2^2 \quad (3.6)$$

Hold for all  $x \in \Sigma^k$ .

If a matrix  $\Phi$  satisfies the RIP of order  $2k$ , then we can interpret (3.6) as saying that  $\Phi$  approximately preserves the distance between any pair of  $k$ -sparse vectors.

If  $\Phi$  satisfies the RIP of order  $k$  with constant  $\delta_k$ , then for any  $k' < k$  we automatically have that  $\Phi$  satisfies the RIP of order  $k'$  with constant  $\delta_{k'} \leq \delta_k$ . Moreover, in [72] it is shown that if  $\Phi$  satisfies the RIP of order  $k$  with a sufficiently small constant, then it will also automatically satisfy the RIP of order  $\gamma k$  for certain  $\gamma$ , albeit with a somewhat worse constant.

The stability of RIP addresses that if a matrix  $\Phi$  satisfies the RIP, then this is sufficient for a variety of algorithms to be able to successfully recover a sparse signal from noisy measurements.

We can also consider how many measurements are necessary to achieve the RIP. If we ignore the impact of  $\delta$  and focus only on the dimensions of the problem ( $n$ ,  $m$ , and  $k$ ) then we can establish a simple lower bound.

**Theorem 3.1** [73] let  $\Phi$  be an  $m \times n$  matrix that satisfy the RIP of order  $2k$  with constant  $\delta \in (0, 1/2)$  then

$$m \geq ck \log \frac{n}{k} \quad (3.7)$$

where  $c \geq \frac{1}{2} \log \sqrt{24 + 1} \approx 0.28$

One can establish a similar result by examining the Gelfand width of the  $\ell_1$  ball. Both fail to capture the precise dependence of  $m$  on the desired RIP constant  $\delta$ . Also, [74] shown that if a matrix  $A$  satisfies the RIP of order  $k = c_1 \log(p)$  with constant  $\delta$ , then  $\Phi$  can be used to construct a distance-preserving embedding for  $p$  points with  $\varepsilon = \delta 4$ .

For application purposes, one often needs to analyze the RIP constants of the products of a matrix  $\Phi$  with known RIP constant  $\delta$  and other matrices. For example, if the size of  $\Phi$  is  $n \times N$  with  $n < N$  one would like to extend  $\Phi$  to  $A\Phi B$  of size  $m \times q$  with  $m < n < N < q$  if possible to give a further reduction on the number of measurements one need to collect: for  $\Phi$  the number of measurements is  $n$ ; while for  $A\Phi B$ , the number of measurements is  $m$ .

### 3.3 Reconstruction Algorithms

The basic theory of CS consists of two components: recoverability and stability [75]. Recoverability answer the following question: what types of measurement matrices and recovery procedures ensure exact recovery of all  $k$ -sparse signals and what is the best order  $m$  for the sparsity  $k$ ? Reconstruction algorithms are amazing. Collecting a few samples (less than that used in Shannon-Nyquist sampling theory) randomly can perfectly reconstruct the signal.

Given noisy compressive measurements  $y = \Phi x + e$  of a signal  $x$ , a core problem in compressive sensing is to recover a sparse signal  $x$  from a set of measurements  $y$ . The most difficult part of signal reconstruction is to identify the location of the largest component in the target signal. The signal recovery algorithm must take a few number of measurements  $M$  in the vector  $y$ , the random measurement matrix  $\Phi$ , and the basis  $\Psi$  and reconstruct the length- $N$  signal  $x$ , or equivalently, its sparse coefficient vector  $s$ . In order to recover a good estimate of  $x$  from the  $M$  compressive measurements, the measurement matrix  $\Phi$  should satisfy the restricted isometry property (RIP). In CS signals recovery achieved by; using nonlinear and relatively expensive optimization-based and iterative algorithms [5, 69].

Designing of sparse recovery algorithms is guided by various criteria. Some important ones are:

- ❖ **Minimal number of measurements:** Sparse recovery algorithms must require approximately the same number of measurements (up to a small constant) required for the stable embedding of  $k$ -sparse signals.
- ❖ **Robustness to measurement noise and model mismatch:** Sparse recovery algorithms must be stable in regard to perturbations of the input signal, as well as noise added to the measurements; both types of errors arise naturally in practical systems.
- ❖ **Speed:** Sparse recovery algorithms must strive towards expending minimal computational resources, keeping in mind that a lot of applications in CS deal with very high-dimensional signals.
- ❖ **Performance guarantees:** Focus on algorithm performance for the recovery of exactly  $k$ -sparse signals  $x$ .

Most of the CS literature has focused on improving the speed and accuracy of the process [76].

Several methods for recovering sparse  $x$  from a limited number of measurements have been proposed [57, 59, 63, 65, 77 - 83]. In some cases the goal is to solve some kind of interface problem such as signal detection, classification, or parameter estimation, in which case a full reconstruction may not be necessary [69, 84 - 86] Most of proposed algorithms have the same process idea (for example orthogonal matching pursuit and matching pursuit). For simplicity we categorized them in groups, and we restrict our attention to the algorithms that reconstruct the signal  $x$ .

The reconstruction methods categorized into the following groups:

- ❖ Convex optimization based approaches,
- ❖ Greedy methods and
- ❖ Combinatorial methods.

Before discussing those algorithms let us give a general overview of a natural first approach to recover sparse signals, this approach is known as the  $\ell_1$ -norm.

Consider a measurement  $y$  and the original signal  $x$  is sparse or compressible, it is natural to attempt to recover  $x$  using  $\ell_0$ -norm by solving an optimization problem of the form

$$\hat{x} = \arg \min_x \|x\|_0 \quad s.t. \quad y = Ax \quad (3.8)$$

Where  $y = Ax$  ensures that  $\hat{x}$  is consistent with the measurements  $y$ . This is the case where the measurements are exact noise-free. When the measurements have been contaminated with a small amount of noise, we solve an optimization problem of the form

$$\hat{x} = \arg \min_x \|x\|_0 \quad s.t. \quad \|Ax - y\|_2 \leq \varepsilon \quad (3.9)$$

In both cases, find the sparsest  $x$  that is consistent with measurements  $y$ .

In (3.8, 3.9) we assume that  $x$  itself is sparse. In the common setting where  $f = \Phi c$  we can easily modify the approach and instead consider

$$\hat{c} = \arg \min_x \|x\|_0 \quad s.t. \quad y = A\Phi x \quad (3.10)$$

This is by noise-free measurements, when considering the noise measurements the form is

$$\hat{c} = \arg \min_x \|x\|_0 \quad s.t. \quad \|A\Phi x - y\|_2 \leq \varepsilon \quad (3.11)$$

By considering  $\hat{A} = A\Phi$  we see that (3.8) and (3.10) are essentially identical. Moreover, in many cases the introduction of  $\Phi$  does not significantly complicate the construction of matrices  $A$  such that  $\hat{A}$  will satisfy the desired properties [59, 65].

One avenue for translating this problem into something more trustable is to replace  $\|\cdot\|_0$  ( $\ell_0$ -norm) with its convex approximation  $\|\cdot\|_1$  ( $\ell_1$ -norm). Specifically we consider

$$\hat{x} = \arg \min_x \|x\|_1 \quad s.t. \quad y = Ax \quad (3.12)$$

Provided that  $y$  is convex, (3.12) is computationally feasible. In fact, the resulting problem can be posed as a linear program [94]. While it is clear that replacing (3.8) with (3.12) transforms a computationally intractable problem into a tractable one, it may not be immediately obvious that the solution to (3.12) will be at all similar to the solution to (3.8). As an example, the solutions to the  $\ell_1$  minimization problem coincided exactly with the solution to the  $\ell_p$  minimization problem for any  $p < 1$ , and notably, was sparse. Moreover, the use of  $\ell_1$  minimization to promote or exploit sparsity has a long history.

Finally, there was renewed interest in  $\ell_1$  minimization approaches within the signal processing community for the purpose of finding sparse approximations to signals and images when represented in overcomplete dictionaries or unions of bases [87].  $\ell_1$  minimization received significant attention in the statistics literature as a method for variable selection in regression, known as the Lasso.

Thus, there is a variety of reasons to suspect that  $\ell_1$  minimization will provide an accurate method for sparse signal recovery. More importantly, this also constitutes a computationally tractable approach to sparse signal recovery.

### 3.3.1 Convex Optimization Based-Approaches

Using convex optimization algorithms to recover sparse signals has been proposed in different articles [40, 57, 63, 70, 88, 89], it is also known as basis pursuit. An important class of sparse recovery algorithms falls under the purview of convex optimization. This algorithms seeks to optimize the convex function  $f(\cdot)$  of the unknown variable  $x$  over a convex subset of  $\mathbb{R}^N$ .

Assume that  $J(x)$  be a convex sparsity-promoting cost function (i.e.,  $J(x)$  is small for sparse  $x$ .) to recover a sparse signal representation  $\hat{x}$  from measurements  $y = \Phi x$ ,  $\Phi \in \mathbb{R}^{M \times N}$ , we may either solve

$$\min_x \{J(x) : y = \Phi x\}; \quad (3.13)$$

When there is no noise, or solve

$$\min_x \{J(x) : H(\Phi x, y) \leq \epsilon\}; \quad (3.14)$$

When there is noise in the measurements. Here,  $H$  is a cost function that penalizes the distance between the vectors  $\Phi x$  and  $y$ .

For convex programming algorithms, the most common choices of  $J$  and  $H$  are usually chosen as follows:

$J(x) = \|x\|_1$ , the  $\ell_1$ -norm of  $x$  and  $H(\Phi x, y) = \|\Phi x - y\|_2^2$ , the  $\ell_2$ -norm of the error between the observed measurement and the linear projection of the target vector  $x$ . In statistics, minimizing  $H$  subject to  $\|x\|_1 \leq \delta$  is known as the Lasso problem [90]. More generally,  $J(\cdot)$  acts as a regularization term and can be replaced by other, more complex functions.

We can conclude that (3.13, 3.14) can exactly recover signal with high possibility using only  $M \geq ck \log(N/k)$  independent and identically distributed Gaussian measurements [63, 68]. Then, the numbers of measurements depend on the length of signal and nonzero coefficient. Also M. Wakin [91] **theorem 2** shows that more than  $k + 1$  measurement are required to recover the sparse signal.

Figure 3-5 shows the recovered signal by using convex optimization. 136 numbers of measurements were used for the reconstruction. The length of the signal is 1024 and the numbers of nonzero are 17.

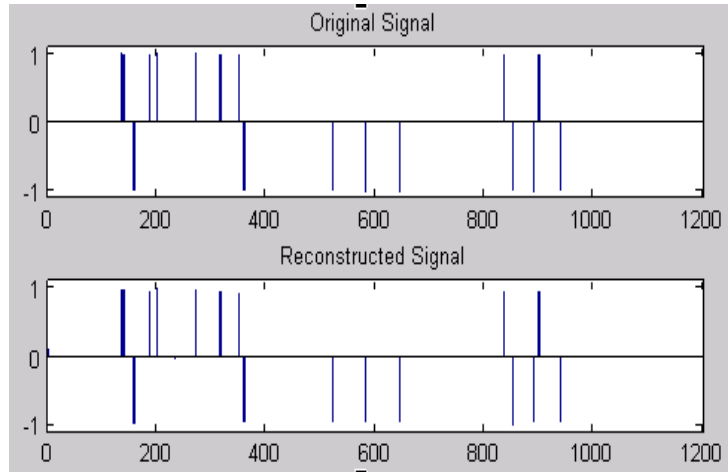


Figure 3-5. Reconstructed signal via convex optimization

Convex optimization methods ( $\ell_1$  minimization) will recover the underlying signal  $x$ . In addition, convex relaxation methods also guarantee stable recovery by reformulating the recovery problem as unconstrained formulation.

The advantages of using convex optimization method provide uniform guarantee for sparse reconstruction and it's stable. The convex optimization method based on linear programming.

### 3.3.2 Greedy Algorithm

While convex optimization techniques are powerful methods for computing sparse representations, there are also a variety of greedy/iterative methods (matching pursuit, orthogonal matching pursuit, stagewise orthogonal matching pursuit, compressive sampling matching pursuit and regularized orthogonal matching pursuit) for solving such problems [62, 76, 92 - 70]. Greedy algorithms rely on iterative approximation of the signal coefficients and support, either by iteratively identifying the support of the signal until a convergence criterion is met, or alternatively by obtaining an improved estimate of the sparse signal at each iteration that attempts to account for the mismatch to the measured data. Some greedy methods can actually be shown to have performance

guarantees that match those obtained for convex optimization approaches. Greedy algorithms are very simple and fast to implement.

### 3.3.2.1 Matching Pursuit

Matching Pursuit (MP) is an iterative greedy algorithm that decomposes a signal into a linear combination of elements from a dictionary.

The concept of MP is very simple. A key quantity in MP is the initial residual  $r \in \mathbb{R}^M$  equal to the input signal  $x$ , which is representing the portion of measurements. At each iteration of the algorithm, we select a vector from the dictionary that is maximally correlated with the residual  $r$ :

$$\lambda_k = \underset{\lambda}{\operatorname{argmax}} \frac{\langle r_{k-1}, \Phi_{\lambda} \rangle \Phi_{\lambda}}{\|\Phi_{\lambda}\|^2} \quad (3.15)$$

Once this column is selected, we possess a “better” representation of the signal, since a new coefficient indexed by  $\lambda_k$  has been added to our signal approximation. Thus, we update both the residual and the approximation as follows:

$$r_k = r_{k-1} - \frac{\langle r_{k-1}, \Phi_{\lambda_k} \rangle \Phi_{\lambda_k}}{\|\Phi_{\lambda_k}\|^2} \quad (3.16)$$

$$\hat{x}_{\lambda_k} = \hat{x}_{\lambda_k} + \langle r_{k-1}, \Phi_{\lambda_k} \rangle \quad (3.17)$$

and repeat the iteration. A suitable stopping criterion is when the norm of  $r$  becomes smaller than some quantity. Although MP is intuitive and can find an accurate approximation of the signal, it possesses major Drawbacks are:

- ❖ It offers no guarantees in terms of recovery error; indeed, it does not exploit the special structure present in the dictionary.
- ❖ The required number of iterations required can be quite large. The complexity of MP for CS recovery is  $O(MNT)$  [69], where  $T$  is the number of MP iterations

### 3.3.2.2 Orthogonal Matching Pursuit

Orthogonal matching pursuit (OMP) algorithm combines the simplicity and the fastness for high-dimensional sparse signal recovery. Hence, it is easy to implement in practice [80, 70]. OMP algorithm begins by finding the column of  $A$  most related with the measurements. The algorithm then repeats this step by correlating the columns with the signal residual, which is obtained by subtracting the contribution of a partial estimate of the signal from the original measurement vector.

Tropp and Gilbert [62] proved that OMP can be used to recover a sparse signal with high probability using CS measurements. Suppose that  $x$  is an arbitrary  $k$ -spares in  $\mathbb{R}^M$ , and let  $\{\alpha_1, \dots, \alpha_N\}$  be a family of  $N$  measurement vectors. From an  $N \times M$  matrix  $\Phi$  whose rows are the measurement vectors, and observe that the  $N$  measurement of the signal can be collected in  $N$ -dimensional data vector:

$$y = \Phi x \tag{3.18}$$

We refer to  $\Phi$  as the measurement matrix and denote its columns by  $\varphi_1, \dots, \varphi_M$ .

It is natural to think of signal recovery as a problem dual to sparse approximation. Since  $x$  has only  $k$  nonzero components, the data vector (3.18) is a nonlinear computation of  $k$  columns from  $\Phi$ . In this language of approximation, we say  $x$  has  $k$ -term representation over the dictionary  $\Phi$ .

Therefore, sparse approximation algorithms can be used for recovering sparse signal. To identify the ideal signal  $x$ , we need to determine which columns of  $\Phi$  participate in measurement vector  $x$ . The idea behind the algorithm is to pick a column in a greedy fashion. At each iteration, we chose the column of  $\Phi$  that is most strongly correlated with the remaining part of  $x$ . Then we subtract off it is a contribution to  $x$  and iterate on the residual. After  $k$  iteration, the algorithms suppose to identify the correct set of columns.

Tropp and Gilbert show that, if we let  $\Phi$  be a  $m \times N$  subgaussian matrix and fix a  $k$ -spares signal  $x \in \mathbb{R}^M$ . Then, OMP recovers signal  $x$  from measurements (3.18) correctly with high probability, provided the number of measurements is  $m \sim k \log N$ .

The steps of OMP for signal recovery [80] are

Let  $M \times N$  measurement matrix  $\Phi$ ,  $M$ -dimensional vector  $y$  and the sparsity level  $k$  of the ideal signal.

Output:

- An estimate  $\hat{x}$  in  $\mathbb{R}^N$  for the signal
- A set  $A_k$  containing  $k$  element from  $\{1, \dots, N\}$
- An  $M$ -dimensional approximation  $a_k$  of the data  $y$ .
- An  $M$ -dimensional residual  $r_k = y - a_k$

Procedure:

1- Initialize the residual  $r_0 = y$ , the index set  $A_0 = \emptyset$ , and the iteration counter  $t = 1$ .

2- Find the index  $\lambda_t$  that solves the easy optimization problem

$$\lambda_t = \mathit{arg} \max_{j=1, \dots, N} |\langle r_{t-1}, \varphi_j \rangle|$$

If the maximum occurs for multiple indices, break the tie deterministically.

3- Augment the index set and matrix of chosen atom  $s$ :  $A_t = A_{t-1} \cup \{\lambda_t\}$  and  $\Phi_t = [\Phi_{t-1}, \varphi_{\lambda_t}]$  we use the convention that  $\Phi_0$  is empty matrix.

4- Solve a least squares problem to obtain a new signal estimate:

$$x_t = \mathit{arg} \min_x \|y - \Phi_t x\|_2$$

5- Calculate the new approximation of the data and the new residual.

$$a_t = \Phi_t x_t, \quad r_t = y - a_t$$

6- Increment  $t$ , and return to step 2 if  $t < k$ .

7- The estimate  $\hat{x}$  for the signal has nonzero indices at the components listed in  $A_k$ .

The value of the estimate  $\hat{x}$  in component  $\lambda_j$  equals the  $j$ th component of  $x_t$ .

Figure 3-6 shows the signal recovered by OMP using signal length 256 and 64 measurements. The recovered signal is the same as the original signal (We plot only 50 samples so as to give a clear signal).

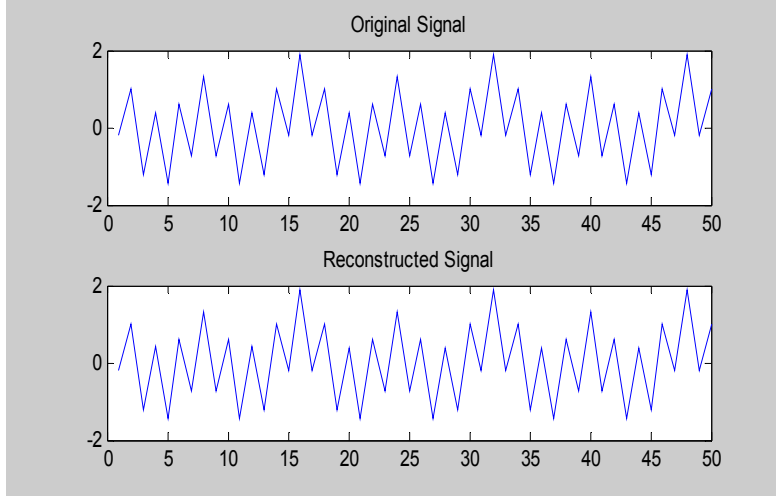


Figure 3-6. Reconstructed signals via OMP

This algorithm is quite fast. The speed of the OMP is a great advantage, but it lacks the strong guarantee that  $\ell_1$  provides [90].

### 3.3.2.3 Stagewise Orthogonal Matching Pursuit

Orthogonal matching pursuit is not effective when the signal is not very sparse as the computational cost increases quadratically with the number of nonzero  $k$ . In this setting StOMP proposed in [96] is a better choice for approximately sparse signals in a large-scale setting.

StOMP offers considerable computational advantages over  $\ell_1$  minimization and Orthogonal Matching Pursuit for large scale problems with sparse solutions. The algorithm starts with an initial residual  $r_0 = y$  and calculates the set of all projections  $\Phi^T r_{k-1}$  at the  $k^{th}$  stage (as in OMP). However, instead of picking a single dictionary element, it uses a threshold parameter  $\tau$  to determine the next best set of columns of  $\Phi$  whose correlations with the current residual exceed  $\tau$ . The new residual is calculated using a least squares estimate of the signal using this expanded set of columns, just as before.

Unlike OMP, the number of iterations in StOMP is fixed. In general, the complexity of StOMP is  $O(KN \log N)$ , a significant improvement over OMP. However, StOMP does not

bring in its work any reconstruction guarantees. StOMP also has moderate memory requirements compared to OMP.

### 3.3.2.4 Compressive Sampling Matching Pursuit

CoSaMP is an iterative recovery algorithm that provides same guarantees as even the best optimization approaches [76]. This algorithm recovers signals using measurement matrices that satisfy the RIP. Thus, the observation vector  $y = \Phi^*u$  serves as a good proxy for the signal  $x$ . With the largest coordinates, an approximation to the signal is formed at each iteration. After each new residual is formed, reflecting the missing portion of the signal, the measurements are updated. This is repeated until all the recoverable portion of the signal is found. CoSaMP algorithm is similar to the OMP, but does a limited search at each step, in the sense that it adds more than one coordinate.

CoSaMP reconstructions steps according to M. Fazel & M. Meila [101] are as:

Initialize residual  $r_0 = y$ , Support  $\Omega = \emptyset$ , Counter  $t = 1$

Repeat

1- Find the  $2s$  columns most correlated with

$$r : \lambda_t = \arg \min_{|T| \leq 2s} \sum_{j \in T} |\langle r_{t-1}, \Phi_j \rangle|$$

2- Add them to the index set  $\Omega = \Omega \cup T$

3- Re-evaluate the solution  $x_t = \arg \min_x \|\Phi_\Omega x - y\|_2$  by least square

4- Prune:  $\Omega =$  the  $k$  largest coefficient of  $x_t$ ,  $x_t \leftarrow x_\Omega$

5-  $r_t = y - \Phi_\Omega x_t$  (note  $x_t \in R^t$ )

Until stopping criterion

In the above, the  $s \leq k$  and in the standard setting  $s = k$ .

The most expensive step is, that is, finding the column (s) most aligned with the residual. The step takes  $O(nN)$  multiplication.

Under certain general assumptions, the computational cost of CoSaMP can be shown to be  $O(MN)$ , which is independent of the sparsity of the original signal. This represents an improvement over both greedy algorithms as well as convex methods. The drawback of

this algorithm is the algorithm requires prior knowledge of the sparsity  $k$  of the target signal. An incorrect choice of input sparsity may lead to a worse guarantee than the actual error incurred by a weaker algorithm such as an MP.

### 3.3.2.5 Regularized Orthogonal Matching Pursuit

Regularized orthogonal matching pursuit (ROMP) is one of the greedy algorithms with strong guarantees similar to those of convex optimization methods. The ROMP algorithm was proposed in [99] for sparse recoveries that achieved properly for all measurement matrices that satisfy the restricted isometry condition (RIC), and requires no prior knowledge about the error vector [79]. The sparsity of the signal is required for reconstruction, several ways proposed to estimate the parameters [99]. Consider the signal represented in equation 3.18.

We want to recover the signal  $x$ , which has a few non-zero coefficient from the linear measurements, using only numbers of measurements fewer than  $N$  the length of the signal [102, 103].

Considering the observation  $u = \Phi^* y$  as a local approximation of the signal  $x$ . the observation vector  $u$  encodes correlation of the measurement vector  $y$  with the columns of  $\Phi$ .  $\Phi$  is a dictionary, and so since the signal  $x$  is sparse,  $y$  has a sparse representation with respect to the dictionary. By the RIC, every  $M$  columns form approximately an orthonormal system. Thus, every  $M$  coordinates of the observation vector  $u$  look like correlations of the measurement vector  $y$  with orthogonal basis and there for being close in the Euclidean norm to the corresponding  $M$  coefficient of  $x$ .

The coordinates are selected to be more regular by selecting only coordinates with comparable size, this lead us to use only the  $M$  biggest coordinate of the observation vector  $u$  instead of using one biggest coordinate as in OMP [102]. Lastly a new regularization step needed to make sure that each of these coordinates gets constant share information. The algorithm for sparse signal recovery by using ROMP as proposed in [99] is as follows:

Input

- Sensing matrix  $\Phi$  in  $N$ -by- $M$
- Measurement vector  $y$
- The signal  $x$  and its support  $T$

Output

- Index set  $I_t$  in  $\{1, \dots, M\}$
- Residual vector  $R_t$  in  $N$ -by- $1$
- Reconstructed signal  $\hat{x}$  in  $M$ -by- $1$

Procedure

- 1- **Initialize:** let the residual vector  $R_t = y$ , the index set  $I_t = \emptyset$ , and start the iteration with counter  $t = 1$ .
- 2- **Identify:** choose a set  $J$  of a biggest absolute values of the observation vector  $u = \Phi^* R_t$ , or all of its non-zero coordinate.
- 3- **Regularize:** divide the set  $J$  into subset  $J_k$  which satisfies

$$|u(i)| \leq 2 \cdot |u(j)| \quad \text{for all } i, j \in J_k$$

And chose the subset  $J_0$  with the maximum energy  $\|u|_{J_0}\|$

- 4- **Update:** set  $I_t = I_{t-1} \cup J_0$

Calculate the new output approximation by solving the least square equation

$$x_t = \operatorname{argmin}_c \|y - \Phi I_t c\|_2$$

Update the residual:  $R_t = y - \Phi I_t x_t$

- 5- **Stopping:** Check the stopping criterion, if not, then keep increasing  $t = t + 1$

The difference between this algorithm and OMP algorithm is in the second and third steps. Instead of choosing only one biggest correlation between the residual and columns of the matrix at each iteration, we choose a set of  $|J_0|$  coefficient from  $J$  biggest absolute coefficients of  $A^* R_t$ . By this the signal can be recovered perfectly without going through all iterations.

### 3.3.3 Combinatorial Optimization Algorithm

In addition to convex optimization and greedy algorithms, there is another important class of sparse recovery algorithms that we will refer to as combinatorial algorithms. These algorithms mostly developed by the theoretical computer science community, it's highly relevant to the sparse signal recovery problem. Combinatorial algorithms were developed in the context of group testing. In the group testing problem, we suppose that there are  $N$  total items, of which an unknown subset of  $k$  elements are anomalous and need to be identified. The goal is to design a collection of tests that allows the user to identify the support of  $x$  while also minimizing the number of test performed. There were several combinatorial optimization algorithms has been developed in literature to reconstruct the sparse signal, (e.g. A non-exhaustive list includes Random Fourier Sampling, HHS Pursuit, Sparse Sequential Matching Pursuit, count-min and count-median [104, 105]).

If we consider the signal  $x$ , which is recovered by solving combinatorial optimization problem, more than  $k$  measurement must be taken to avoid ambiguity. Some authors [63, 91, 106] show that  $k + 1$  random measurement will be sufficient to recover the signal. If we know that the measurement  $x$  has very few non-zeros components (high sparse signal), then a reasonable decoding model is to look for sparsest signal among all those that produce the measurement  $x$  by using  $\ell_0$  minimization.

$$\hat{x} = \underset{x}{\operatorname{argmin}} \|x\|_0 \quad \text{subject to } y = \Phi\psi x \quad (3.19)$$

Where  $\psi \in \mathbb{R}^N$  is an orthogonal basis,  $\Phi$  is  $M \times N$  measurement matrix.

The signal with the length of 700, the numbers of spikes is 70 and using numbers of measurements equal to 210, is shown in figure 3-7. The signal was reconstructed by using a combinatorial algorithm ( $\ell_0$  minimization). According to the theory we have to used number of measurement  $M \geq k + 1$  to recover the sparse signal.

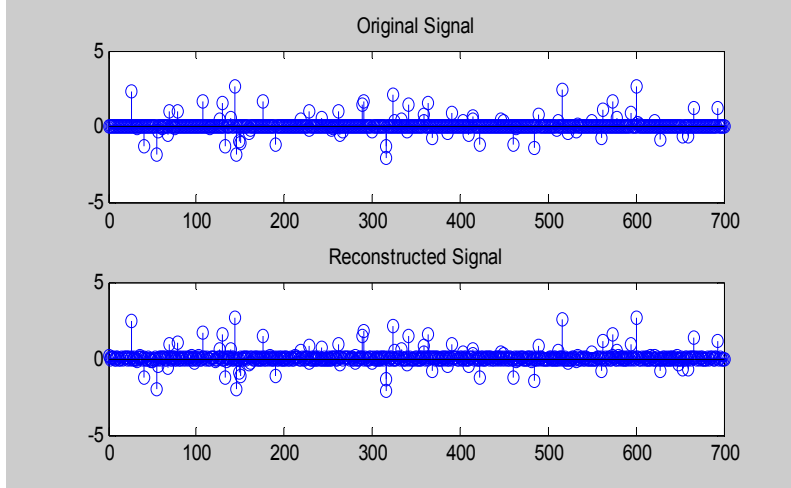


Figure 3-7. Reconstructed signals via combinatorial algorithm

The algorithm based on  $\ell_0$  optimization, which is both numerically unstable and NP-hard, requiring an exhaustive enumeration of all possible locations of the non-zero entries in  $x$ .

### 3.3.4 Total variation minimization

The total variation (TV) based on filtering was introduced by Rudin, Osher, and Fatemi [107], TV have been used in many applications in image processing, ever since, in particular for image reconstruction, blind deconvolution, resolution enhancement and decompression. In all the application mentioned above, TV is used as a regularization term that permits to select, among several competing solutions. TV of an image is the total length of its level sets. It is computed as the  $\ell_1$  norm of the gradient, viewed as a complex operator, which is the sum of the length of the all gradient vectors. The main idea of the algorithm is to minimize numerically  $TV + L^2$  norm via dual problem.

TV minimization is closely related to  $\ell_1$  minimization; it considers as a recovery method. If we minimize the total variation and take the total variation minimizer, we choose the one possibility with the least amount of oscillation to reconstruct the original image. Thus, the image, which is reconstructed with total variation minimizer will be less noisy and it is smooth. This result is exactly what is expected.

We can recover an approximate image  $\hat{x}$  from measurements  $y = \Phi \Psi \hat{x}$  by solving:

$$f^* = \operatorname{argmin} \|\Psi \hat{x}\|_{TV} \text{ s. t. } y = \Phi \Psi \hat{x} \quad (3.20)$$

Where  $\|f\|_{TV} = \sum_{s,t} \sqrt{(f(s+1, t) - f(s, t))^2 + (f(s, t+1) - f(s, t))^2}$ ,  $y$  is  $m \times l$  vector of sub-sampled measurements,  $\Phi$  in form of  $m \times n$  sensing matrix,  $\Psi$  is  $n \times n$  orthogonal basis,  $\hat{x}$  is  $n \times l$  coefficient vector and  $\|f\|$  is the sum of the magnitudes of the gradient of  $f(s, t)$ . From the mathematical expression of total variation, we see that there will be several signals that fulfill the equality constraints.

### 3.4 Robust Compressive Sensing

In reality, signals do not have an exact sparse representation. Such signals are modeled as compressive signals; with a threshold such that any values above the threshold are considered non-zeros and values below are treated as zeros. This approximates the sparsity model. Signals also have inherent noise, in the form of measurement noise or instrument noise.

In all sensor applications, one should not expect to measure signal without any error. As we know one can recover sparse signals from just a few measurements, but in order to be really powerful, CS needs to be able to deal with both sparse signals and noise. The issue here is whether or not it's possible to obtain accurate reconstructions of such objects from highly under-sampled measurements. In a real application measured data will invariably be corrupted by small amount of noise as sensing devices do not have infinite precision. It is, therefore, imperative that CS be robust in relation to such nonidealities.

Suppose the observations are not inaccurate and consider the model

$$y = \Phi x + e \quad (3.21)$$

Where  $\Phi$  is an  $M \times N$  sensing matrix giving us information about  $x$  and  $e$  is a stochastic or deterministic unknown error with bounded energy  $\|e\|_2 \leq \varepsilon$ . The (3.21) reconstructed program given as

$$\min \|\hat{x}\|_{\ell_1} \quad \text{subject to} \quad \|\Phi\hat{x} - y\|_{\ell_2} \leq \varepsilon \quad (3.22)$$

The reconstruction is within the noise level.

### 3.5 Application of Compressed Sensing

Compressive sensing can be potentially used in all applications where the task is the reconstruction of a signal or an image from linear measurements, while taking many of those measurements in particular, a complete set of measurements is costly, lengthy, difficult, dangerous, impossible or otherwise undesired procedure. Compressed sensing appears to be promising for a number of applications in signal acquisition and compression. CS has been applied in various areas [108, 109], which is categorized as the following:

- ❖ Compressive medical imaging.
- ❖ Group testing and data stream algorithm.
- ❖ Analog-to-information conversion.
- ❖ Single pixel camera.
- ❖ Hyperspectral imaging.
- ❖ Compressive processing of manifold-modeled data
- ❖ Compressive sensing network.
- ❖ Genomic sensing.
- ❖ Inference using compressive measurements.

There is a widespread body of literature on image compression, but the essential concept is straightforward; we transform images into a suitable basis and then code only

the important expansion coefficients. A problem of finding a good transform has been studied extensively from both theoretical and practical standpoint.

Image compression algorithms convert high-resolution image into relatively small bit streams, in effect turning a large digital data set into a substantially smaller one. But is there a way to avoid the large digital data set to begin with? Is there a way we can build the data compression directly into the acquisition? The answer is yes; by using CS it is possible to reduce the number of data used to reconstruct the image. In this part we want to concentrate on the application of CS in imaging, particularly medical imaging.

In our research we applied CS theory into Doppler ultrasound imaging system data, which is used to measure and imaging the blood flow within the body so as to overcome the current data acquisition limitation, such as processing time reduction, reduction of the data used for the reconstruction and increasing the patient safety level.

### **3.5.1 Application of CS in Medical Imaging**

Compressed sensing becomes popular and increasing rapidly in various fields of biomedical signal and image processing. CS has been applied to different medical imaging systems such as Magnetic resonance imaging (MRI), computed tomography (CT), electroencephalogram (EEG), Ultrasound RF echoes, Doppler ultrasound signal and ... ect. More information regarding application of CS in medical imaging can be viewed at [56, 110 - 117].

Increasing in biomedical measurement's techniques for diagnosis and follow-up of human disease strongly requires compression in order to keep the data-flow tractable.

#### **3.5.1.1 Application of CS in computerized tomography**

For example, in computerized tomography, for instance, one would like to obtain an image of inside a human body by taking X-ray images from different angles. Taking an almost complete set of images would expose the patient to a large and dangerous dose of radiation, so the amount of measurements should be as small as possible, and

nevertheless guarantee a good enough image quality. Such images are usually nearly piecewise constant and therefore nearly sparse in the gradient, so there is a good reason to believe that compressive sensing is well applicable.

### **3.5.1.2 Application of CS in Magnetic Resonance Imaging**

Also, Compressed Sensing applied to magnetic resonance imaging (MRI). MRI is an essential medical imaging tool with an inherently slow data acquisition process. Applying CS to MR offers potentially significant scan time reductions, with benefits for patients and health care economics. MRI scanners have traditionally been limited to imaging static structures over a short period of time, and the patient has been instructed to hold his or her breath. But now, by treating the image as a sparse signal in space and time, MRI scanners have begun to overcome these limitations, for example, produce images of a beating heart. Example of MR reconstruction was shown in figure 3-8; 2-D frequency measurements were used. Figure 3-8 (a) describes such a sampling set of a 2-D Fourier transform. Since a length scanning procedure is very uncomfortable for the patient it is desired to take only minimal amount of measurements. A total variation, considered as the recovery algorithm. Figure 3-8 (b) shows the recovered image by a traditional backprojection algorithm. Figure 3-8 (c, d) shows the recovered image by using TV algorithm, (c) represents the image after 26 iterations and (d) after 126 iterations, it's exact.

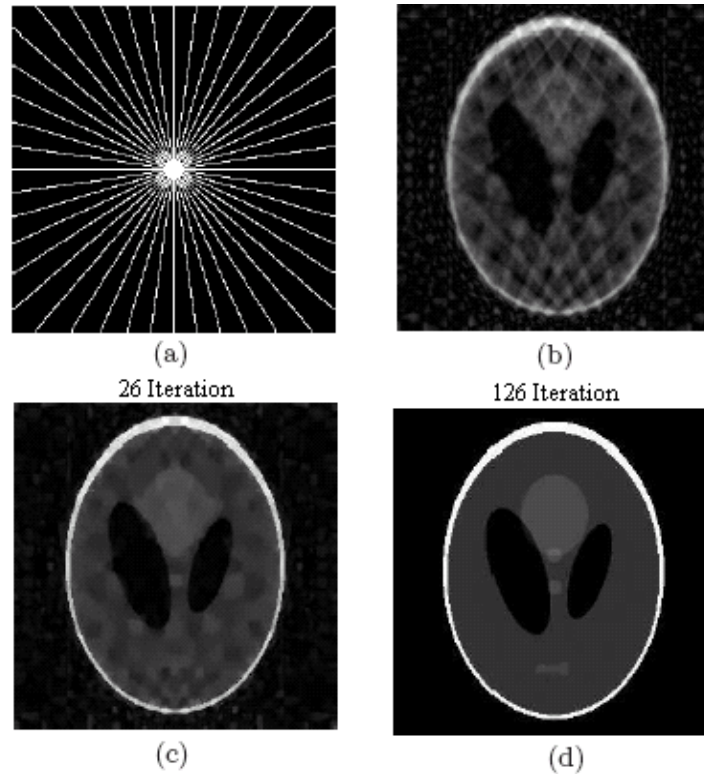


Figure 3-8. (a) Sampling data of MR image in the Fourier domain which correspond to only 0.11% of all samples. (b) Reconstructed by back-projection. (c) Intermediate iteration of an efficient algorithm for large scale TV minimization. (d) The exact reconstruction [56].

### 3.5.1.3 Application of CS in Doppler Ultrasound Signals

Finally we will give a brief introduction about our work on the application of compressed sensing on Medical Doppler Ultrasound Signal which is demonstrated in [117, 118]. Ultrasound imaging is arguably the most widely used cross-sectional medical imaging modality worldwide. Indeed, ultrasound has a number of potential advantages over other medical imaging modalities because it is non-invasive, portable and versatile, it does not use ionizing radiation and it is relatively low-cost [1].

The acquisition of Doppler ultrasound data relies on repeatedly transmitting ultrasound pulses to acquire data from a particular region of interest selected by the sonographer. Such acquisition must be extremely precise in its periodicity to ensure that the Doppler signal is uniformly sampled for further spectrogram processing. This can be a major constraint to ultrasound imaging systems when this Doppler signal acquisition is done in

such modes as Duplex or Triplex imaging where B-mode or color flow signals are acquired concurrently.

Doppler ultrasound signal was nonuniformly sampled in a random fashion and then reconstructed using CS via  $\ell_1$  minimization to regenerate the Doppler ultrasound spectrogram from much fewer samples. The measurement model is

$$f = A x \quad (3.23)$$

Where  $f$  is the  $M \times 1$  vector containing the compressive measurements, and  $A$  is the  $M \times N$  measurement matrix. Using the  $M$  measurement in the first basis given the sparsity property on the other basis, the original signal was recovered by using convex optimization recovery algorithm ( $\ell_1$  minimization) expressed as

$$\min \|x\|_{\ell_1} \text{ s. t. } \|Ax - f\|_{\ell_1} \leq \varepsilon \quad (3.24)$$

Software programs written in Matlab (Mathworks, MA) were developed and used to generate an original Doppler spectrogram. Then, the same signal was undersampled in a random manner to reduce the length of the signal to either different lengths (here, we show lengths of 128 or 256 points). The Optimization based on  $\ell_1$ -norm was used to recover exactly the Doppler signal.

The recovered signals were used to regenerate the Doppler ultrasound spectrograms as shown in figure 3-9. The sonogram was recovered exactly. Different reconstruction algorithms applied to Doppler ultrasound signal will be discussed in more details in the next chapter

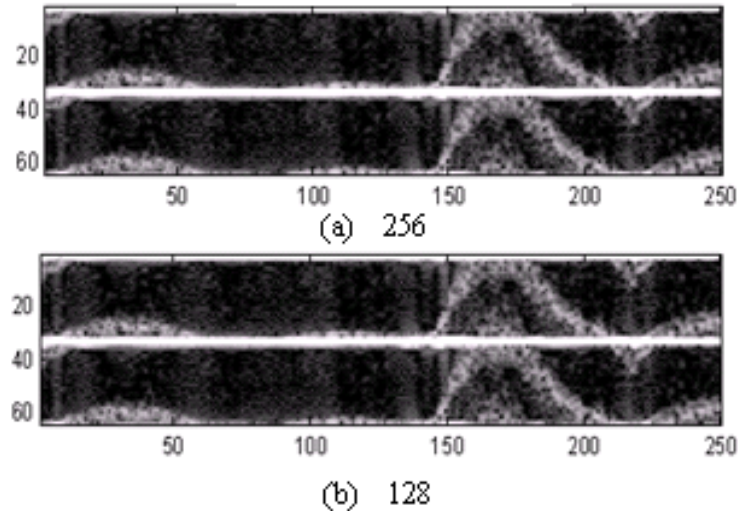


Figure 3-9. Reconstructed Doppler sonograms using two different numbers of measurements

### 3.6 Parallel Computing

The goal of parallel computing is speed up computation by using multiprocessor and utilize more memory than available on a single machine, using one of the parallel programs such as message passing interface (MPI), which is used to exchange the data and control information between the processors.

Several authors show that the parallel computational algorithms can be used for reconstruction time reduction [42, 119]. In this part of our work we want to make use of CS and parallel algorithms, by integrating the CS reconstruction algorithms used for Doppler ultrasound spectrogram reconstruction spatially convex optimization ( $\ell_1$ -norm) algorithm and parallel algorithms so as to reduce the relative recovery time. The combination has done using systems widely available, multicore CPUs.

The reconstruction time depends on the number of measurements used for reconstruction and the reconstruction algorithm. CS reconstructions involve nonlinear optimization, which can be time consuming even for a few numbers of measurements. This problem can be overcome by using the novel performance of the central processing unit (CPU). Unfortunately, the power consumption and physical layer size were limiting the computation power growth using higher CPU clock frequency. Modern process

design is moving toward multicore architecture. The availability of duo-core, quad-core central processing unit and graphical processing unit (GPU) offer new platforms for implementing parallel computation algorithms to speed up the reconstruction of the Doppler ultrasound spectrogram. Matlab and Parallel computing toolbox provides a useful code that can work well in a multicore system enabling the user to select the most appropriate program to the application. In this work we will use MPI to achieve the reduction.

The parallel computing toolbox (PCT) and long with Matlab distributed computing server (MDCS) are commercial products offered by MathWorks Inc. The PCT provides functionality to run Matlab code on multicore system and cluster, besides providing functions in parallel for-loop execution, creation/manipulation of distributed array as well as message passing functions for implementing fine gained parallel algorithms.

The MDCS gives the capability to scale parallel algorithms to larger cluster sizes. The MDCS consist of Matlab worker processes that run on a cluster and is responsible for parallel code execution and process control [119]. Figure 3-10 illustrates the architecture of PCT and MDCS.

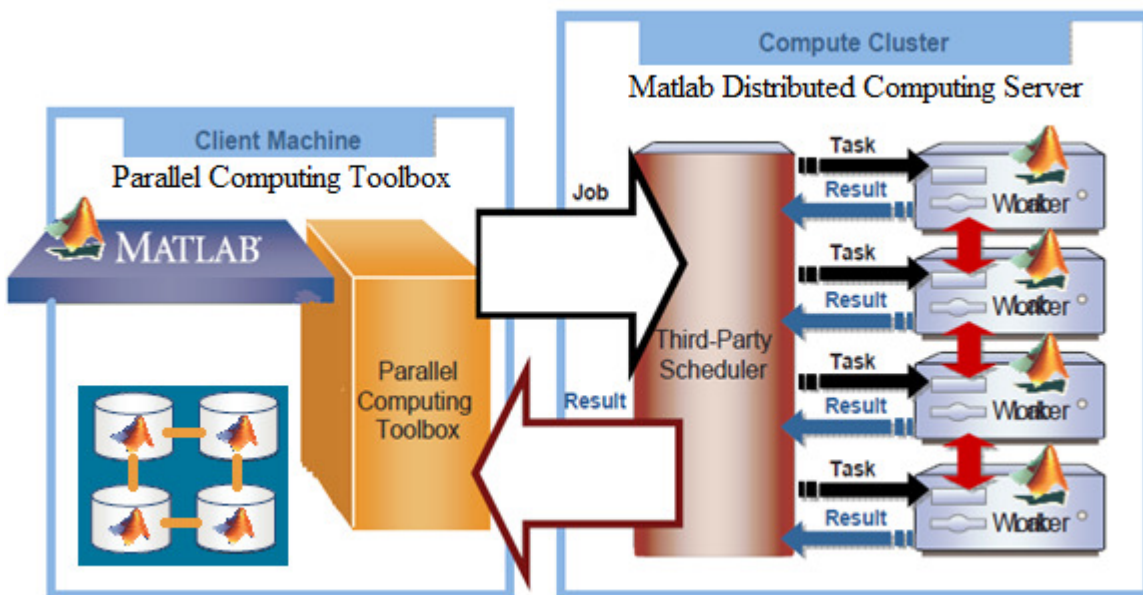


Figure 3-10. The PCT and MDCS [119]

In this work we will consider only PCT because its easily experiment with explicit parallelism in multicore machines, rapidly develop parallel applications on local computer, take full advantage of desktop power and separate computer cluster not required. Figure 3-11 illustrates the multicore system with parallel computing toolbox.

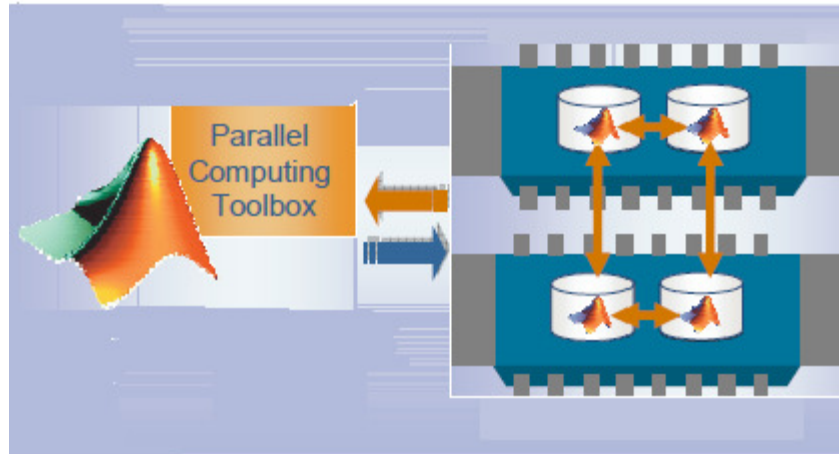


Figure 3-11. Multicore system and PCT

The combination of CS and parallel computing to reduce the reconstruction time has been applied in different areas such as real-time MRI reconstruction [120]. We want to make use of this combination to reduce the recovery time in the Doppler ultrasound spectrogram, using duo-core systems and Matlab PCT.

# Chapter 4

## Application of CS & Parallel Algorithm in Doppler Signal

In this chapter we want to discuss the proposed data acquisition by showing how different CS algorithms from sparse approximation applied to the Doppler ultrasound data so as to reconstruct the Doppler ultrasound sonogram using a few numbers of measurements. Doppler ultrasound signal was sampled randomly and constructed by using CS via one the reconstruction algorithms to regenerate a reconstructed Doppler signal, which is used to generate a Doppler ultrasound spectrogram using a much fewer number of measurements  $M$ . Figure 4-1 illustrated the block diagram of present methods and the new methods. Also we will discuss application of parallel methods for reconstruction time reduction.

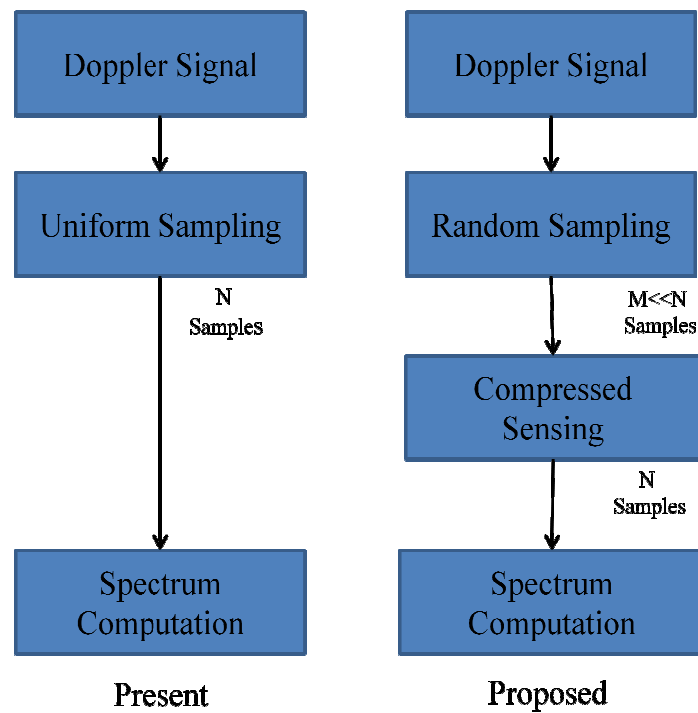


Figure 4-1. Comparison of present method vs new methods

## 4.1 The Doppler Data

The proposed Doppler data acquisition performed by using a real Doppler ultrasound data (heart data). The data downloaded from the H. Torp group website. The length of the Doppler data was 2032 point and the numbers of measurement used for reconstruction are, 5%, 20%, 40%, 60% and 80%. Software programs written in MATLAB (MathWorks, Inc., Natick, MA) were developed and used to generate the Doppler ultrasound spectrogram, before and after applying the CS theory. Also all the reconstruction algorithm developed in MATLAB program.

## 4.2 Doppler Signal Reconstruction

Different reconstruction algorithms proposed for signal and image reconstruction via CS theory. In the work four different algorithms were used to reconstruct the Doppler ultrasound signal, the algorithms are

- 1- Reconstruction via  $\ell_1$  Minimization ( $\ell_1$ -norm)
- 2- Reconstruction via Orthogonal Matching Pursuit (OMP)
- 3- Reconstruction via Compressive sampling Matching Pursuit (CoSaMP)
- 4- Reconstruction via Regularized Orthogonal Matching Pursuit (ROMP)

### 4.2.1 Reconstruction via $\ell_1$ Minimization

The Doppler ultrasound data were loaded into Matlab, The coefficient matrix  $A$  in term of  $M \times N$  have been selected non uniformly at random, which is done with normalized vectors sampled independently and uniformly using the sparse model, the Doppler signal represented linearly as follows:

$$f = Ax \tag{4.1}$$

The basis  $A$  selected to suit the discrete cosine transform and assume that most of the coefficients  $x$  are zero, so  $x$  is sparse. In real signal it's not possible to collect signal without noise, thus the noise  $z$  added to the signal, the linear signal described as:

$$f = Ax + z \quad (4.2)$$

Where the vector  $f$  is  $M \times 1$ ,  $z$  in an  $M$ -dimensional measurement noise vector and  $M \ll N$

For solving the Doppler signal (4.2), another linear operator is needed. The linear operator chosen to be as follows:

$$S = g f \quad (4.3)$$

Where,  $S$  is a random sample from  $f$  and  $g$  is the subset of the rows of the identity operator.

To recover the signal we need to recover the coefficient by solving  $Z \hat{x} = S$  where  $Z = g A$ .

Then solving

$$f = A \hat{x} \quad (4.4)$$

By using  $\ell_1$ -norm

$$\min \|x\|_1 \quad \text{subject to } \|\Psi x - y\|_1 < \delta$$

Recover the sparse signal. The recovered signal  $\bar{x}$  applied into the Matlab code to generate the recovered Doppler spectrum.

## 4.2.2 Orthogonal Matching Pursuit

Orthogonal matching pursuit algorithm from sparse approximation used to reconstruct the Doppler ultrasound signal. Doppler ultrasound signal was sampled randomly and constructed by using CS via OMP algorithm to create a reconstructed Doppler signal, which is used to generate a Doppler ultrasound spectrogram using a much fewer number of measurements  $M$ . The data constructed by using OMP begins by finding the column of  $A$  most related to the measurements. The algorithm then repeats this step by correlating the columns with the signal residual, which is obtained by subtracting the contribution of a partial estimate of the signal from the original measurement vector. The measurement model is:

$$y = A x \quad (4.5)$$

Where  $A$  is a measurement matrix in  $N \times M$ ,  $y$  is an  $M$ -dimensional and  $x$  is a sparse signal with  $k$  nonzero.

The signal  $x$  reconstructs by solving the relation (4.5) with the OMP algorithm as follows:

Input: Loaded Doppler signal vector  $A$

Output: sparse signal vector  $x$

Initialize the residual  $r_0 = y$ . At each iteration, the observation vector is set,  $y = A^* r$ , and add the index to the coordinate of its the largest coefficient in the magnitude. By solving the least square problem, the residual is updated  $r = u - Ay$ . Repeating this  $m = 2*k$  times give the recovered Doppler signal  $x$ . The recovered signal used to generate Doppler spectrogram by using MATLAB.

## 4.2.3 Compressive Sampling Matching Pursuit

To reconstruct the Doppler signal using CoSaMP algorithms we first need to generate the measurement matrix  $A$ , later we generate the sparse coefficient, which have a problem

specific structure. We intend to reconstruct a vector  $x$ , the Doppler ultrasound signal in our case, with a few numbers of non-zero components, that is, with a CoSaMP recovery algorithm. Many others algorithms exist for signal recovery proposed in [76].

The Doppler signal with a length of 2032 was sampled randomly and constructed by CoSaMP using a few numbers of measurements  $M$ . To reconstruct the signal as mentioned before the measurement matrix  $A$  was selected randomly and then reconstruct the signal by solving the measurement vector  $y$ . The measurement vector is given in equation (4.5).

Applying CoSaMP to reconstruct the Doppler data by solving the measurement vector (4.5), lead to a good approximation of Doppler signal  $x$ . By using the largest coordinates, an approximation of the signal is found at each iteration. After each new residual is formed, reflecting the missing part of the signal, the measurements are updated. This is repeated until all the recoverable portion of the signal is found. The whole CoSaMP algorithm for reconstructing the signal described below:

**Initialize**

Residual  $r_0 = y$   
 Support  $\Omega = \emptyset$   
 Counter  $t = 1$

**Repeat**

- 1- Find the  $2s$  column most correlated with  $r$  :  $\lambda_t = \underset{|T| \leq 2s}{\operatorname{argmin}} \sum_{j \in T} |\langle r_{t-1}, \theta_j \rangle|$
- 2- Add them to the index set  $\Omega = \Omega \cup T$
- 3- Re-evaluate the solution  $x_t = \underset{x}{\operatorname{argmin}} \|A\Omega x - y\|_2$  by least square
- 4- Prune:  $\Omega =$  the  $k$  largest coefficients of  $x_t$   $x_t \leftarrow x_\Omega$
- 5-  $r_t = y - A\Omega x_t$  (note  $x_t \in \mathbb{R}^t$ )

Until stopping criterion

#### 4.2.4 Regularized Orthogonal Matching Pursuit

ROMP algorithm used to reconstruct Doppler ultrasound signal using a few numbers of points. The reconstruction performed using the Doppler signal of length 2032 and five different numbers of measurements.

Doppler ultrasound signal with a length of 2032 was sampled randomly and constructed by ROMP using a few numbers of measurements  $M$  and sparsity level  $n$ . To reconstruct the signal, an  $N \times M$  Gaussian measurement matrix  $A$  was selected randomly and then reconstructs the signal with ROMP by solving the measurement vector  $y$ . The measurement model was given in relation (4.5).

The reconstructed signal used later to generate the reconstructed Doppler spectrogram.

### 4.3 Reconstruction Time

The reconstruction time was calculated for each number of measurements in all the recovery algorithms used to reconstruct the Doppler signal. We have computed the process time by using Matlab program v. 7.0.1, which allow us to run the CS recovery algorithms. The recovery algorithms run on a TOSHIBA laptop model 2008 with Intel® Celeron @ 2.6 GHz, 3.0 GB of main memory and 512 MB RAM. The operating system of the laptop was Windows XP Home Edition Service Pack 2.

Each algorithm with specific numbers of measurements runs several times, the average relative time was calculated and compared for each.

The number of iterations for  $\ell_1$ -norm algorithm only was evaluated at each numbers of measurements used. The process was repeated several times and the average was calculated at each measurements. The result shows that there is no significant difference in the number of iterations by using different numbers of measurements.

### 4.4 Reconstructed Image Evaluation

Root mean Square Error (RMSE) and Peak Signal-to-Noise Ratio (PSNR) expressed in dB were used to evaluate the quality, accuracy of the reconstructed images and compared

between the resulting images. Those methods are widely used for evaluating the recovered images using random sampling.

#### 4.4.1 Root Mean Square Error (RMSE)

The efficient of reconstructed images evaluated by using the root mean square error (RMSE) which is widely-used quantitative measurement. The RMSE calculated for two images  $I$  and  $II$  with dimension of  $(m-by-n)$ , where  $I$  is the original image and  $II$  is the reconstructed image. The RMSE measurement is easily computed by the square root of (mean square error MSE) the average squared difference between every pixel in recovering image and the original image. The RMSE calculated as follows:

$$MSE = \frac{1}{nm} \sum_{i=0}^{m-1} \sum_{j=0}^{n-1} [I(i, j) - II(i, j)]^2 \quad (4.6)$$

$$RMSE = \sqrt{MSE} \quad (4.7)$$

Where,  $I(i, j)$  and  $II(i, j)$  are the pixel values of the original and recovered image respectively and  $m, n$  are the size of an image.

#### 4.4.2 Peak Signal-to-Noise Ratio (PSNR)

PSNR reflects the differences of the information contained between an original and recovered image. The PSNR numbers are reported in Decibels (dB) as a measure of the relative weight between two images. A higher number in dB indicates a higher correlation. The PSNR is directly proportional to the image quality. When PSNR is higher this indicates that the reconstruction is of higher quality. PSNR calculated as follows:

$$PSNR = 20 \log_{10} (255/RMES) \text{ dB} \quad (4.8)$$

## 4.5 Applying Parallel Computing to the Doppler Signal

Parallel computing is an effective method proposed for process time reduction or analysis large set of data. During reconstruction the Doppler spectrogram it's very important to keep the time of reconstruction very low so as to display the image in real-time. The use of parallel computing techniques can enable us to utilize the number of processors to run comprehensive analysis in a reasonable amount of time.

The Matlab program for the reconstruction was run on serial implantation first, and then we run the same file in parallel implementation using Matlab parallel computing toolbox package in duo-core CPU. Parallelization techniques applied to the Doppler data after prepare the data for compressed sensing, before solving the CS algorithm the parallel algorithm was started as shown in figure 4-2.

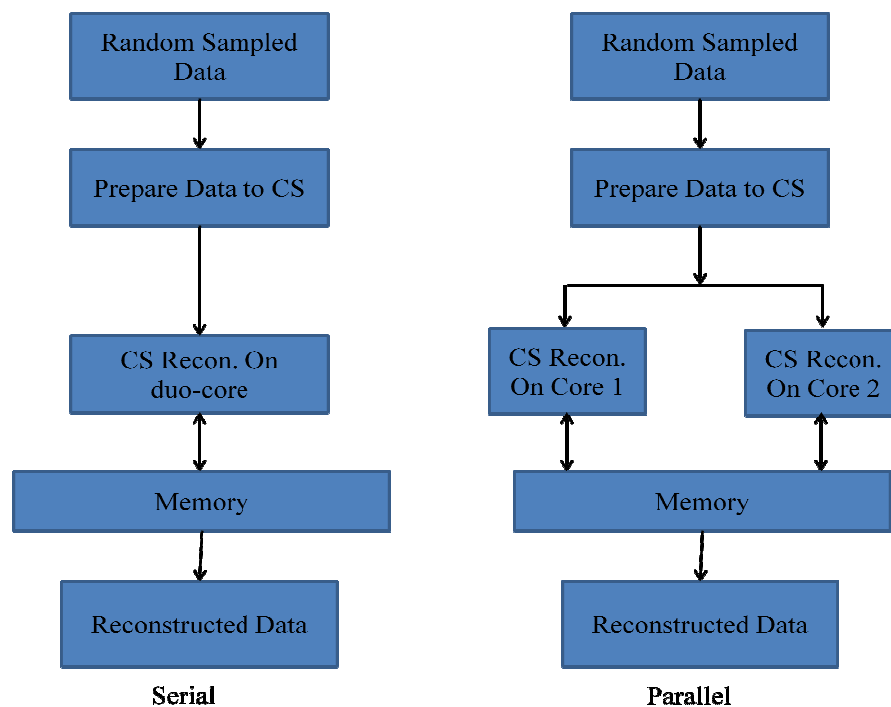


Figure 4-2 Serial and parallel methods for CS reconstruction

The parallel initialized using the Matlab command as stated in [121], which allows multiple Matlab processes run on parallel computer clusters or multicores. In our case

duo-core CPU, two Matlab started at the beginning of the initialization. The data separated between the channels, then the data on each channel reconstructed and then sum up to get the final recovered Doppler signal.

# Chapter 5

## Clutter Rejection Filters (Wall Filters)

In this chapter filters applied to Doppler signals to separate the blood flow from stationary or slow moving tissue will be discussed. Two types of filters will be considered, Non adaptive filters and adaptive filters. In Non adaptive filters we will discuss in details the three types of filters, finite impulse response, infinite impulse response and polynomial regression filters. The frequency response of the filters will be compared. In adaptive filters the proposed filters for cluttering will be considered and discussed in details. All the clutter rejection filters discussed in this chapter were implemented in software, using MATLAB (MathWorks, Inc., Natick, MA) as a part of this thesis.

### 5.1 Motivation

Doppler ultrasound is widely used diagnostic tool for measuring and detecting blood flow. To get a Doppler ultrasound spectrum image with a good quality, the clutter signals generated from stationary and slowly moving tissue must be removed completely. The clutter signals originated from moving tissue and vessel walls are much stronger than the signal originated from blood cell; the clutter-to-signal ratio may in some case exceed 100 dB [122]. The signal scattered from the moving blood cells has stronger Doppler frequency shift than that reflected from slowly moving tissue and surrounding walls. Thus, a high pass filter is needed to separate the blood flow signal from the clutter signal. Figure 5-1 shows clutter filter, and power spectrum for clutter and blood cell signals. To achieve accurate cluttering or Doppler spectrum image with high quality, a clutter filter with high quality has to be developed. Thus, selection of a good clutter rejection filter method based on clutter characteristics is a challenging problem.

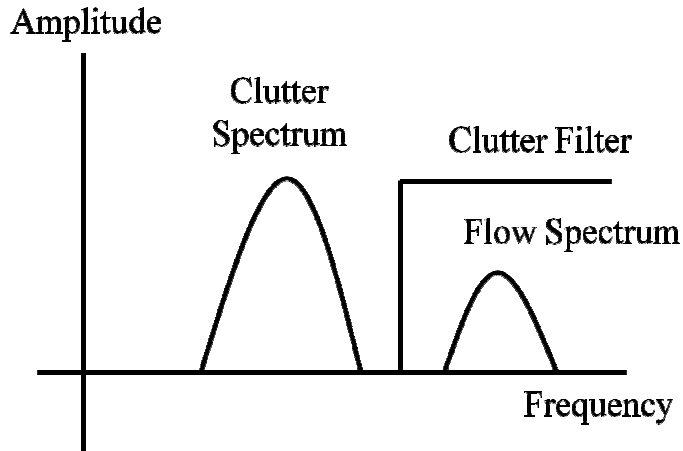


Figure 5-1. The clutter filter and spectrum of clutter and flow signals

## 5.2 Clutter Rejection Filters

Clutter rejection in Doppler ultrasound signals is a challenging signal processing problem. The objective is to suppress the signal from blood flow that summed with clutter signals (echoes from stationary slowly moving tissue). The clutter strength is typically 40 – 60 dB larger than the desired flow signal [123]. The velocities (clutter signal) from surrounding tissues and vessels are lower than that from blood flow, but a wide range of both velocities exists in the body. To acquire data with an ultrasound radio frequency lower than 20 MHz a clutter rejection filter must be applied to remove high amplitude, low frequency echoes from the Doppler signal, in order to estimate the blood flow velocity. The clutter rejection filter is known as stationary echo cancelling in literature [1, 2], also known as wall filter in some cases. Several approaches have been developed for separating the blood flow signal from the clutter signals [7, 11, 14, 15, 49, 124, 125]. To select a better clutter rejection filter among different approaches, a list of important attribute for a good clutter rejection must be considered.

- *Selectable cutoff frequency*: The Doppler frequency cutoff for clutter rejection filters selected either by user or adapted to the clutter or automatically. Body propagates various flow and tissue velocities yielding various Doppler flow and

clutter frequency spectra. Therefore, it's necessary to provide user interaction in designing systems.

- *High pass-band to stop-band attenuation ratio*: The clutter signals need to be removed down the noise level, to ensure accurate blood flow estimation.
- *Narrow transition band*: To suppress the clutter signal to the noise level, the low flow weakness should be maximized, thus narrow transition band is essential.

Various types of clutter filters have been proposed to suppress the clutter from the backscattered signals, each with unique advantages and disadvantages. General clutter rejection filter design illustrated in figure 5-2. In this work we proposed new clutter rejection filter for Doppler ultrasound signals and compared the performance of the present clutter rejection filters with the proposed methods. The present (non adaptive) clutter rejection filters are:

- Finite Impulse Response (FIR)
- Infinite Impulse Response (IIR)
- Polynomial Regression (PR)

The proposed (adaptive) clutter rejection filters are:

- Principal Component Analysis (PCA)
- Independent Component Analysis (ICA)

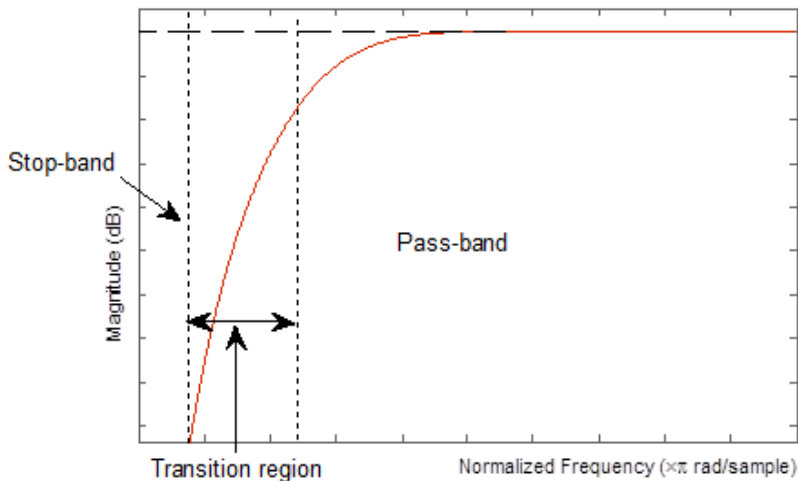


Figure 5-2. General clutter rejection filter

### 5.2.1 Finite Impulse Response (FIR) Filter

One of the challenges in filter design problem is to find a filter meet the design specification. Finite impulse response (FIR) filters are usually implemented in a non-recursive way which guarantees a stable filter, and are mainly useful for applications where exact linear phase response is required [126]. The designed filters should have minimum stop band attenuation or a maximum pass band ripple. One of the challenges in an FIR filters design, it is necessary to use a large order to meet the design specifications. The FIR has a difference equation of

$$y(n) = \sum_{k=0}^{M-1} b_k x(n - k) \quad (5.1)$$

If the package size is  $N$ , and filter order of  $k$ , the number of valid output is  $N - k$ . The  $z$ -transform of an  $M$ -point FIR filter (the frequency response of the system) is given by

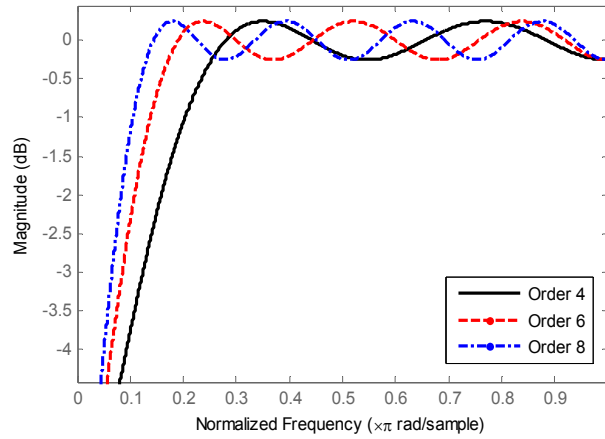
$$H(z) = b_0 + b_1 z^{-1} + \dots + b_{M-1} z^{1-M} = \sum_{k=0}^{M-1} b_k z^{-k} \quad (5.2)$$

The parameters used for designing different types of filters are shown in table 5.1.

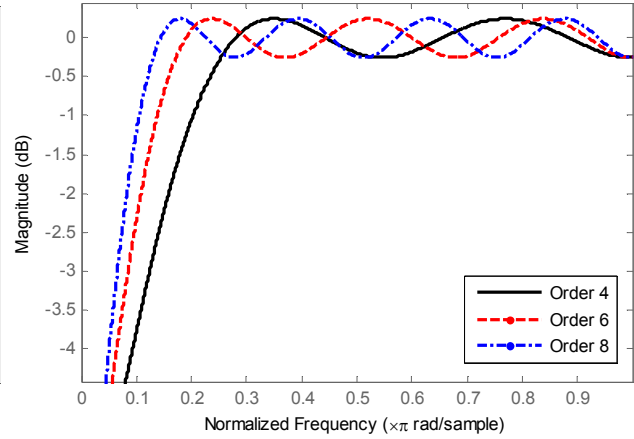
Table 5.1. FIR and IIR Filters design parameters

Filters Parameters	Values
Finite Impulse Response Filter	
Stop-band frequency ( $F_{\text{stop}}$ , $w_{\text{stop}}$ )	0.02 Hz
Pass-band frequency ( $F_{\text{pass}}$ , $w_{\text{pass}}$ )	0.5 Hz
Stop-band weight ( $W_{\text{stop}}$ )	-80dB
Pass-band weight ( $W_{\text{pass}}$ )	-0.5 dB
Infinite Impulse Response Filter	
Pass-band frequency ( $F_{\text{pass}}$ )	0.2 Hz
Transition width ( $F_{\text{stop}}$ )	0.02 Hz
Pass-band ripple ( $A_{\text{pass}}$ )	-3 dB
Stop-band attenuation ( $A_{\text{stop}}$ )	-80 dB

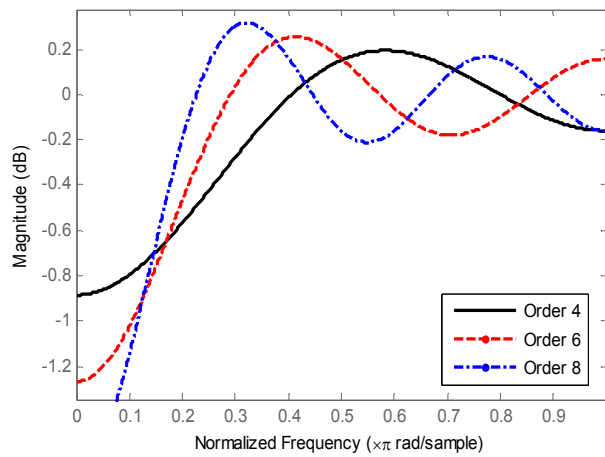
All types of FIR filters were tested and compared between them using the parameters in table 5.1 and different orders. The FIR filters with a transition width and maximum pass-band / stop-band ripple that do not exceed the allowable value will compare with other types of filters. The results illustrated in figure 5-3, we show in the figure only six types of filters for simplicity.



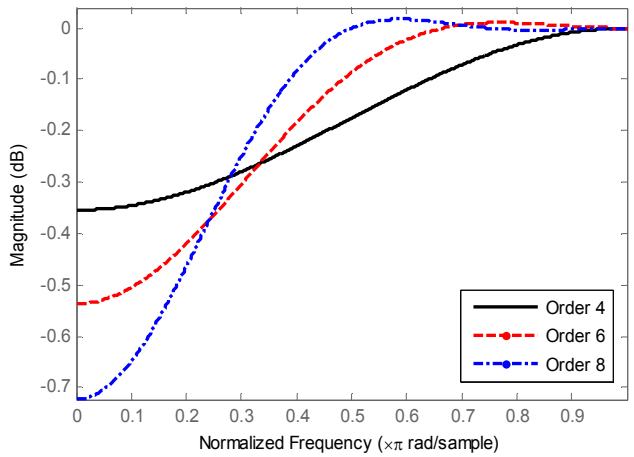
(a) Constrained Equiripple



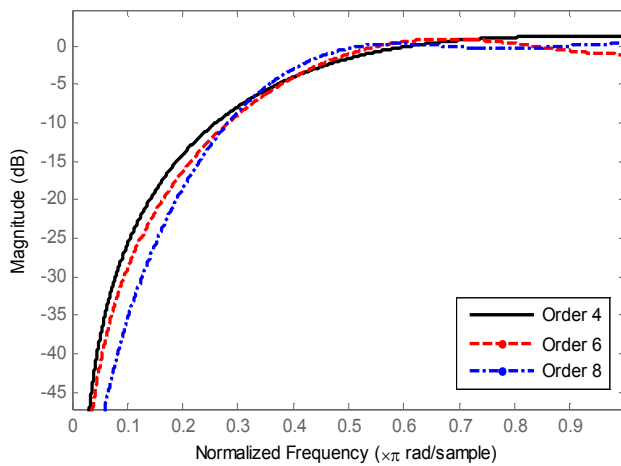
(b) Least-Square FIR



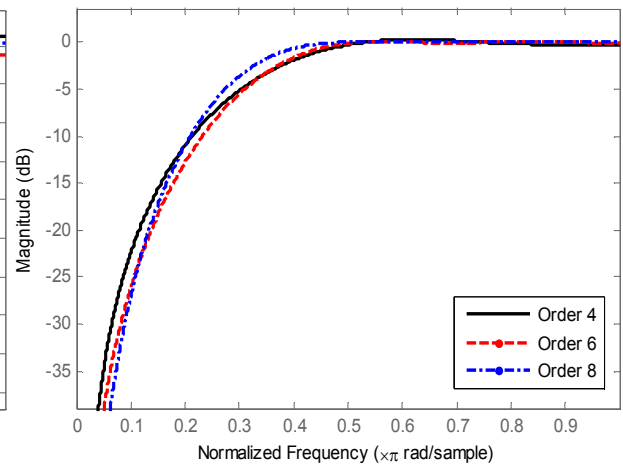
(c) Window (Kaiser)



(d) Window (hanning)



(e) Linear-phase



(f) Minimum-phase

Figure 5-3. The frequency response of FIR filters designed with using same parameters and three different orders (a) Constrained Equiripple (b) Least-Square FIR (c) Window (Kaiser) (d) Window (Hanning) (e) Linear-phase (f) Minimum-phase

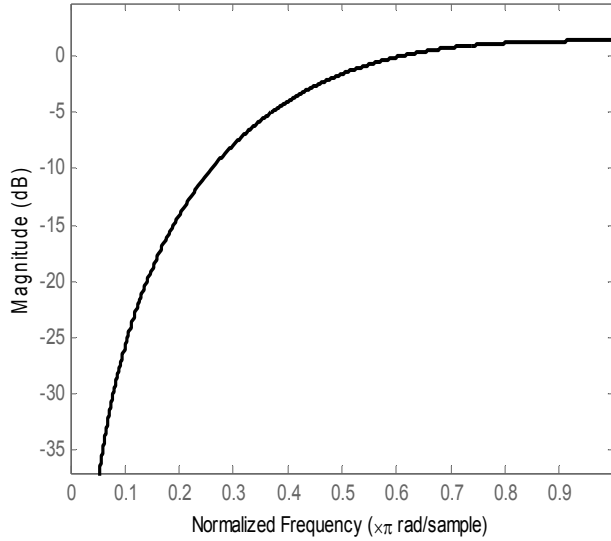
The result shows that most FIR filters types designed using the same parameters gives very low minimum stop band (higher than  $-30$  dB), only three types give lower minimum stop band reach up to  $-60$  dB. Those are linear phase FIR, minimum phase FIR and equiripple FIR filters.

### **5.2.1.1 Linear Phase FIR Filter**

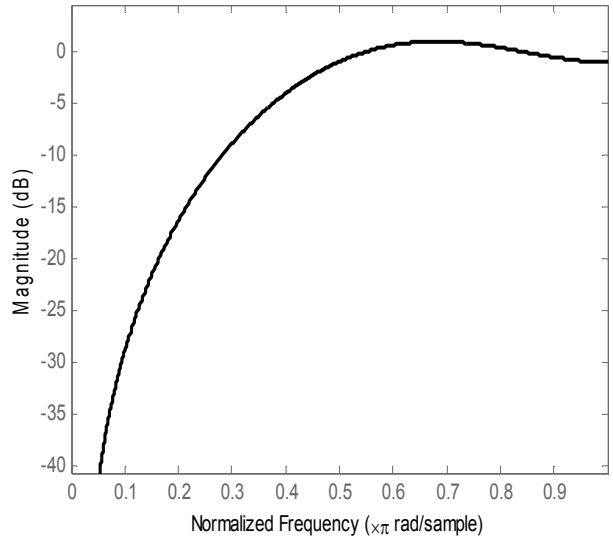
The most suitable FIR filters to be compared with each others are linear phase, minimum phase and equiripple filters. The filter with narrower bandwidth, narrower stop-band and narrower transition band [7, 9, 126], will be used to be compared with IIR, PR and our adaptive filters for clutter rejection.

The linear phase response filter is attractive in many applications, especially in image processing and data transmission [126]. The filters were designed by using fixed stop band cut off frequency, pass band ripple (the same parameters used for FIR filter design) and four different orders 4, 6, 8 and 10. Linear-phase FIR filters have impulse response that is either symmetric or asymmetric. The frequency response of the linear-phase FIR filters illustrated in figure 5-4. At each time the minimum cut off frequency ( $\omega_{pas}$ ) was estimated.

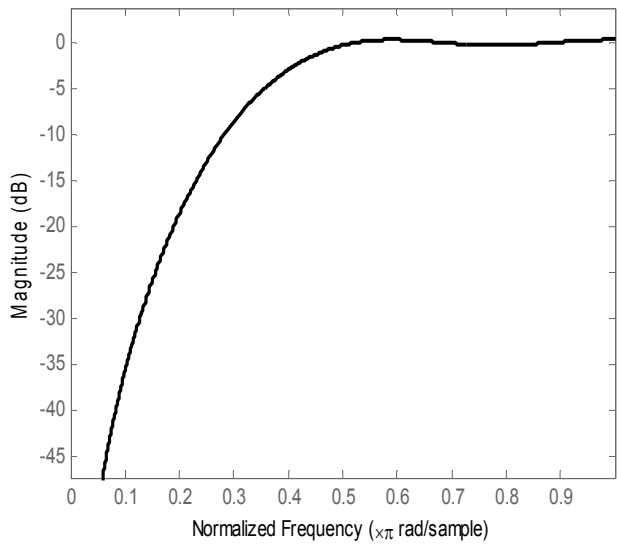
The result shows that the transition width of the linear phase filter decreased with increasing the filter order. The pass band cut off frequency of  $0.44\pi$  was obtained when order 4 filters used, when order 10 used the pass band cut off frequency decreased to  $0.37\pi$ . The minimum  $d_s$  decreased from  $-57$  dB to  $-83$  dB when filter of order 4 and 10 were used respectively. Table 5.2 shows pass-band cutoff frequency and minimum  $d_s$  for different orders.



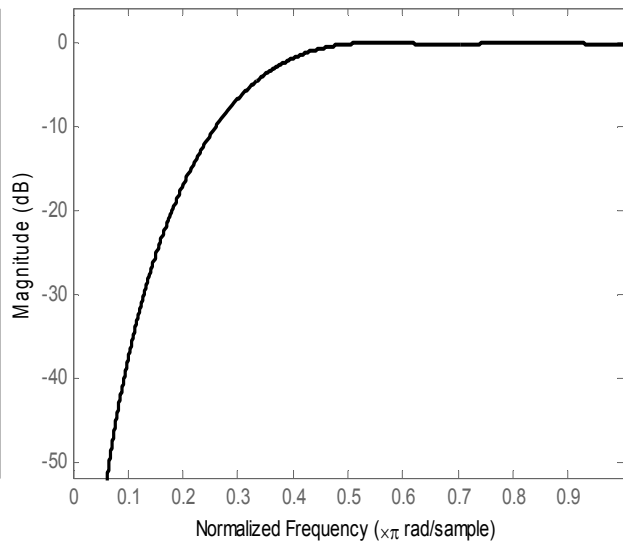
(a) Linear phase FIR filter using order 4



(b) Linear phase FIR filter using order 6



(c) Linear phase FIR filter using order 8



(d) Linear phase FIR filter using order 10

Figure 5-4. The frequency response of the linear-phase FIR filters using different orders (a) Linear phase FIR filter using order 4 (b) Linear phase FIR filter using order 6 (c) Linear phase FIR filter using order 8 (d) Linear phase FIR filter using order 10

To suppress the clutter from Doppler signal it's necessary to design a high pass filter with a suitable cutoff frequency, which is given high stop-band attenuation, short transition region and flat pass-band so as to avoid any loss of blood flow information.

Thus, from the compression we found that for cluttering the unwanted signal originated from surrounding and slowly moving tissue, the clutter filters with order 6 is the best for clutter suppression. The frequency response of linear-phase FIR filters using different orders shown in figure 5-5.

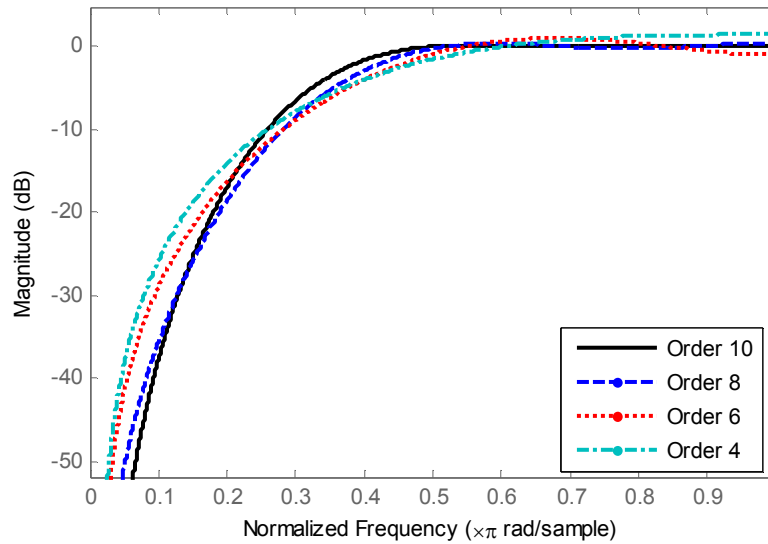
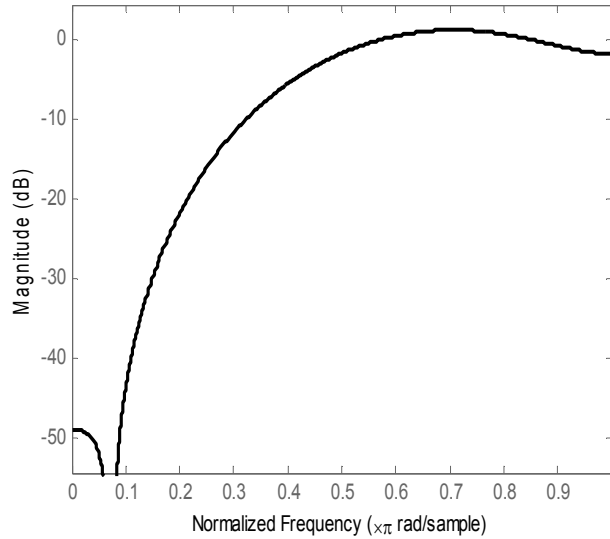


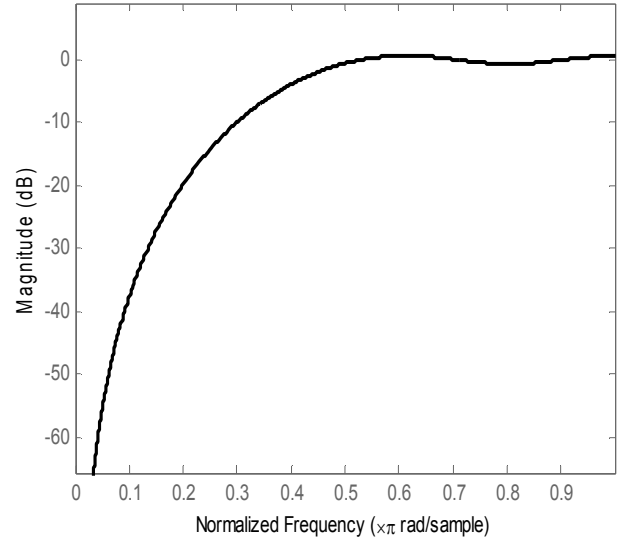
Figure 5-5. Linear phase FIR filter designed using different orders

### 5.2.1.2 Minimum Phase FIR filter

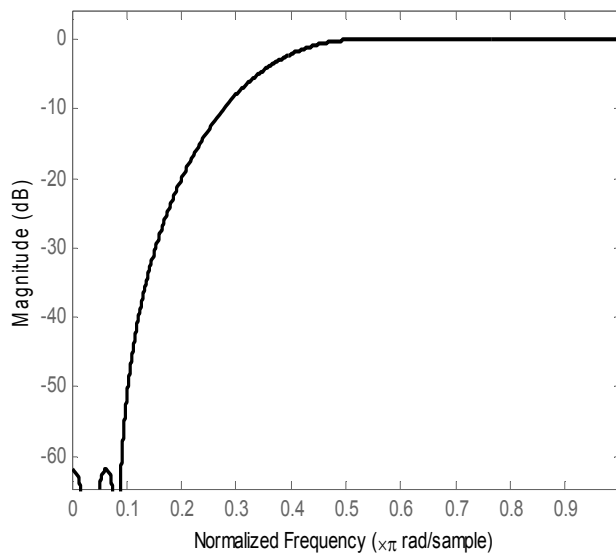
Same procedures used for designing the linear phase FIR filters were used to design the minimum phase FIR filters. The frequency response illustrated in figures 5-6. Different orders were used, at each the minimum cut off frequency ( $\omega_{pas}$ ) and minimum ds were estimated.



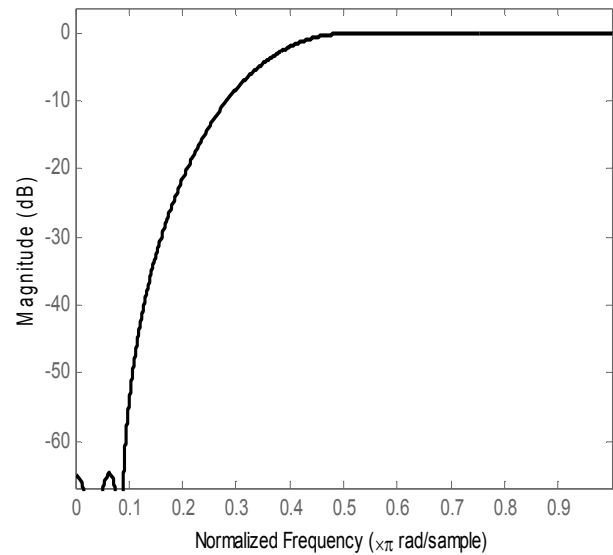
(a) Min. phase FIR filter using order 4



(b) Min. phase FIR filter using order 6



(c) Min. phase FIR filter using order 8



(d) Min. phase FIR filter using order 10

Figure 5-6. The frequency response of the minimum-phase FIR filters using different orders (a) Min. phase FIR filter using order 4 (b) Min. phase FIR filter using order 6 (c) Min. phase FIR filter using order 8 (d) Min. phase FIR filter using order 10

Different order has been used for designing the minimum phase FIR filters; the result shows that lower orders have higher pass band cutoff frequency. When the filter with

orders 4 design the minimum pass band cut off frequency was  $0.36\pi$ , but when orders 10 used the minimum pass band cutoff frequency decreased to  $0.30\pi$ . Moreover the result shows that Minimum ds improved when higher order filter used. The pass-band cutoff frequency and minimum  $d_s$  for different orders of the minimum phase FIR filters illustrated in table 5.2.

The minimum phase filter by order 6 will be used for designing the clutter rejection filter to avoid loss of Doppler signals and be sure to reject all the clutter level of the Doppler signal. Minimum phase FIR filter by order 6 will be used for comparison with other types of FIR filters. The comparison of the frequency response for minimum phase FIR filters using different orders was shown in figure 5-7.

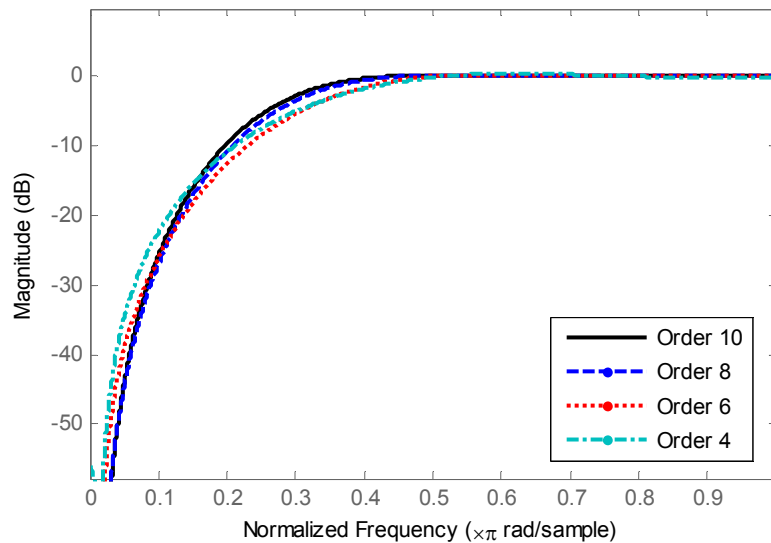
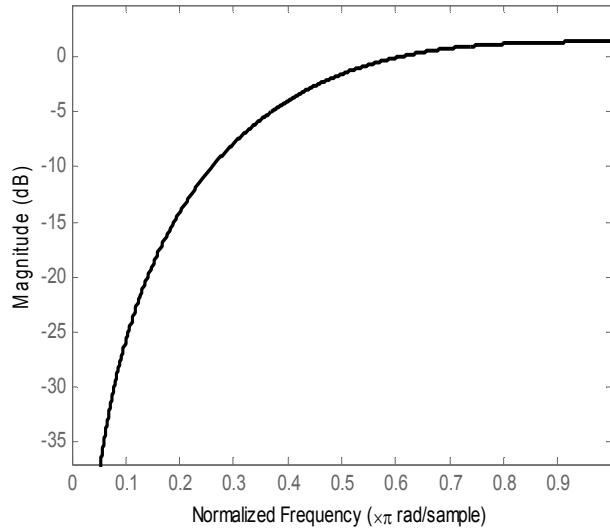


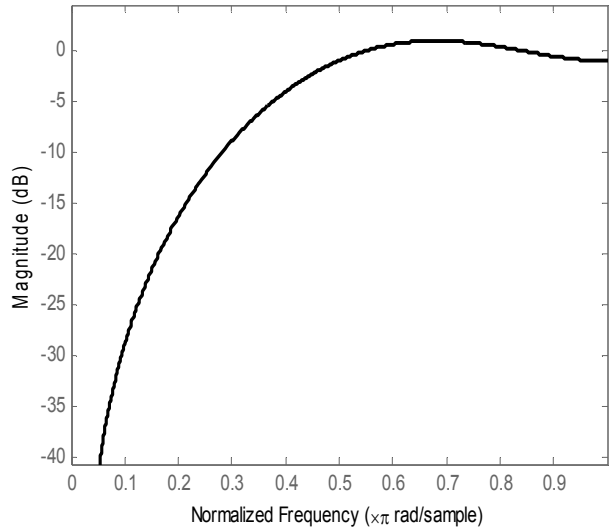
Figure 5-7. Min. phase FIR filter designed using different orders

### 5.2.1.3 Equiripple FIR Filter

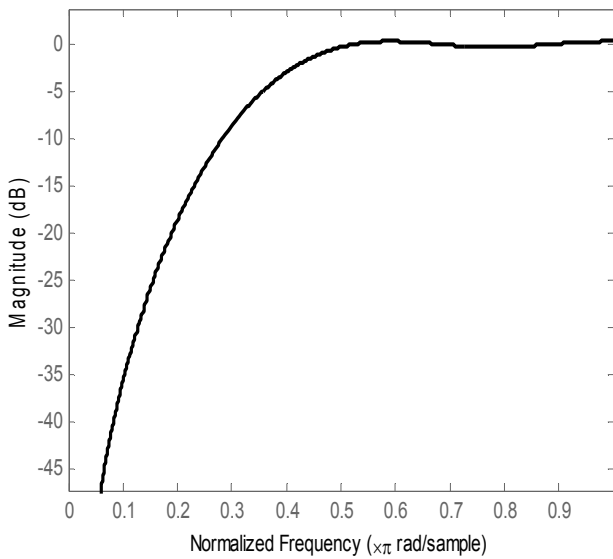
Equiripple gives the smallest maximum deviation from the ideal filter. Equiripple filters are used in applications where a specific tolerance must be met [126]. The filter designed with parameters in table 5.1 and the result illustrated in figure 5-8.



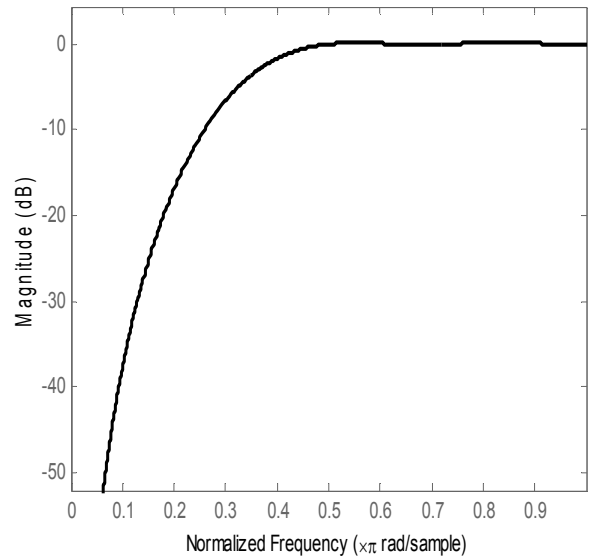
(a) Equiripple filter using order 4



(b) Equiripple filter using order 6



(c) Equiripple filter using order 8



(d) Equiripple filter using order 10

Figure 5-8. The frequency response of the equiripple FIR filters using different orders (a) Equiripple filter using order 4 (b) Equiripple filter using order 6 (c) Equiripple filter using order 8 (d) Equiripple filter using order 10

The equiripple FIR filters with order 4 gives pass-band cut off frequency of  $0.44 \pi$  and order 10 gives  $0.36 \pi$ . The pass-band cutoff frequency and minimum  $d_s$  for equiripple

FIR filters using different orders shown in table 5.2. The comparison of the frequency response for equiripple FIR filters using different orders shown in figure 5-9.

Table 5.2. Pass-band cut off frequency and Minimum  $d_s$  for the filters using different order

Filter type	Orders	4	6	8	10
Linear phase FIR filter	Passband cut off frequency $\omega_{pas}$	$0.44 \pi$	$0.43 \pi$	$0.40 \pi$	$0.37 \pi$
	Minimum $d_s$ (dB)	-57.0	-62.0	-70.5	-82.9
Minimum phase filter	Passband cut off frequency $\omega_{pas}$	$0.36 \pi$	$0.35 \pi$	$0.314 \pi$	$0.30 \pi$
	Minimum $d_s$ (dB)	-56.0	-61.2	-69	-78.5
Equiripple FIR filter	Passband cut off frequency $\omega_{pas}$	$0.44 \pi$	$0.43 \pi$	$0.40 \pi$	$0.364 \pi$
	Minimum $d_s$ (dB)	-59.4	-62.9	-71	-83

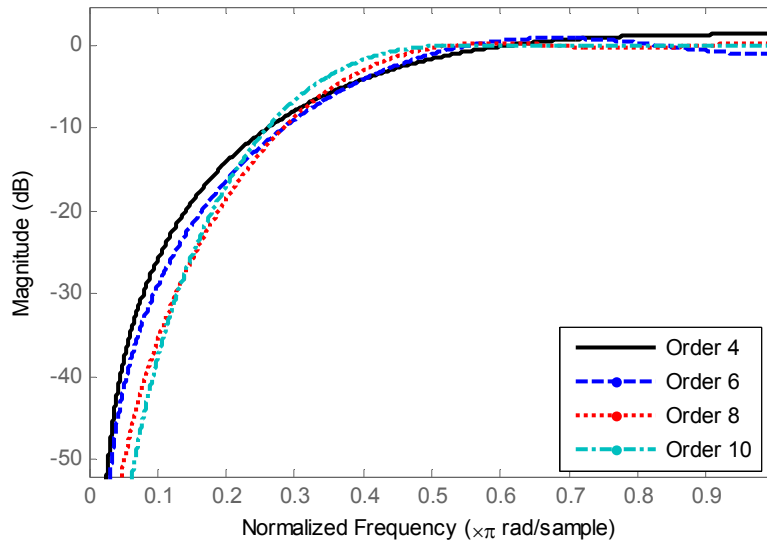


Figure 5-9. Frequency response of different orders equiripple filters

### 5.2.1.4 FIR Filters Comparison

Three types of FIR filter considered in the comparison, equiripple, linear phase and minimum phase FIR filters. All filters designed using parameters mentioned in table 5.1 and order 6. The comparison between the filters based on analyzing the frequency

response (measure the pass-band cut off frequency  $W_{pass}$  and minimum  $d_s$ ). The results of the frequency response illustrated in figure 5-10. The result shows that the minimum phase filter has a much smaller transition region compared to the others FIR filters types moreover; the minimum phase filter has flatter pass-band and higher stop-band attenuation. Equiripple and linear phase filters gives an equal frequency response. The minimum phase filter gives pass-band cutoff frequency of about  $0.35\pi$  when designed using order 6, but equiripple and linear phase filters with same order give the pass band cutoff frequency of  $0.43\pi$ . To get equiripple or linear phase filter with same minimum phase filter transient, we need to increase the order. Thus, the two filters are not comparable with minimum phase filter. In order to compare them we need to increase the order in equiripple or linear phase filter until we get the same frequency response that the minimum phase filter gives. We have got the same pass band cut off frequency that gene from minimum phase by using equiripple and linear phase filters when the filters designed using order 10. Increasing in filter order increased the delay of the filter. Thus when comparing the FIR filter with others classes of filters, the minimum phase FIR filter will be used.

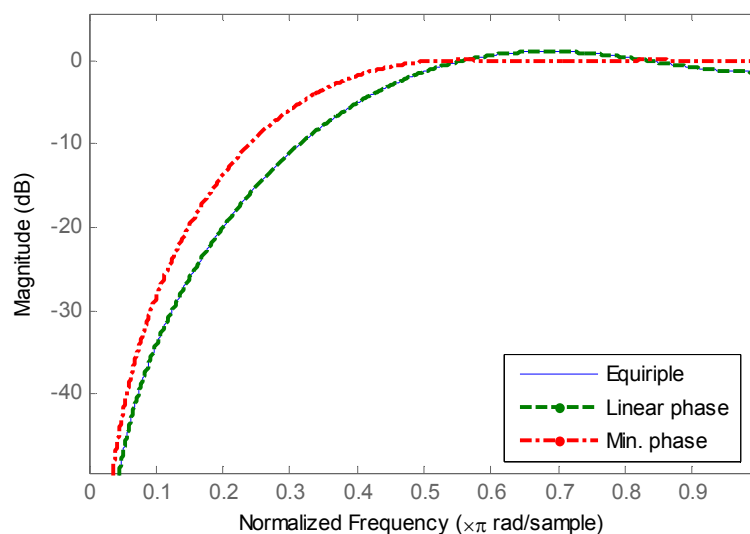


Figure 5-10. Frequency response of minimum phase, linear phase and equiripple FIR filters

## 5.2.2 Infinite Impulse Response (IIR) Filter

An infinite impulse response (IIR) filter designed by using the bilinear transformation approach. The IIR filter computed by using the basic formula that combines the input and output as following

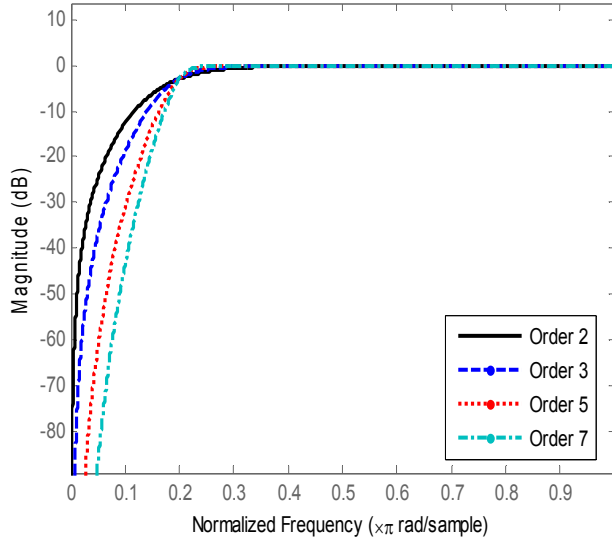
$$y[n] = \sum_{k=0}^M b_k x[n-k] - \sum_{k=1}^N a_k y[n-k] \quad (5.3)$$

The coefficient  $b_k$  act only with the input signal  $x[n]$ , thus it is known as “feedforward” coefficient, and the coefficient  $a_k$  act with output  $y[n]$ , is known as feedback coefficient. The transfer function of IIR filter is

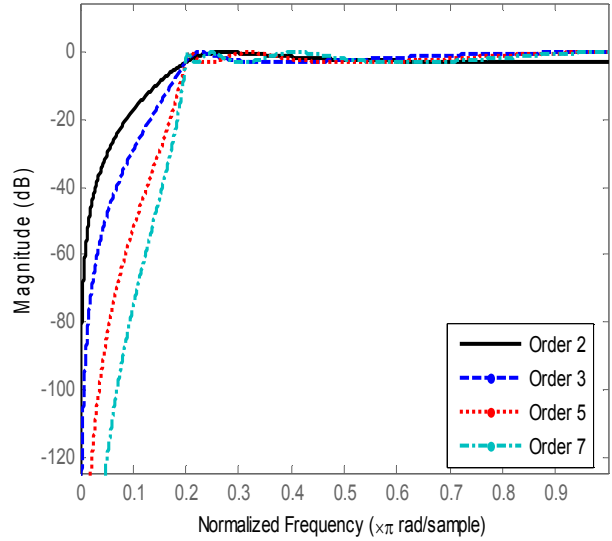
$$H(z) = \frac{B(z)}{A(z)} = \frac{\sum_{k=0}^M b_k z^{-k}}{\sum_{k=0}^N b_k z^{-k}} = \frac{b_0 + b_1 z^{-1} + \dots + b_M z^{-M}}{1 + a_1 z^{-1} + \dots + a_N z^{-N}} \quad (5.4)$$

There are different types of IIR filters, all types of IIR filters were compared with each other's. The filter with best and suitable frequency response will be used for comparison with the other types of filters. The IIR filters were designed using the parameters in table 5.1 and different orders.

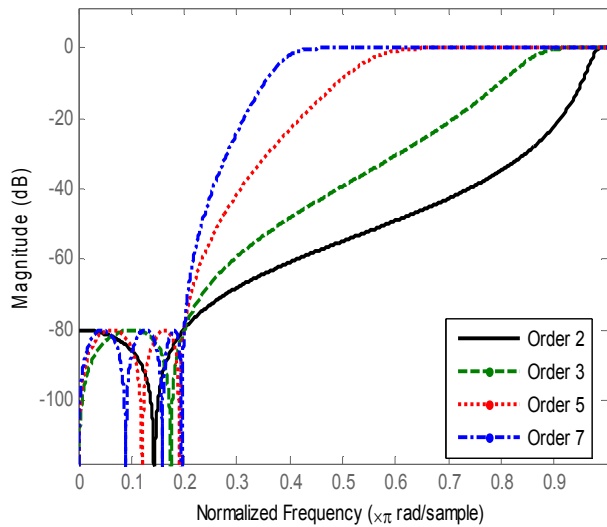
There are about seven different types of IIR filters, their design based on steady-state magnitude response. The most common types filter used are Butterworth, Elliptic and Chebyshev type I and II filters, more detail about IIR filter design can be found in [126, 127]. The filters were designed using the parameters in table 5.1 and different orders, all types of IIR filter were compared, the filter with the best transition region will be compared with FIR and PR filters. Figure 5-11 shows the effect of a different order in the frequency response for different types of IIR filters, only four types (Elliptic, Butterworth and Chebyshev type I, and II filters) were shown.



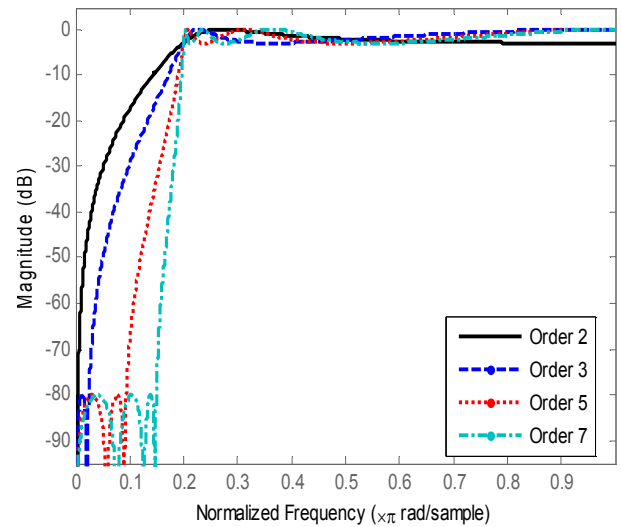
(a) Butterworth



(b) Chebyshev type I



(c) Chebyshev type II



(d) Elliptic

Figure 5-11. The frequency response of different IIR filters using four different orders

The result shows that the frequency response of the filters improved by increasing the filter orders. To compare different types of IIR filters, order 3 was used. The filter with better transient response will be used for clutter rejection, and compared with other types of filters. However, several studies showed that IIR filters can be used for separating the blood flow signal from clutter signal [7, 11, 14].

### 5.2.2.1 IIR Filters Comparison

All types of IIR filters designed using order 3 and the parameters in table 5.1, so as to select a filter with better performance for clutter rejection and compared with other classes of filters. The frequency response of different types of IIR filters was illustrated in figure 5-12. The result shows that the Butterworth and chebyshev type I filters gives the smaller transient region, but Butterworth filter gives better stop-band.

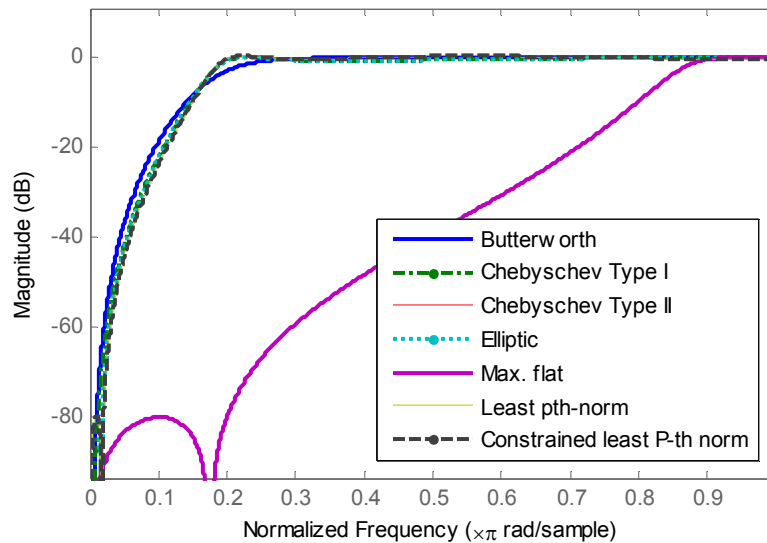


Figure 5-12. IIR filter comparison designed with order 3

For IIR filter transient response improvement [15, 128] initialization of the inner states of the filters suggested. Initialization of IIR filter reduces the time the transient responses dominates the output of the IIR filter and yield a suppression of the transient response.

The most widely used techniques for reducing the IIR filter's frequency response is a state space formulation [15]. The state space formulation used to investigate different ways of minimizing the transient response. The three different initialization techniques used to minimize the transient are examined in [7].

- Zero initialization: The state vector of the filter set to zero. Zero initialization gives insufficient stop-band rejection.

- Step initialization: The state vector of the filter is set to constant determined by filter coefficients and data values. Step initialization gives zero at zero frequency and very narrow stop-band.
- Projection initialization: The filtered signal is decomposed into steady-state and transient components. Projection initialization gives stop-band equal to steady state and wider transient rejoin.

The projection initialization gives response equal to the steady-state and wider transition region [7]. Among all different types of IIR filters, projection initialization Chebyshev type I IIR filters is the best, because of his a steep transition. Therefore, Chebyshev type I filter with projection initialization will be used when comparing IIR filters with other filter classes. The stop-bandwidth of the projection initialization Chebyshev IIR filters can be increased with either increasing order or the cutoff frequency of the steady-state response. The frequency response for Chebyshev IIR filters with different initialization illustrated in figure 5-13.

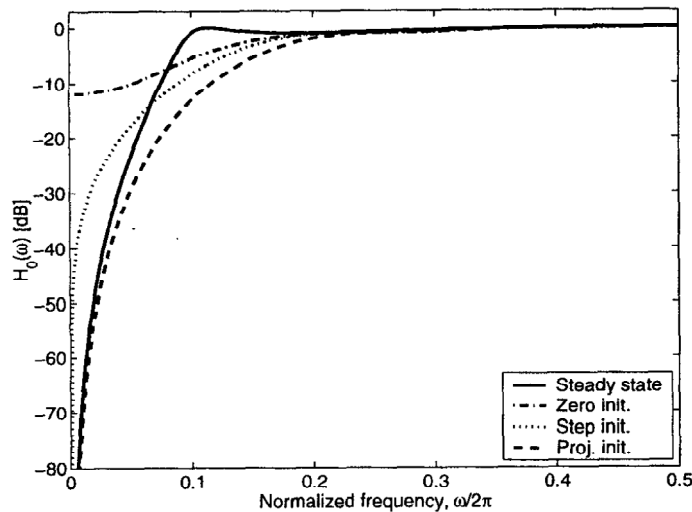


Figure 5-13. The frequency response for Chebyshev IIR with different initialization [7]

### 5.2.3 Polynomial Regression (PR) Filter

Regression filter works on different concept to FIR and IIR, which are based on theories that signals are superposition of sinusoids. It operates on the assumption that the

slowly varying component can be approximated by polynomial [11, 122]. Regression filter approximates the input signal with polynomial function in the time domain, and the filter design is not based on impulse of frequency response [129, 130]. Regression filter calculates the best least square fit of the input signal to set of curves from modeling the clutter signal and then subtracts this clutter estimate of the original signal. The linear filtering can be expressed as:

$$y = Ax \quad (5.5)$$

Where  $x$  is complex input signal,  $y$  is complex output signal and  $A$  is an  $N \times N$  matrix given by:

$$A = I - \sum_{k=0}^{K-1} b_k b_k^* \quad (5.6)$$

The frequency response of this relation given by

$$H_0(\omega) = I - \frac{1}{N} \sum_{k=0}^{K-1} |B_k(\omega)|^2 \quad (5.7)$$

Where  $b_k$  is a set of orthogonal basis in  $k$ -dimensional clutter space,  $I$  is the identity matrix and  $B_k(\omega)$  is the Fourier transform of orthonormal basis vector  $k$ . In order to design high pass filters,  $k$  must be small compare to the length of signal  $N$ .

The filter matrix in relation (5.6) depends only on  $P$  and  $k$ -dimensional clutter so it can be recomputed for real-time application and the recompilation is not required if the sampling does not change. Figure 5-14 illustrated the block diagram of polynomial regression filters.

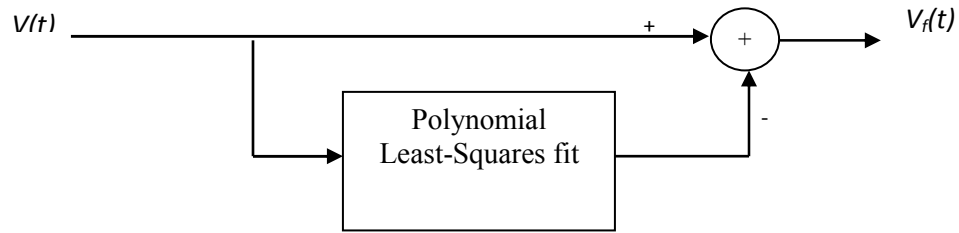


Figure 5-14 Polynomial regression filter block diagram

The frequency response for polynomial regression filters with different dimensions of the clutter space shown in figure 5-15. The figure shows that the polynomial regression filters have a smooth frequency response, which will be used to when regression filter compared with other filter classes. The frequency response of polynomial regression filters changes in discrete steps with space dimension (clutter order) as shown in the figure. A better frequency response obtains with low clutter order. Also the frequency response varies with the package size, as shown in figure 5-16. To obtain the same stop bandwidth with the large package size, the clutter order has to be increased.

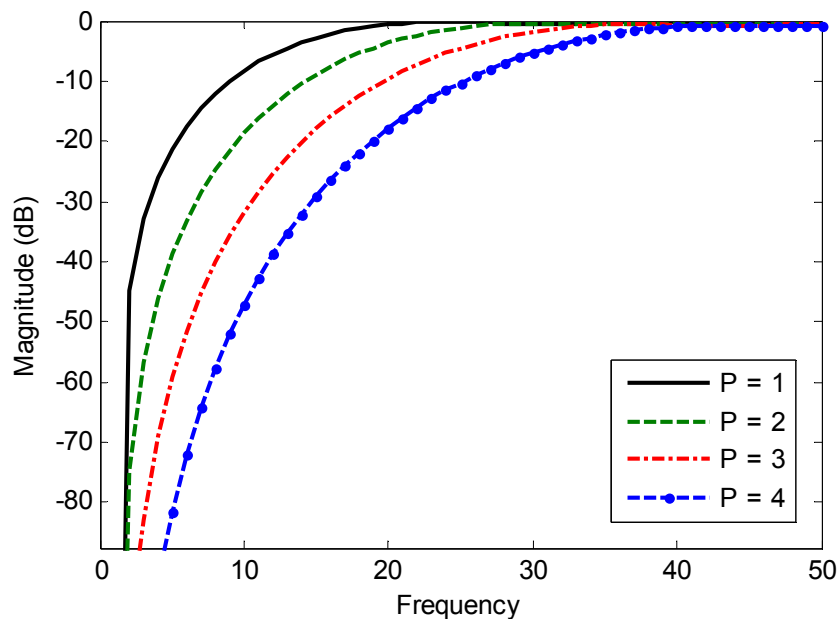


Figure 5-15. Frequency response of PR filters using different clutter space dimension.

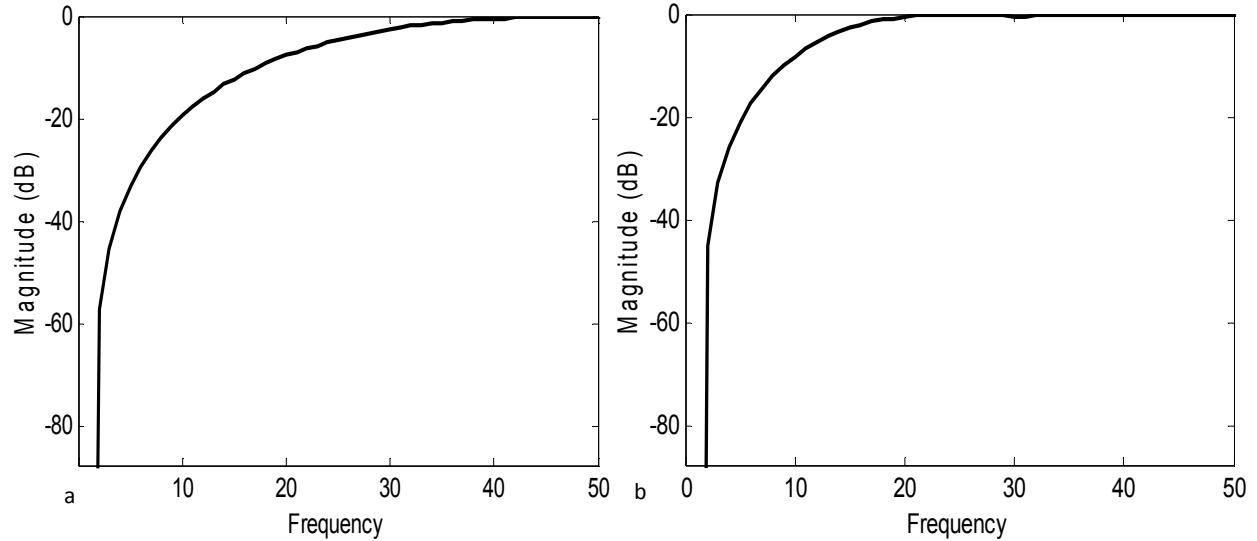


Figure 5-16. Frequency response for PR filters with different package size and order  $P = 1$ . (a) With package size 8. (b) With package size 16.

The polynomial regression filter matrix in relation (5.6), multiplied by a constant factor to test the behaviors of the filter. The result matrix given by:

$$A = I - \sum_{k=0}^{K-1} C_k \cdot b_k b_k^* \quad (5.8)$$

Where  $C_k$  is the real constant

The filter was tested by multiplying the function with constant factors  $C_k$ , for clutter order equal to three and package size 8, the factor used are as follows:  $C_0 = C_1 = 1$  and  $C_2 = 0.25, 0.5$  and  $0.75$  [7]. Figure 5-17 shows the frequency response of polynomial regression filters from relation (5.6) (conventional polynomial regression filters) with clutter dimension one and the frequency response from the relation (5.8) with clutter dimension equal to three. The conventional polynomial regression filters give wider transition rejoin and best performance. There is no significant difference for both at  $-80$  dB stop-bandwidth. Thus for comparison with other clutter rejection filters (FIR, IIR) the conventional polynomial regression filters will be considered.

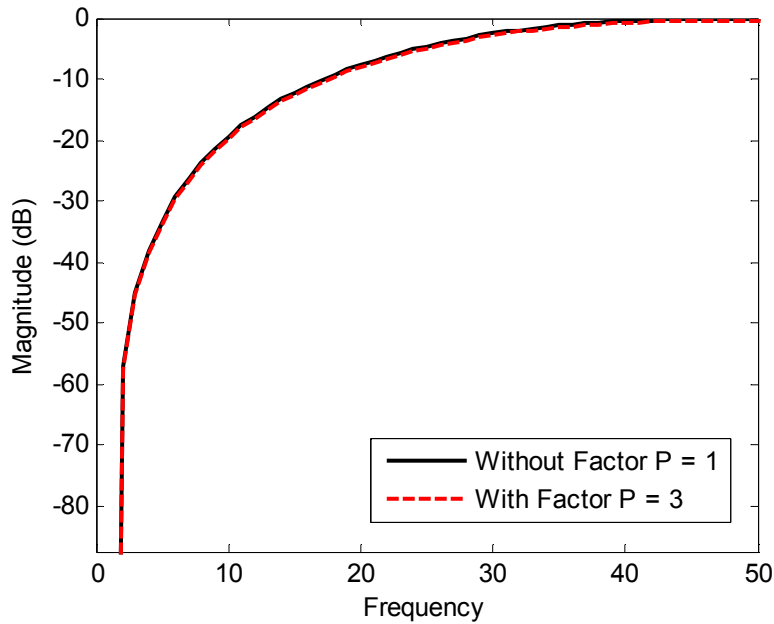


Figure 5-17. Frequency responses of conventional PR filters and filter from relation 5.6 using package size 8

## 5.2.4 Filters Comparison

The filter with the best frequency response within the three types of filters FIR, IIR and PR filters were found in the previous subsections. The frequency response of projection initialization Chebyshev IIR filters, Minimum phase FIR filter and polynomial regression filters were compared. The filters were designed with parameters given in table 5.3 proposed in [7], to achieve filters with equal frequency responses. These parameters were chosen to achieve filters with a comparable frequency response.

The projection initialization Chebyshev IIR filters has frequency responses almost identical to that in the polynomial regression filters. Minimum phase FIR filters have largest transition region, which is not preferable in Doppler clutter rejection. The FIR filter requires a higher order in order to have a same narrow transition band given when IIR filter used, which is one of the requirements of a good wall filter. The comparison of the frequency response of projection initialization Chebyshev IIR filters, minimum phase FIR filters and polynomial regression filters illustrated in figure 5-18.

Table 5.3. Filter design parameters

Parameters	values
Projection initialization IIR Chebyshev	
order	4
$\omega_p$	$0.2 \pi$
dp	0.5 dB
Minimum phase FIR	
Order	6
Minimum $\omega_s$	$0.02 \pi$
Maximum dp	0.5 dB
Minmum ds	- 80 dB
Polynomial regression	
Clutter space dimension	2

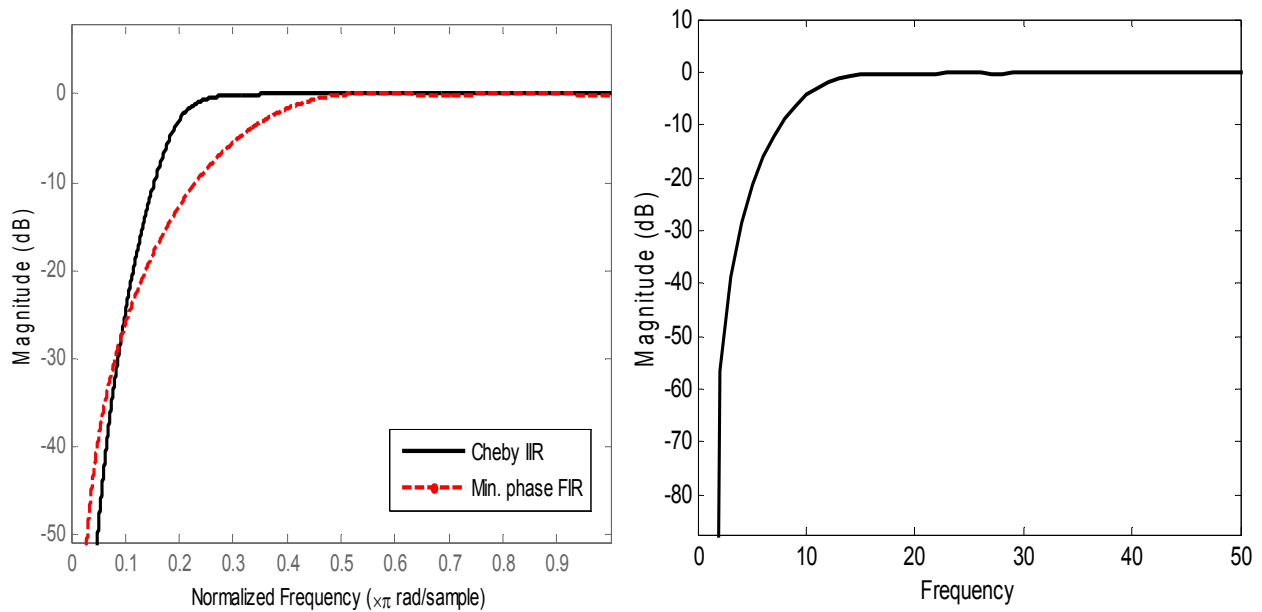


Figure 5-18. The frequency response of IIR and FIR (left), and PR (right)

### 5.2.5 Principal Component Analysis

Principal component analysis (PCA) is a tool used to analyze the data because it is simple, non-parametric methods for extracting relative information from confusing data set. The idea behind PCA is the dimensionality reduction of a data set which has a large number of uncorrelated variables, in the other words identifies most meaningful basis to re-express the data set. For reducing the dimensionality of large data set, PCA uses a vector to transforms [131]. The hope is that this new basis filters out the noise and reveals hidden structure. This achieved by transforming the data set to a new data set of the principal components (PCs), which are uncorrelated. The PCs are calculated as the eigenvectors of the matrix covariance of the data [19, 132, 133]. It is easier to handle a small set of uncorrelated variables and use for further analysis than a large set of correlated variables.

PCA tools are very important tools for data analysis this importance comes from, it's optimal linear scheme for data reduction from high dimensional vector to a low dimensional vectors and then reconstruct the original set, the model parameters can be computed from the data directly and it is need only matrix multiplication for compression and decompression.

A multi dimensional data are often difficult to visualize. Thus, data reduction is essential. PCA has been applied in different field, because it reveals simples underlying structures in complex data sets using analytical solutions from linear algebra.

Extracting the PCs in PCA can be made using either original data set or using covariance matrix. In some cases for deriving PCs, the correlation matrix is used instead of the covariance matrix.

Assuming that the data set represented as a matrix,  $X$  in terms of an  $m \times n$ , where the  $n$  columns represent the samples (observations) and  $m$  are the variables. If the new representation of the data set represented as a matrix,  $Y$  in terms of a  $m \times n$  matrix and a linear transformation is  $P$ , then the PCA model can be represented by

$$Y = PX \quad (5.9)$$

This relation represents changes in basis. Considering the row of  $P$  to be a row vector  $p_1, p_2, \dots, p_m$ , and the columns of  $X$  to be column vectors  $x_1, x_2, \dots, x_n$  then the relation (5.9) can be written as follows:

$$PX = \begin{bmatrix} p_1 \cdot x_1 & p_1 \cdot x_2 & \dots & p_1 \cdot x_n \\ p_2 \cdot x_1 & p_2 \cdot x_2 & \dots & p_2 \cdot x_n \\ \vdots & \vdots & \ddots & \vdots \\ p_m \cdot x_1 & p_m \cdot x_2 & \dots & p_m \cdot x_n \end{bmatrix} = Y \quad (5.10)$$

The common approach in analysis of noisy data is to use data averaging strategies. Hoping that errors due to noise canceled out when a data mean is calculated. Thus, the first step of the analysis is to express each attribute as a difference between an original data set and the mean of all such values. The mean of the original data computed as follows

$$\bar{x}_i = \frac{1}{n} \sum_{k=1}^n x_i^{(k)} \quad i = 1, 2, \dots, m \quad (5.11)$$

Then the data matrix entries replaced by its difference with mean, this generate a data set whose mean is zero.

Then the covariance of the matrix calculated. A large positive value indicates positive correlation and large negative value indicate negative correlations. Since the resulting matrix from subtracting the mean of the data consist of a row vector for each variable, each vector contains all samples for one particular variable. The data set covariance matrix can be calculated using the following relation

$$S = \frac{1}{n-1} \sum_{i=1}^n (x - \bar{x})(x - \bar{x})^T \quad (5.12)$$

The result  $S$  is a square symmetric matrix in term of the  $M \times M$ . The diagonal terms of the resulting matrix are the variance of exacting measurement. The off diagonal terms of the matrix are the covariance between the measurements.

Since the covariance matrix is a square in term of the  $M \times M$ , this matrix can be used to calculate the eigenvector and eigenvalue. The eigenvector and eigenvalue give quite different values for eigenvalues. So the eigenvector  $e_1, e_2, \dots, e_m$  of the data sets with highest eigenvalue  $\lambda_1, \lambda_2, \dots, \lambda_m$  represent the principal components of the data set.

The eigenvectors  $e_i$  calculated by solving the set of the following relations

$$(S - \lambda_i I)e_i = 0 \quad i = 1, 2, \dots, d \quad (5.13)$$

After the calculation, the eigenvectors are sorted by magnitude of corresponding eigenvalues. Then the largest values of the eigenvalues are chosen. The projection matrix of the PCA then calculated as:

$$W = E^T \quad (5.14)$$

Where  $W$  is a matrix in term of  $m \times d$  and column of  $E$  has the  $m$  eigenvectors.

One of the most important advantages for selecting the PCA for clutter rejection does not need to transform the data into another space (e.g. self-learning techniques [134]), it is working on the input data vector space directly. The dimensional reduction in PCA achieved by calculating first PCs of the input data vectors that have a higher variance, without the need to perform any transformations in the input space.

### 5.2.6 Independent component analysis

Independent component analysis (ICA) is a technique for instructive hidden factors that underlies set of measurements or signals. There are several transformation methods proposed for data analysis and finding a suitable representation of the multivariable data

such as PCA. A recent developed transform method is independent component analysis (ICA), which is used to minimize the statistical dependent of the component of the representation. The used ICA to estimate the original data set of mixed data. In other words separate the noise from original signals. This is referred to as the blind source separation (BSS) problem [135 - 137].

ICA technique based on non-Gaussianity and use higher order statistics rather than second order to separate the signal from the noise [135, 138]. Beside the non-Gaussian, ICA assumes the components to be independent [139]. This is powerful and attractive set of assumption that make ICA very aggressive tasks, however, ICA treat the observed signal as a set of random variables without considering the dependency of adjacent time point.

Since ICA uses higher order statistics rather than second order moments to determine the basis vectors that are statistically independent as possible, ICA can consider as an extension of PCA [138, 140]. This made ICA gives a better separation result in most applications.

Signals originated from different sources are statistically autonomous from each others, thus the signals can be separated from each by ICA, which is able to distinguish different signal from each other from linear combinations of their sources, the signal separation process illustrated in figure 5-19. This made ICA applied to different signal processing approaches such as, filtering, source separation, data analysis, features extraction, ect.

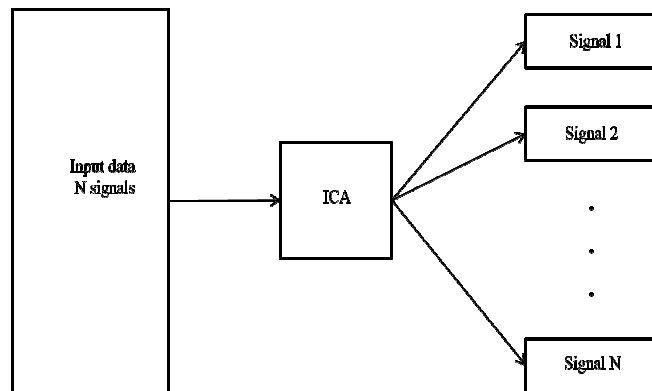


Figure 5-19. Block diagram of signal separation process in ICA

Let  $X$  represents the observed data vector, which is modeled by

$$X = AS = \sum_{j=1}^n a_j s_j \quad j = 1, \dots, n \quad (5.15)$$

Where  $A$  is a matrix with column vector  $a_j$  and  $S$  is n-dimensional vector consist of source signals  $s_1, s_2, \dots, s_n$ . The signals are assumed statistically independents. The ICA approach used to estimate a matrix  $P$  such that

$$Y = PX \quad (5.16)$$

are statistically independent using the observed data.

There are five assumptions must be meet, in the ICA process.

- The source vector  $S$  assumed to be statistically independent.
- The matrix  $A$  (mixing matrix) must be square.
- The source matrix  $S$  is the only source of stochasticity in the model
- The data centered (zero mean) and the vectors must be whitened
- The source signal must not have a Gaussian probability density function (pdf)

The first step in ICA after removing the means of the row vectors of the data, is the whitening (sphere) of the data set. Whiten is a process used to remove any correlation in the data and mathematically similar to PCA. The new data set is whitened via a linear transformation. Whitening is very important that make the subsequent separation task easier. Also whitening help in estimating the independent component from the first larges PCs. After whitening, only the first most significant terms are preserved in a fast fixed-point algorithm (FastICA) calculation. FastICA process used to implement ICA, FastICA process proposed by Hyvarinen and Oja in [141]. The next step is to search for non-mixing matrix mutually independent. Mutual information or kurtosis (forth order moment) measure the non-Gaussianity, can be used to find the ICA information.

If the random variables are  $x_1, x_2, \dots, x_m$  with pdf  $f(x_1, x_2, \dots, x_m)$ , the variables  $x_i$  is mutually independent if

$$f(x_1, x_2, \dots, x_m) = f_1(x_1)f_2(x_2), \dots, f_m(x_m) \quad (5.17)$$

Considering the random centered variables, uncorrelatedness is represented by the following equation

$$E[x_i x_j] - E[x_i]E[x_j] = 0 \quad \text{for } i \neq j \quad (5.18)$$

Where  $E[.]$  is the expectation

Then the Kurtosis principle is maximized by applying the FastICA algorithm, to estimate the independent component.

# Chapter 6

## Cluttering Doppler Data

In this chapter we will discuss the types of the data used in this work, to validate and compare different types of clutter rejection filters discussed in chapter 5, two types of data were used, the real Doppler data and simulated data. The simulated data generation and signal models were also discussed.

### 6.1 The Data

Two types of data were used, real Doppler data and simulated data to validate and compare different types of clutter rejection filters.

#### 6.1.1 Real Data

The real data used to validate the clutter rejection filters are the same data used for Doppler ultrasound signal reconstruction, discussed in chapter 4.

#### 6.1.2 Simulated Data

To quantify the performance of a new clutter for rejecting the clutter, the Doppler data from URI downloaded and generate Doppler IQ using MATLAB (MathWorks, Inc., Natick, MA). Ultrasound research interface (URI) and Ultrasound research interface offline processing tools (URI-OPT) are software and sample data. In this work we will concentrate on URI-OPT. URI-OPT are a Matlab based program for reading and processing the RF data acquired from a URI-equipped Antares system. URI-OPT can be used to display different Doppler imaging mode. One of the most important modes that we are interested in is spectral Doppler mode, which is used to display the Doppler

spectrum of RF data. The speed of flow information within the Doppler range gate is displayed as gray scale intensities at a time versus velocity plot.

The data used are data of Doppler spectrum collected from URIDmode. The data tested first on the program to display the spectrum, and then the data extracted and stored in Matlab. Matlab program was developed to read the saved data and then generate Doppler In-phase/Quadrature (IQ) data, which is used to test our proposed clutter rejection filters and comparisons between different types of clutter filters. The parameters used to generate the Doppler IQ data illustrated in table 6.1. The generated Doppler IQ data is a complex matrix  $X$  in  $100 \times 7923$ .

Table 6.1. Parameters used to generate Doppler IQ

Data Parameters	Values
First value	1
Last value	7923
Range gate start	1100
Range gate size	100
Vector group	0
Real group	1000
Frequency	7.2727
PRF	2441

The complex data matrix  $X$  obtained can be expressed as:

$$X = \begin{bmatrix} x_{11} & x_{12} & \cdots & x_{1N} \\ x_{21} & x_{22} & \cdots & x_{2N} \\ \vdots & \vdots & \ddots & \vdots \\ x_{M1} & x_{M2} & \cdots & x_{MN} \end{bmatrix} \quad (6.1)$$

Where  $M$  is the number of pulses and  $N$  is the axial sample volume. Each column in the matrix  $X$  represents a vector with length  $M$ .

The input sample vector to clutter rejection filter with index depth equal to  $n$ , can be represented by the following expression:

$$x_n = [x_{1,n}, x_{2,n}, \dots, x_{M,n}]^T, n = 1, \dots, N \quad (6.2)$$

## 6.2 Signal Model

The generated Doppler signal data originated not only from blood flow, but also it originated from different tissue regions with different motion patterns, the clutter Doppler signal is a sum of contributions from different regions, and figure 6-1 shows the Doppler signal from blood. We assume that the resulting signal consists of a blood signal component  $b$  originated from the reflected echo from the moving red blood cells, a clutter component  $c$  originated from surrounding and moving tissue and white noise  $n$  originated from electronics or any other component. The signal can be modeled as:

$$X = b + c + n \quad (6.3)$$

The signal characterized by the correlation matrix [3]. The correlation matrix  $R_x$  given by:

$$R_x = E\{xx^{*T}\} \quad (6.4)$$

In our case the correlation matrix expressed as

$$R_x = R_c + \sigma_n I + R_b \quad (6.5)$$

Where,  $R_c$  is the clutter correlation matrix,  $\sigma_n$  is the noise variance,  $R_b$  is the blood correlation matrix and  $I$  is the identity matrix.

The three components originated from different source and are statistically independent. Thus with the proposed methods we can easily determine the basis vectors that are statistically independent [142].

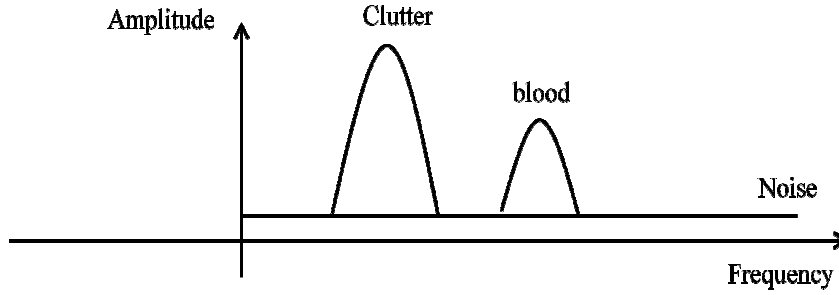


Figure 6-1 Doppler signal spectrums

The Doppler IQ data prepared to satisfy our proposed clutter rejection method based on ICA and PCA by doing some preprocess steps, such as applying discrete Fourier transform (FFT) and the absolute value to the data so as to remove the imaginary values. Assume that our input signal  $f(x,y)$  is a function of 2-D space define over an x-y plane. The two-dimensional FFT takes a complex array and expressed by using the following form:

$$f(u, v) = \frac{1}{MN} \sum_{i=1}^M \sum_{j=1}^N f(x, y) e^{-2j\pi(ux/M+vy/N)} \quad (6.6)$$

A small window has taken for testing our clutter rejection filters. The result Doppler IQ signal illustrated in figure 6-2, only 8 signals were shown for simplicity.

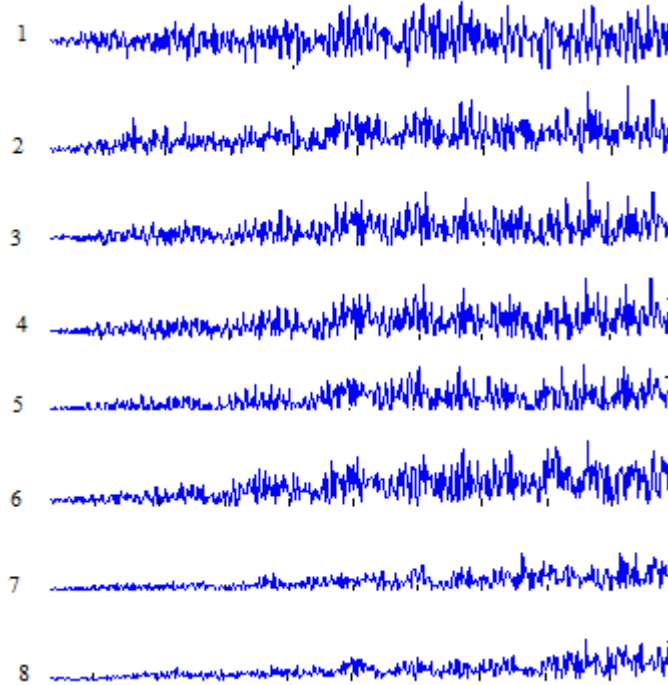


Figure 6-2. The generated Doppler IQ signal for simulation

The Doppler data preparation and cluttering process illustrated in figure 6-3, in data preparation the Doppler data generated and prepared for cluttering, in cluttering steps the Doppler signal with two peaks (clutter and flow peak) applied to the filter, and then the spectrum of the filtered signal calculated to give the blood flow signal spectrum only.

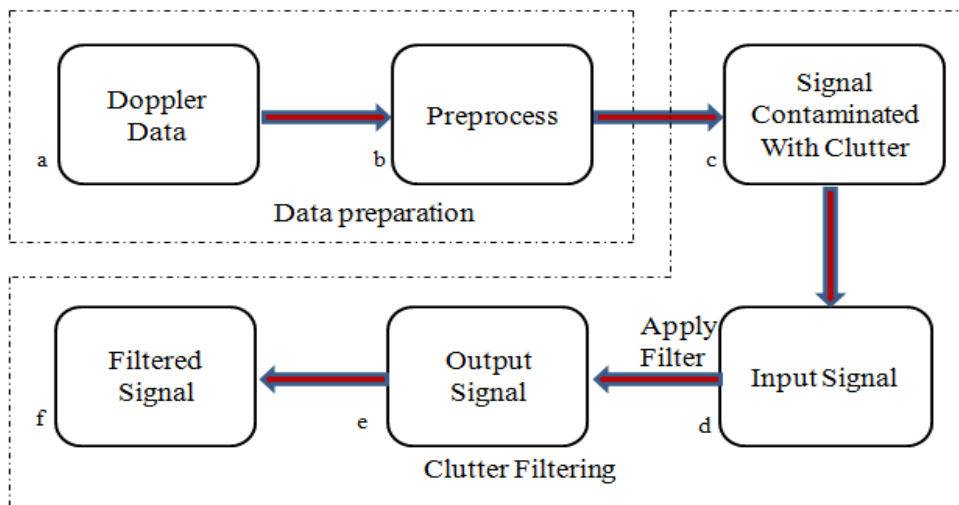


Figure 6-3 Pre-preparation and cluttering process with different filters

### 6.3 Cluttering with PCA

Principal component analysis (PCA) is the techniques that based on sophisticated mathematical principle to transform correlated variables into smaller numbers of variables known as principle components (PCs). The PCs are calculated as the eigenvectors of the covariance matrix of the data [26]. The variance corresponding to these eigenvectors are denoted as the eigenvalues. PCA is one of the most useful tools in modern data analysis, because it is simple and non-parametric methods for extracting useful information from perplexing data set. PCA uses a vector space transform to achieve the reduction and de-noising of the large number of data set. This is particularly useful in application of PCA if a set of data used has many variables lies in actuality, close to two-dimensional plane [19, 131]. Using PCA will help to identify the most meaning full basis to re-represent the desired data set. This new basis filters out the noise and reveals hidden structure.

The input data  $X$  is a matrix represented in term of the  $M$ -by- $N$  with observation (samples) in columns and variables in its rows. The main approach to analysis the data is to use the data averaging strategies to expose the hidden input intrinsic nature of the data. The error due to noise will be canceled out when a mean of data is calculated. The mean of the data matrix calculated by:

$$\hat{X} = \frac{1}{n-1} \sum_{m=1}^n X_i^m \quad (6.7)$$

The mean of each of the measurements, subtracted from original input data matrix  $X$ , each entry in the matrix is replaced by its difference with mean. This produces a data with zero mean. Then the covariance was calculated from the resulting matrix, so as to measure the degree of linear relationship between a pair of variables. A large positive value indicates positive correlation and large negative value indicate negative correlations. Since the resulting matrix from subtracting the mean of the data consist of a

row vector for each variable, each vector contains all samples for one particular variable. The covariance expressed as a dot product matrix [50], and given by:

$$Cx = \frac{1}{n-1}DD^T \quad (6.8)$$

Where,  $D$  is the matrix resulting from subtracting the mean from the original data and  $T$  is transposed.

The result is a square symmetric matrix in term of the  $M$ -by- $M$ . The diagonal terms of the resulting matrix are the variance of exacting measurement. The off diagonal terms of the matrix are the covariance between the measurements.

Since the covariance matrix is a square in term of the  $M$ -by- $M$ , this matrix can be used to calculate the eigenvector and eigenvalue. The eigenvector and eigenvalue give quite different values for eigenvalues. So the eigenvector with highest eigenvalue represent the principal components of the data set.

After getting the eigenvectors of the covariance matrix, they ordered by eigenvalues, highest to lowest. If the lesser significant component ignored this lead to losing some information, but if the eigenvalues are small, there have not much lost in information. Leave out some information lead to reduction in data set dimension.

Considering some of eigenvectors from the list of eigenvectors, and forming a matrix with these eigenvectors in term of columns, gives a matrix of vector (feature vector). Finally to get the PCA filtered of the data set  $X$ , the data mean-adjusted matrix of each axial line was projected onto the selected basis function, as described by

$$Y = P * X \quad (6.9)$$

Where,  $Y$  represent the final filtered data set,  $P$  is the matrix with eigenvectors in columns transposed so that the eigenvectors are now in the rows, with the most significant eigenvector at the top and  $X$  is the mean-adjusted data transposed.

## 6.4 Cluttering with ICA

There are several transformation methods proposed for data analysis and finding a suitable representation of the multivariable data such as PCA. A recent developed transform method is independent component analysis (ICA), which is used to minimize the statistical dependent of the component of the representation. Our goal is to use ICA to estimate the original data set of mixed data with clutter noise. In other words separate the clutter from the blood flow data. This is referred to as the blind source separation (BSS) problem [20, 136, 137].

ICA technique based on non-Gaussianity and use higher order statistics rather than second order to separate the signal from the clutter [20, 138]. Beside the non-Gaussian, ICA assumes the components to be independent [139]. This is powerful and attractive set of assumption that make ICA very aggressive tasks, however, ICA treat the observed signal as a set of random variables without considering the dependency of adjacent time point.

Since ICA uses higher order statistics rather than second order moments to determine the basis vectors that are statistically independent as possible, ICA can consider as an extension of PCA [138, 140]. This made ICA gives a better separation result in most applications. A fast fixed-point algorithm (FastICA) for Matlab is a program package used for implementing ICA [20, 140]. The first step in ICA is whitening (sphere) the data. Before applying the ICA to the data and after centering, the observed vector transformed linearly so as to obtain a new vector that is white, its component uncorrelated and their variance equal to unity (the covariance of a new vector equals the identity matrix). The covariance matrix expressed as:

$$E\{\hat{x}\hat{x}^T\} = I \quad (6.10)$$

Several methods proposed for whitening, the most popular used is eigenvalue decomposition (EVD) of the covariance matrix

$$E\{xx^T\} = EDE^T \quad (6.11)$$

Where,  $x$  is the observed vector,  $\hat{x}$  is a new vector,  $E$  is the orthogonal matrix of eigenvectors of  $E\{xx^T\}$  and  $D$  are the diagonal matrix of its eigenvalues. The whitening expressed by:

$$\bar{x} = ED^{-1/2}E^T x \quad (6.12)$$

Dimension reduction was performed, besides whitening the data, the reduction done by discarding the small eigenvalues, which perform in statistical technique of PCA. Three conventional methods can be used for utilizing higher-order information. The projection pursuit technique was used to find linear combinations of maximum non-Gaussianity. The central limit theory shows that the distribution of a sum of independent random variables tends toward a Gaussian distribution. Thus, a sum of two independent random variables usually has a distribution that is closer to Gaussian than any of the two original random variables. The non-Gaussianity was measured for solving the ICA problem, several methods proposed for measuring non-Gaussianity. The classical measure of non-Gaussianity is kurtosis or fourth-order cumulant. Kurtosis is zero for Gaussian random vector and nonzero for non-Gaussian random vector. Kurtosis can be positive or negative. The Kurtosis principle is maximized by applying the FastICA algorithm, to estimate the independent component.

## 6.5 Cluttering with Non-adaptive Filters

The non-adaptive filters FIR, IIR and PR used for cluttering the Doppler signals were designed using the parameters presented in table 6.2. The filter designed to give same characteristics.

Table 6.2. FIR, IIR and PR filters design parameters

Filter Type	Order	Cutoff frequency	Maximum $d_p$	Minimum $d_s$
FIR	5	$0.09 \pi$	-0.5	- 80
IIR	3	$0.2 \pi$	-0.5	-
PR	2	-	-	-

## 6.6 Clutters Evaluation

The proposed methods for Doppler signal clutter compared with present clutter rejection methods. The present filters designed using the parameters illustrated in table 6.2 to achieve filters with the same characteristics. Root mean square deviation (RMSD) or root mean square error (RMSE) and error are commonly used to measure the differences between values predicted by a model or an estimator and the values truly observed. RMSE and error are a good measure of accuracy. The accuracy of each method was computed, the result from the proposed methods compared with the result from present cluttering methods.

The error was calculated by subtracting the output signal from clutter filter with the input signal to the clutter filter. The error calculated using the following expression:

$$Error = f(i, j) - g(i, j) \quad (6.13)$$

RMSE was computed using the following expression:

$$MSE(f, g) = \frac{1}{mn} \sum_{i=0}^{m-1} \sum_{j=0}^{n-1} [f(i, j) - g(i, j)]^2 \quad (6.14)$$

$$RMSE(f, g) = \sqrt{MSE(f, g)} \quad (6.15)$$

Where,  $f$  is the reference matrix signal,  $g$  is the output signal from the clutter filter and mean square error (MSE) is the square of the difference.

Beside the error also the performance used to evaluate the clutter rejection filters. The performance categorized from 1 to 5, the clutter with highest performance gives lower error and the clutter with lower performance gives highest error value.

# Chapter 7

## Experimental Results and Discussions

We will discuss the result of the reconstruction using different CS reconstruction algorithms, parallel computing algorithm and the cluttering using different clutters types. The performance of each algorithm is analyzed. At the end of section one the result from the algorithms used for Doppler signal reconstruction were compared. In section two filters are investigated to suppress the clutter from real and simulation Doppler ultrasound signal. The performance of each clutter was evaluated. The result of present clutter methods was compared with the proposed clutter methods. Parts of the experimental results shown in this thesis are already published [117, 118] and others are submitted for publication in [143 - 145].

### 7.1 Reconstructions Results

The reconstruction performs using four different reconstruction algorithms,  $\ell_1$  Minimization, OMP, CoSaMP and ROMP, their result is as follows.

#### 7.1.1 $\ell_1$ Minimization

Doppler ultrasound signal was nonuniformly sampled in a random and then reconstructed using CS via  $\ell_1$  minimization to regenerate the Doppler ultrasound spectrogram from much fewer samples. The measurement model is:  $f = A x$ , where  $f$  is the  $M \times 1$  vector containing the compressive measurements, and  $A$  is the  $M \times N$  measurement matrix. Using the  $M$  measurement in the first basis given the sparsity property on the other basis, the original signal was recovered by using convex optimization recovery algorithm ( $\ell_1$  minimization) expressed as  $\min \|x\|_{\ell_1}$  subject to

$\|Ax - f\|_{\ell_1} \leq \varepsilon$ . The numbers of measurements used for reconstruction are 5%, 20%, 40%, 60% and 80%.

Solving the linear system by using  $\ell_1$ -norm minimization, gives the reconstructed signal  $\hat{x}$ , which is used to generate the recovered Doppler sonograms. Both reconstruction and Doppler spectrogram were performed with software program written in Matlab (Mathworks, MA).

The resulting signal  $\hat{x}$  used to generate the Doppler ultrasound spectrograms shown is figure 7-1. The result shows that the Doppler spectrogram has been reconstructed successfully by using a few numbers of measurements with compressed sensing theory using convex optimization ( $\ell_1$ -norm minimization) algorithm with a good quality.

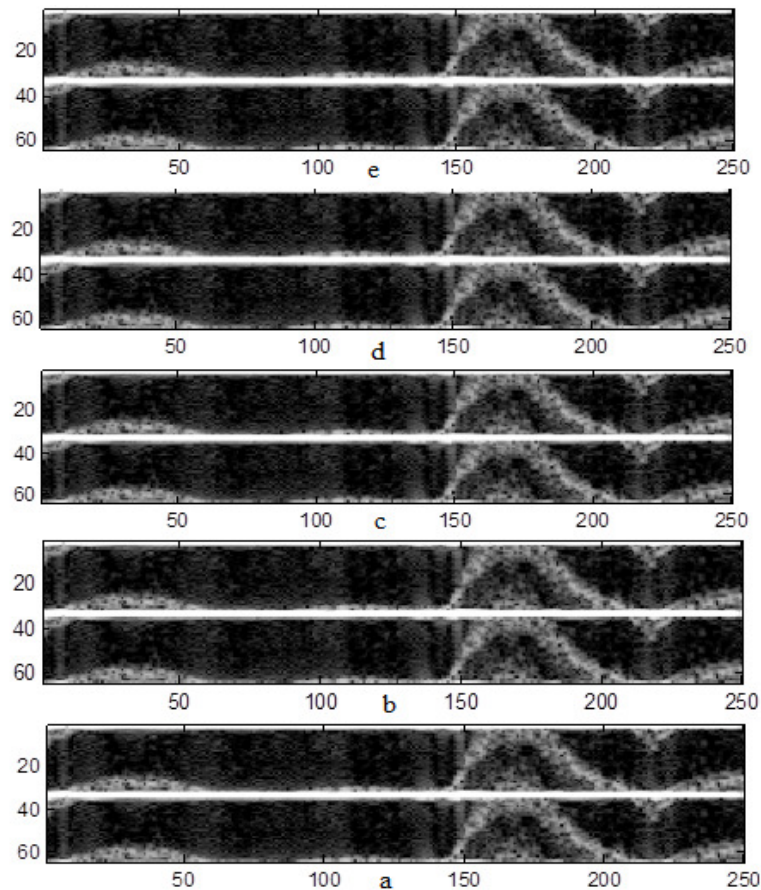


Figure 7-1. Reconstructed Doppler spectrogram via  $\ell_1$ -norm using different number of measurements (a) using 5% points (b) using 20% points (c) using 40% points (d) using 60% points (e) using 80% points

The recovered images were evaluated by calculating the error between each reconstructed and original image, peak signal-to-noise ratio, root mean square error and the reconstruction time.

The error between the original and the recovered image was calculated, the results shown in figure 7-2. The result shows that the error decreased by increasing the numbers of measurements, the reconstructed image with 5% of the data gives error higher than that given when 80% of the data were used.

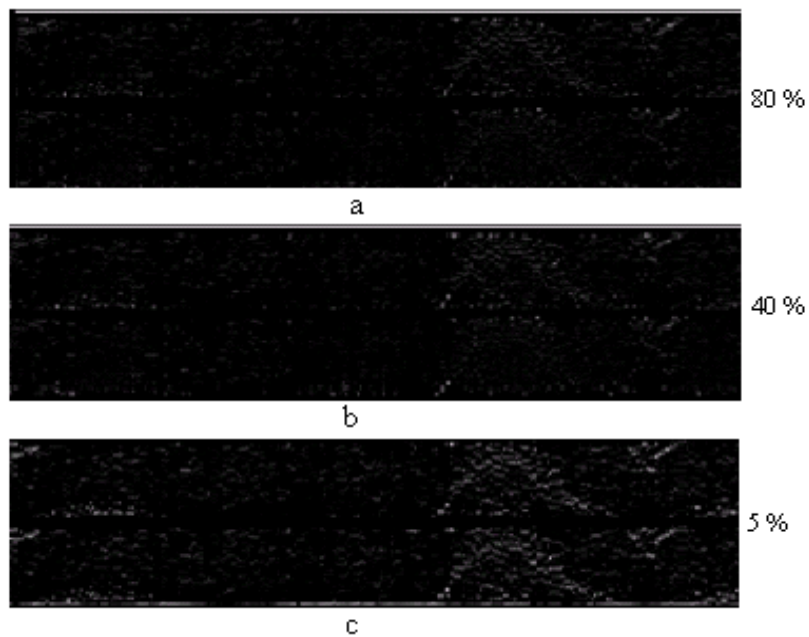


Figure 7-2. The error of the reconstructed image via  $\ell_1$ -norm (a) using 80% (b) using 40% (c) using 5%

The reconstruction time calculated by running the program several times, for each number of measurements and then the average from each was calculated. The result shows that when a few numbers of measurements used the time was low, the reconstruction time increased by increasing the number of measurements. The higher number of measurements 80% gives higher recovery time about 9.044 second and 5% of the data gives 4.855 second. Figure 7-3 illustrated the reconstruction time for different numbers of measurements.

The number of iterations at each number of measurements used for reconstruction was registered. The process was repeated several times and the average was calculated at each measurement. The result shows that there is no significant difference in the number of iterations by using different numbers of measurements. The difference in the time is related to the time between iterations during the process, when we used few numbers of measurements the time interval during the process is low, but the large number measurements take longer time. The iteration was calculated for reconstruction with  $\ell_1$  minimization algorithm only. The result of iteration using different number of points illustrated in table 7.1.

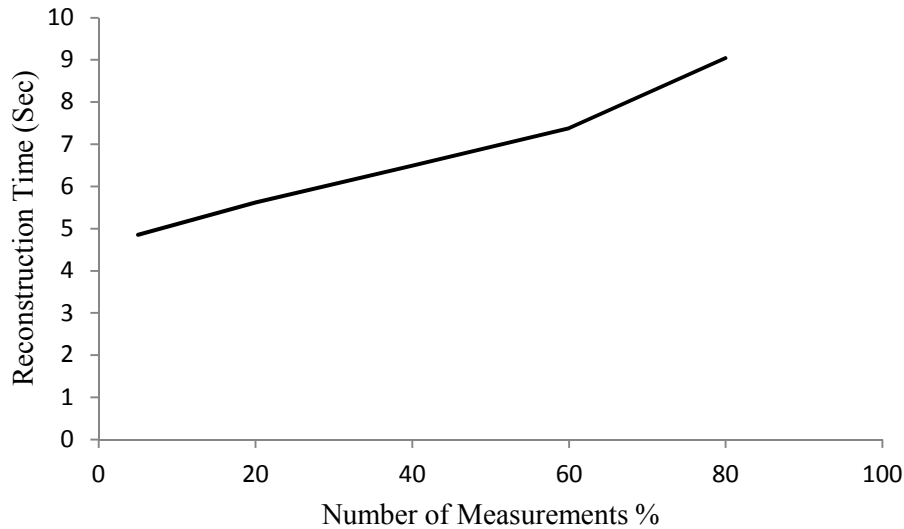


Figure 7-3. Number of measurements vs reconstruction time

The accuracy of the recovered images evaluated by calculating peak signal-to-noise ratio for each recovered image, the PSNR result was shown in figure 7-4. The result shows that the PSNR increased by increasing the number of measurements, the PSNR reaches up to 30 dB when 80% of the data were used. The quality of the reconstructed images that gives high PSNR are better than that gives low PSNR.

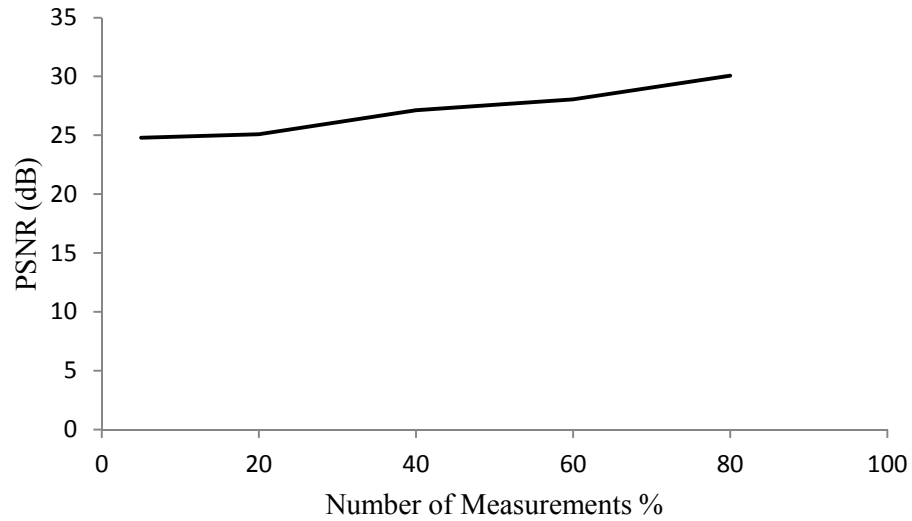


Figure 7-4. Number of measurements versus PSNR

The root mean square error is one of the most important measurements used for evaluating the accuracy of the recovered images. The RMSE calculated from the reconstructed image using different numbers of measurements sampled randomly, and was found that 80% point of the sample gives lower RMSE and for fewer number of point values increased and reach up-to 14.7 when 5% points were used. Figure 7-5 shows the RMSE using different numbers of measurements, the figure shows that the value decreased by increasing the number of points used for reconstructing. Table 7.1 shows the relation between the number of measurements versus recovery time, RMSE and PSNR.

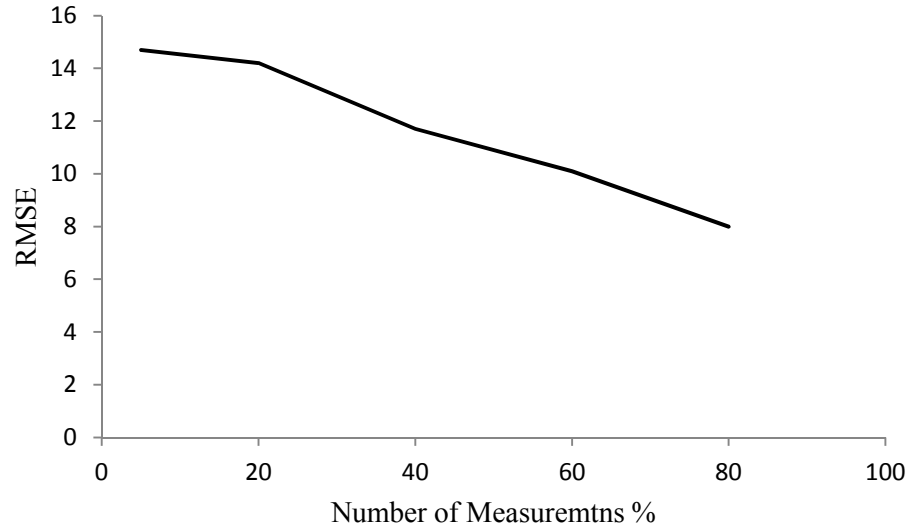


Figure 7-5. Number of measurements versus RMSE

Table 7.1. Number of points, Recovery time, MSE, number of iteration, RMSE and PSNR

Number of measurements %	5	20	40	60	80
Elapsed time (s)	4.855	5.619	6.494	7.377	9.044
MSE	216.09	201.64	136.89	102.01	64
RMSE	14.7	14.2	11.7	10.1	8
PSNR	24.78	25.08	27.14	28.04	30.08
Iteration	16	18	18	16	18

### 7.1.2 Orthogonal Matching Pursuit

The experiment conducted using Doppler ultrasound imaging RF data of length 2032 points. Reconstruction of the Doppler ultrasound data was performed by using Orthogonal matching pursuit algorithm, which is used to identify the nonzero elements of the signal in an iteratively and reconstruct the signal using the pseudo-inverse. The Doppler data sampled randomly, different number of measurements  $M$  was used for reconstruction. Both reconstruction and Doppler spectrogram were performed with software program written in Matlab (Mathworks, MA).

The recovered signals via OMP were used to generate a Doppler ultrasound spectrogram, the result illustrated in figure 7-6. The result shows that the spectrum was reconstructed perfectly even by using a few numbers of measurements.

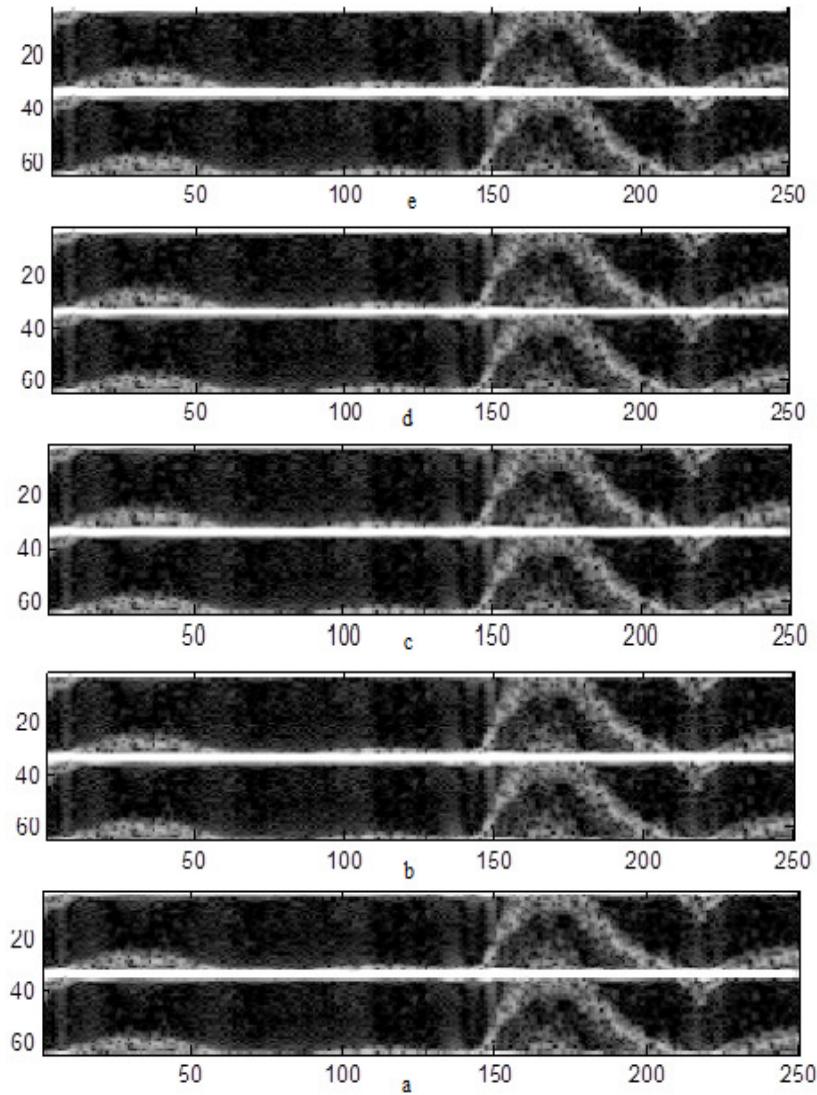


Figure 7-6. Reconstructed Doppler spectrogram via OMP algorithm using different number of points (a) using 5% points (b) using 20% points (c) using 40% points (d) using 60% points (e) using 80% points

The error from the recovered images was calculated to compare to the original image, the result shown in figure 7-7. The result shows that the error in the image decreased by

increasing the number of measurements, the image reconstructed with the number of measurements equal 80% point has a lower error. From the figure, comparing the images in figures (c) and figure (b), the result shows that there is no significant difference between them and comparing figure (a) and figure (c), the result shows a variation between the two images.

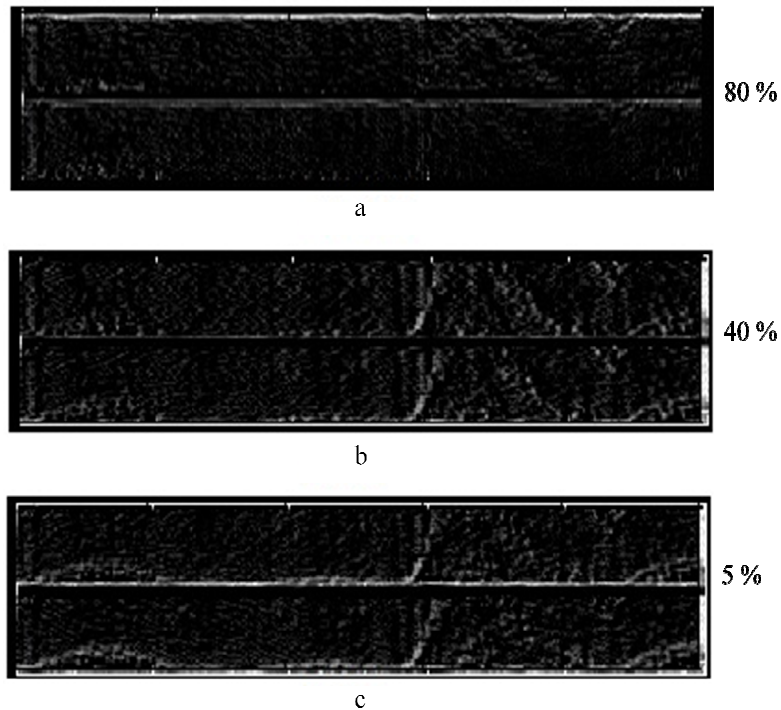


Figure 7-7. The error of the reconstructed image via OMP algorithm (a) using 80% (b) using 40% (c) using 5%

The process time was calculated for different random samples of measurements, the elapsed time shown in figure 7-8. The result shows that when numbers of measurements equal to 5% were used, the elapsed time was about 0.6 seconds and when 80% were used, the elapsed time was about 1.8 second. This indicates that the lower number of points performed faster. At each number of measurements the program runs several times to calculate the reconstructed time, and then the average was calculated.

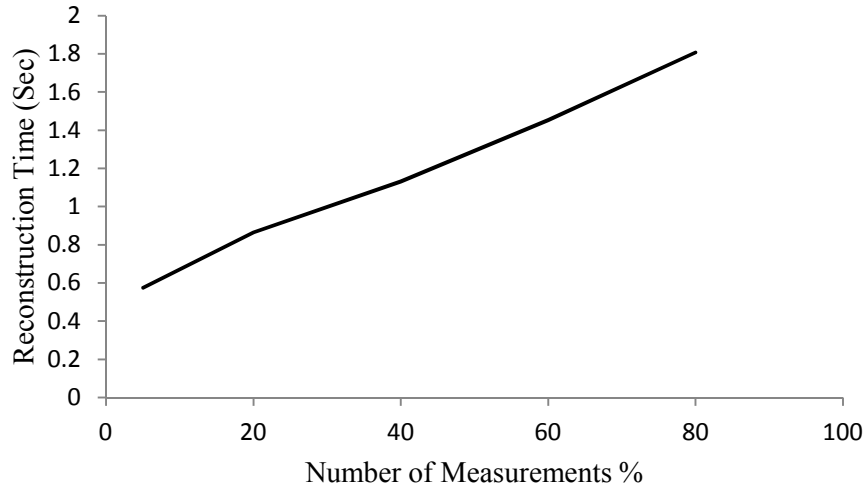


Figure 7-8. Number of measurements vs reconstruction time

The analysis of the results was performed by calculating the PSNR from each recovered image for different random sample measurements compared to the original spectrogram images, PSNR result shows that the reconstructed image with fewer number of measurements 5% has less PSNR and higher number of measurements 80% gives higher PSNR. This indicates that the quality of the image increased by increasing the number of measurements. Figure 7-9 shows the relation between the numbers of measurements and PSNR in dB.

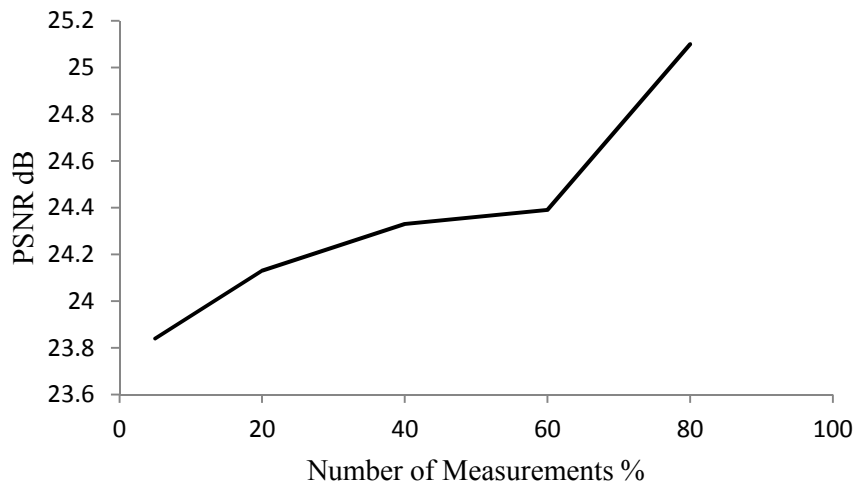


Figure 7-9. Number of measurements versus PSNR

The root mean square error is one of the most important measurements used for evaluating the accuracy of the recovered images. The RMSE calculated from the reconstructed image by using different numbers of measurements sampled randomly, and was found about 25.1 dB for 80 % (1600) point of sample and for fewer number of point values increased and reach up-to 23.84 for 5 % (101) point of the sample. Figure 7-10 shows the RMSE for different numbers of measurements, the figure shows that the value decreased by increasing the number of points used for reconstructing.

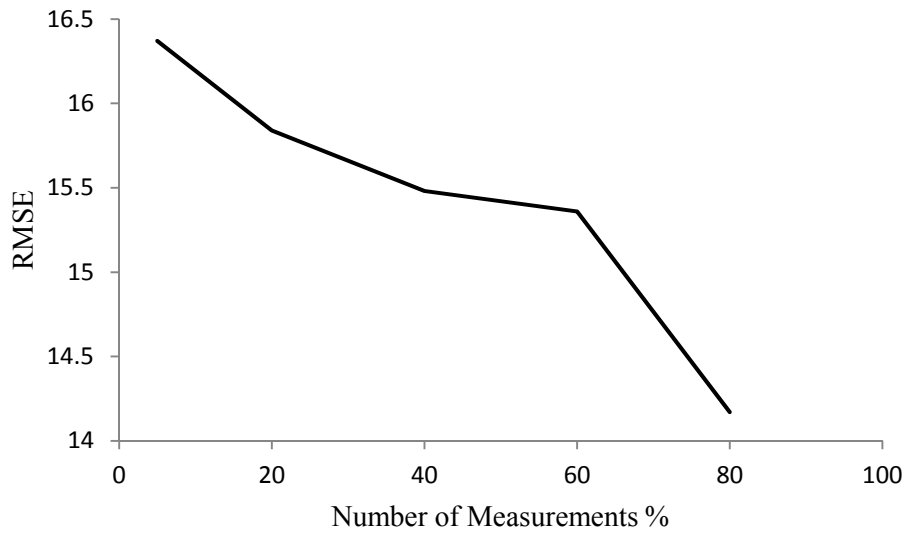


Figure 7-10. Number of measurements versus RMSE

Table 7.2 shows the relation between the number of measurements versus recovered time and number of measurements versus NRMSE.

Table 7.2. Number of points, Recovery time, MSE, RMSE and PSNR from OMP algorithm

Number of measurements %	5	20	40	60	80
Elapsed time (s)	0.575	0.865	1.131	1.453	1.807
MSE	267.48	250.45	239.84	236.13	200.9
RMSE	16.37	15.84	15.48	15.36	14.17
PSNR dB	23.84	24.13	24.33	24.39	25.1

### 7.1.3 Compressive Sampling Matching Pursuit

The experiment validates with using Doppler ultrasound RF data with a length of 2032 points. Reconstruction of the Doppler ultrasound data performed by using compressive sampling matching pursuit algorithm, which is used to identify the nonzero elements of the signal in an iteratively and reconstruct the signal using the pseudo-inverse. The data with a length of 2032 sampled randomly, different number of measurements  $M$  was used for reconstruction. Both reconstructions and Doppler spectrum were performed with software program written in Matlab (Mathworks, MA).

The recovered signal illustrated in Figure 7-11. The Doppler ultrasound signal recovered using different number of measurements, which is used then to generate Doppler spectrum. The recovered signal was performed via CoSaMP algorithm. The result shows that the spectrum was reconstructed with good performance even by using a few numbers of measurements.

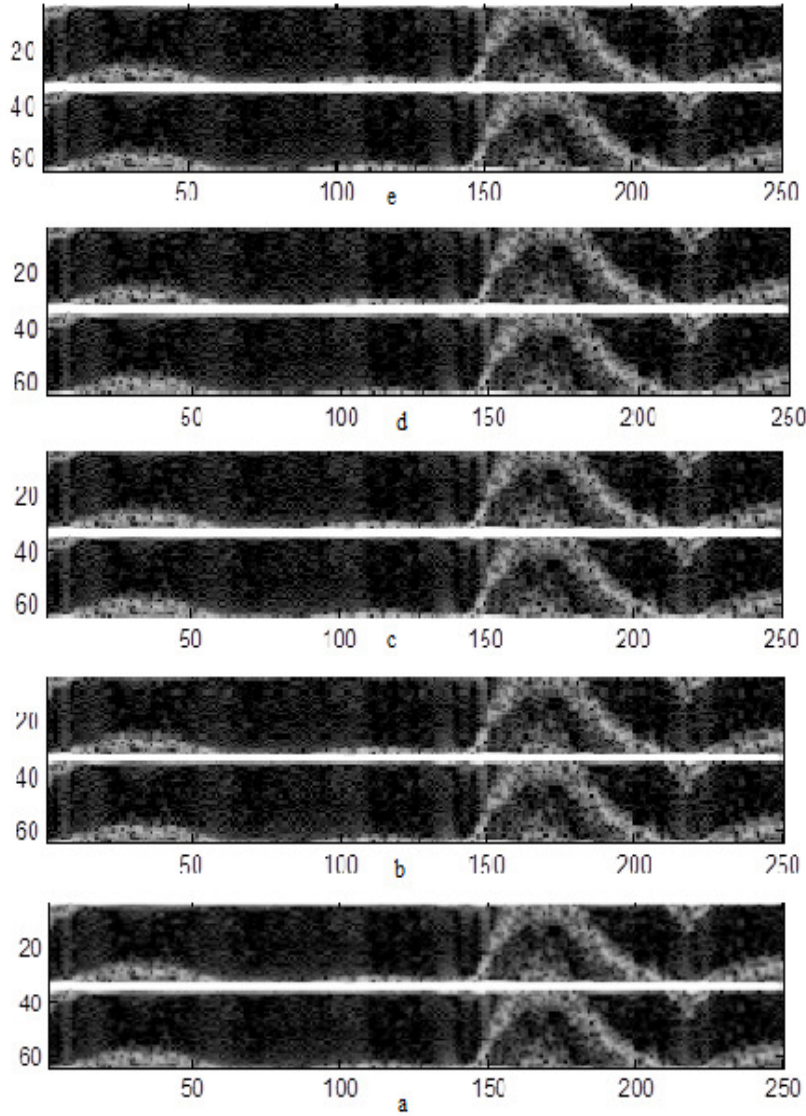


Figure 7-11. Reconstructed Doppler spectrogram via CoSaMP algorithm using different number of points (a) using 5% points (b) using 20% points (c) using 40% points (d) using 60% points (e) using 80% points

The error from the result images were calculated by subtracting the recovered image from the original image, the results were shown in figure 7-12. The result shows that the error in the image decreased with increasing the number of measurements. Image reconstructed with the number of measurements equal to the 80% point gives error lower than that reconstructed with the number of measurements equal to 5% points. This result will be judged by quantitative evaluation.

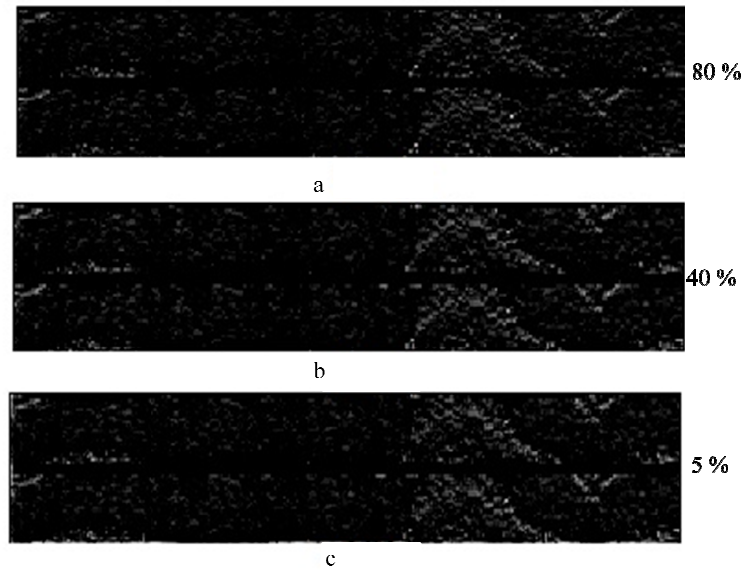


Figure 7-12. The error of the reconstructed image via CoSaMP algorithm (a) using 80% (b) using 40% (c) using 5%

The process time was calculated for different random samples of measurements, the elapsed time shown in figure 7-13. The result shows that when the lower number of measurements used the elapsed time was very low and when higher numbers of measurements used the elapsed time was becoming higher. This indicates that the lower number of points performed faster.

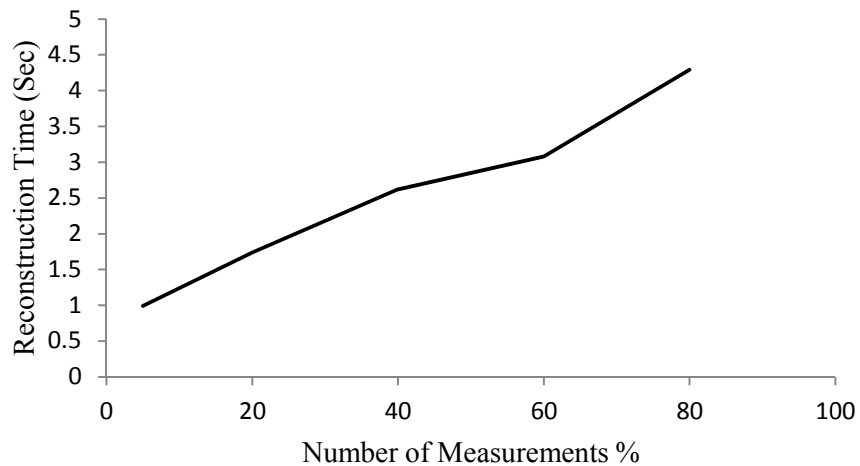


Figure 7-13. Number of measurements versus recovery time

Root mean square error (RMSE) is one of the most important measurements used for evaluating the accuracy of the recovered signals and images. The RMSE calculated from the reconstructed image by using different numbers of measurements sampled randomly, and was found that the RMSE when higher numbers of measurements were used gives lower error, when fewer numbers of points used for the reconstruction the images, the error increased by increasing the point numbers. Figure 7-14 shows the RMSE for different numbers of measurements, the figure shows that the value increased by decreasing the number of points used for reconstructing; so we can conclude that with compressed sensing we can achieve a comparable RMSE even with a very low number of points.

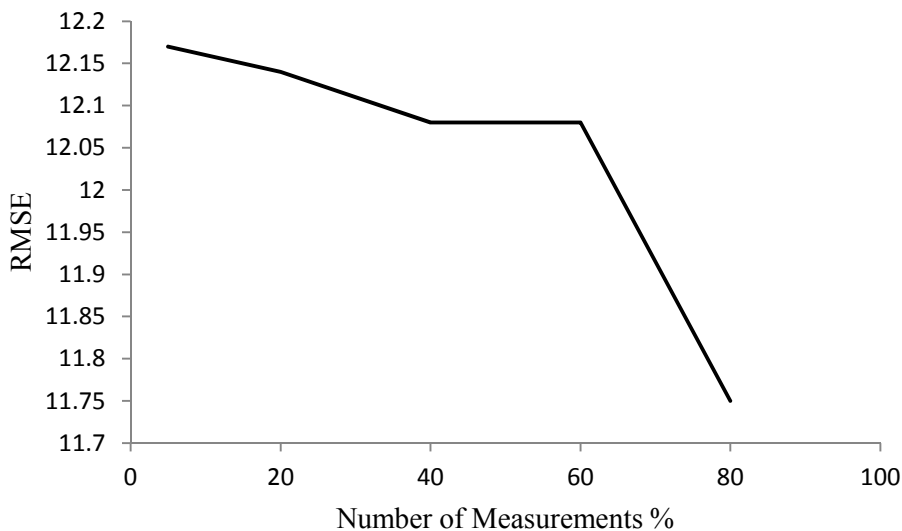


Figure 7-14. Number of measurements versus RMSE

The peak signal-to-noise for the reconstructed images was calculated for different random number of points compared to the original image. The results show that the reconstructed image with fewer numbers of measurements gives lower PSNR, and it increased by increasing the number of points used for reconstruction. This indicates that the quality of the image increased by increasing the number of measurements. Figure 7-15 shows the PSNR uses different numbers of measurements.

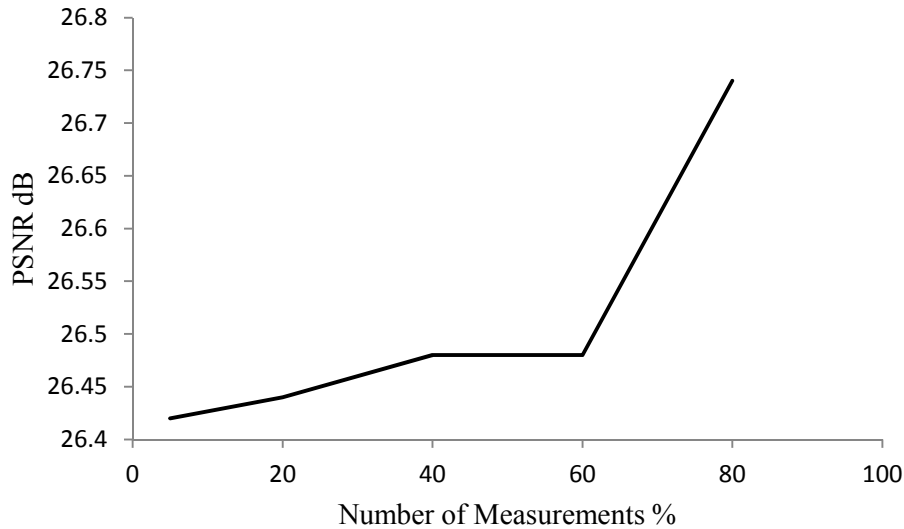


Figure 7-15. Number of measurements versus PSNR

Table 7.3. Shows the peak signal to noise ratio, process time, mean square error, root mean square error versus different numbers of measurements

Table 7.3. Number of points, Recovery time, MSE, RMSE and PSNR from CoSaMP algorithm

Number of measurements %	5	20	40	60	80
Elapse time (sec)	0.99	1.74	2.62	3.08	4.29
MSE	148.2	147.4	146.0	146.0	137.4
RMSE	12.174	12.142	12.084	12.084	11.725
PSNR dB	26.422	26.445	26.487	26.487	26.748

### 7.1.4 Regularized Orthogonal Matching Pursuit

The experiment validated using Doppler ultrasound imaging spectrogram. ROMP algorithm used to identify the nonzero elements of the Doppler signal. The data of length 2032 sampled randomly, different number of measurements  $M$  were used for reconstruction (128, 406, 812, 1219 and 1625 points). Both reconstructions and Doppler spectrum were performed with software program written in Matlab (Mathworks, MA).

Doppler ultrasound signal recovered using different number of measurements, the result signal then used to generate Doppler spectrogram. The reconstruction performed via ROMP algorithm, the resulting spectrogram shown in figure 7-16. The result shows that the spectrum was reconstructed even with a few numbers of measurements.

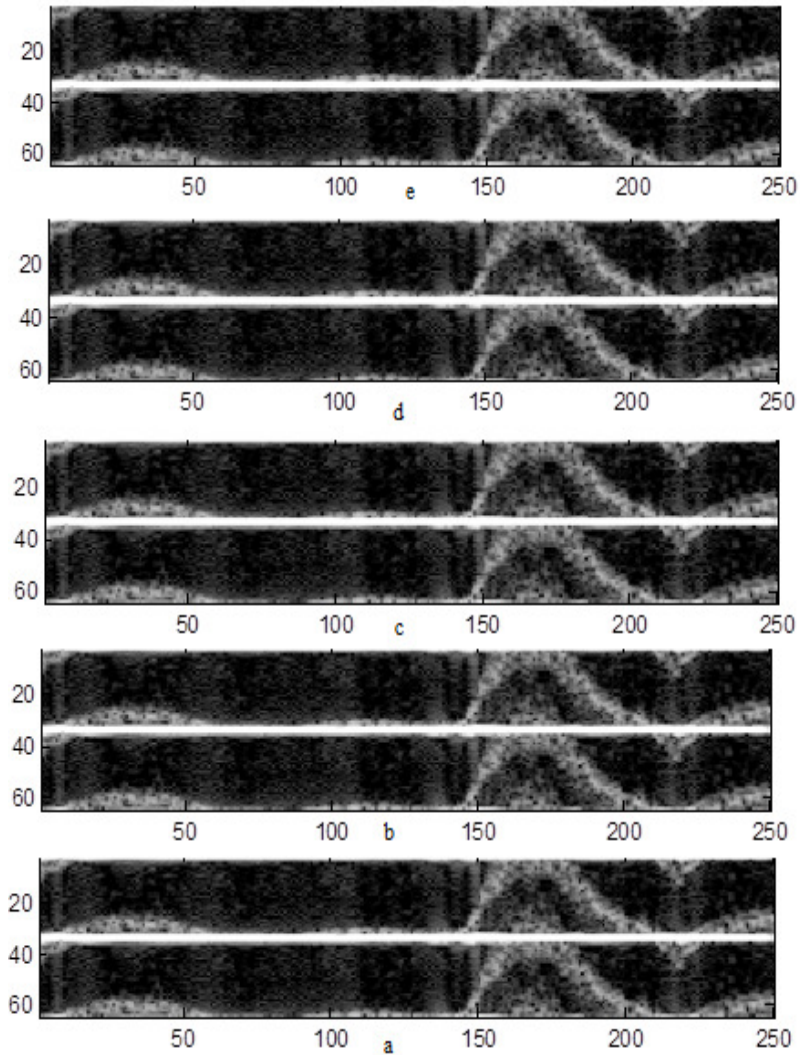


Figure 7-16. Reconstructed Doppler spectrogram via ROMP algorithm using different number of points (a) using 5% points (b) using 20% points (c) using 40% points (d) using 60% points (e) using 80% points

The error from the recovered images was calculated to compare to the original image, the result shown in figure 7-17. The result shows that the error in the image decreased by

increasing the number of measurements, the image reconstructed with the number of measurements equal to the 80 % point has a lower error.

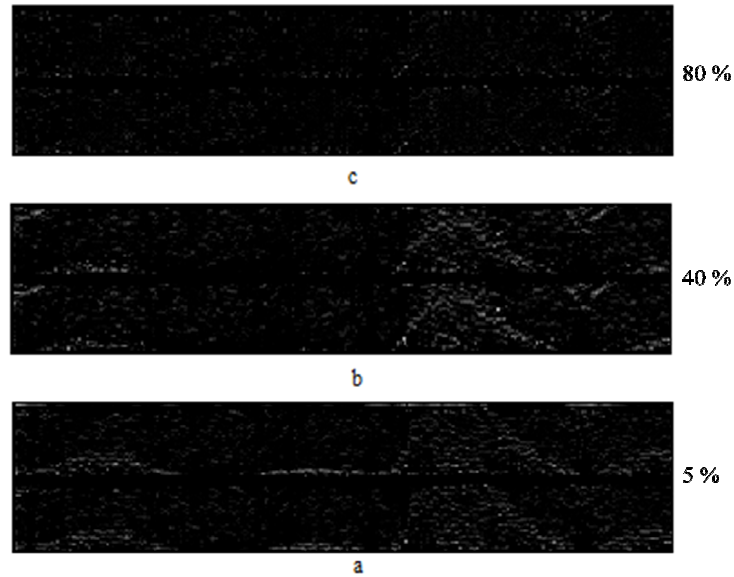


Figure 7-17. The error of the reconstructed image via ROMP algorithm (a) using 5 % (b) using 40 % (c) using 80 %

The process time was calculated for different random samples of measurements, the result of elapsed time shown in table 7.4 and figure 7-18. The result shows that when a few numbers of points were used, the reconstruction will be performed faster (take very low time) and when the higher numbers of points were used the reconstruction takes more time (the reconstruction time increased). In other word the reconstruction time decreased by decreasing the number of reconstruction points.

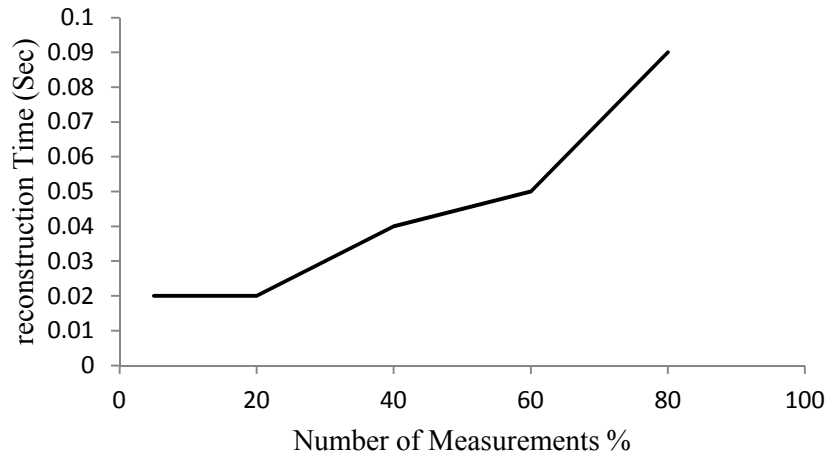


Figure 7-18. Number of measurements versus recovery time

The recovered images evaluated by calculating the RMSE for each, the result shown in figure 7-19. The result shows that when data less than 40 % used for reconstruction, there is no variation in the error. Higher numbers of measurements give low error it reached up to 8 when 80 % of data were used.

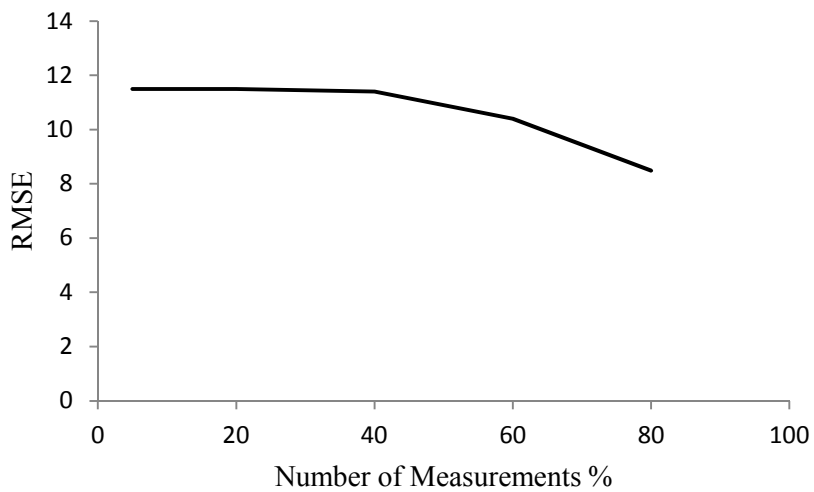


Figure 7-19. Number of measurements versus RMSE

The peak signal-to-noise for the reconstructed images was calculated for different random number of points compared to the original image. The results show that the

reconstructed image with fewer numbers of measurements gives lower PSNR, and it increased by increasing the number of points used for reconstruction, figure 7-20 shows the results. This indicates that the quality of the image increased by increasing the number of measurements. The figure shows that when using less than 40 % of the data for reconstruction, the PSNR are same, in the other word give images with the same quality. The quality improved when more than 60 % of the data were used for reconstruction. Table 7.4 shows the relation between the number of measurements versus reconstruction time, MSE, RMSE and PSNR. All the measurement in the tables calculated by running the program at each number of measurements many times and then calculates the average for each measurement.

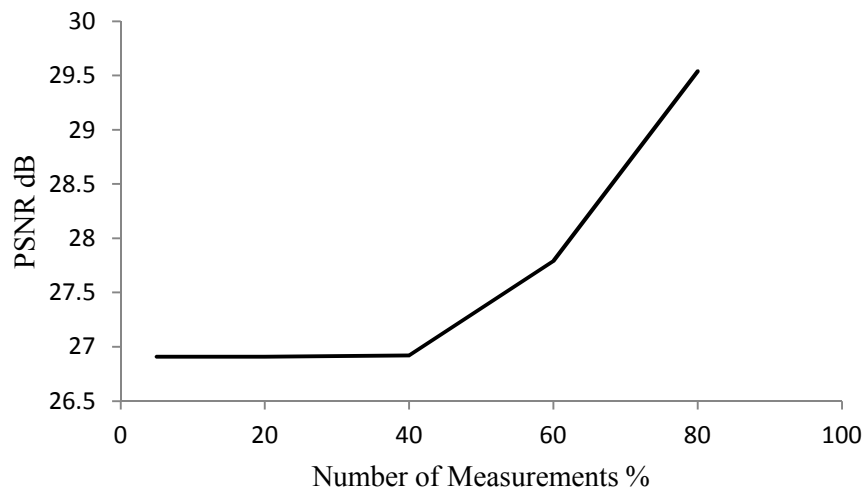


Figure 7-20. Number of measurements versus PSNR

Table 7.4 Number of points, Recovery time, MSE, RMSE and PSNR from ROMP algorithm

Number of measurements %	5	20	40	60	80
Elapse time (sec)	0.02	0.02	0.04	0.05	0.09
MSE	132.34	132.34	132.05	108.15	72.23
RMSE	11.5	11.5	11.4	10.4	8.49
PSNR dB	26.91	26.91	26.92	27.79	29.54

Using compressed sensing theory for Doppler spectrogram reconstruction, lead to reduction in acquisition time, decreased the number of samples, which is lead to decreasing in the average power per unit area. The quality of the generated spectrograms were visually judged by an expert monographer to be very close to the original in diagnostic quality and to have no missing diagnostic features.

From the performance evaluation, as a large number of measurements were used gives more information. However, using a large number of measurements is undesirable because increasing the number of measurements cause in increasing the process time and other acquisition problems. Thus compressed sensing can be considered as an effective tool for Doppler ultrasound data acquisition and can overcome all limitation of the present Doppler signal data acquisition.

The reconstruction time from the four algorithms were compared, the result shown in figure 7-21. The result shows that  $\ell_1$  minimization algorithms give higher reconstruction time among all the recovery algorithms considered in this thesis. The lowest reconstruction time obtained by regularized orthogonal matching pursuit algorithm. When a few numbers of measurements were used, compressive sampling matching pursuit gives reconstruction time closer to that from orthogonal matching pursuit. In general the reconstruction time increased with the amount of measurements, the fewer numbers of points reconstructed faster.

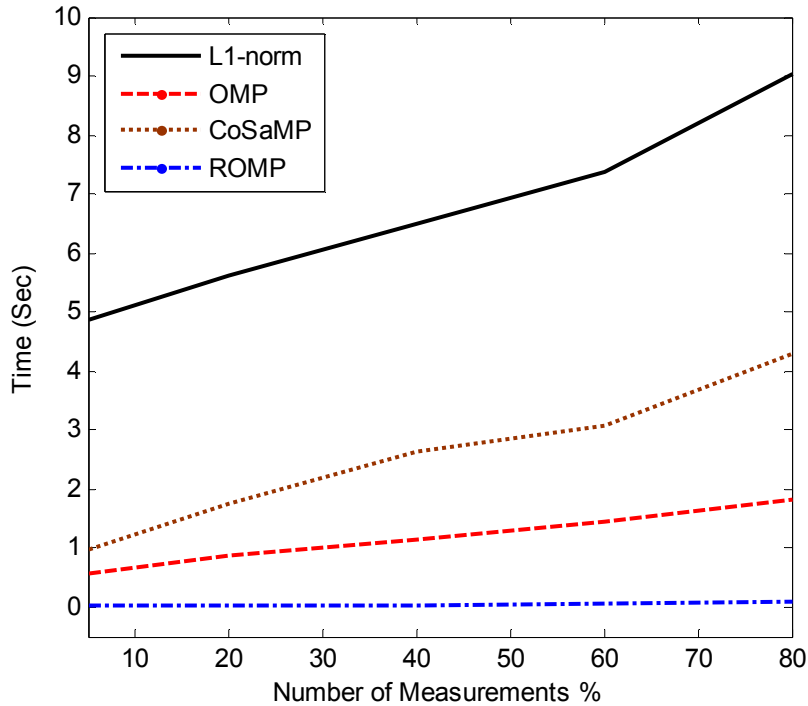


Figure 7-21. Number of measurements vs recovery time for different algorithms

The root mean square error from all algorithms also compared, the result illustrated in figure 7-22. The result shows that the OMP algorithm gives higher RMSE among all the others algorithms. When a few numbers of points used for the reconstruction ROMP gives lower RMSE, but when higher numbers of measurements were used  $\ell_1$  minimization gives the lowest error.  $\ell_1$ -norm and ROMP gives same RMSE when the reconstruction measurements used were about 50 %. There is no big variation in the error when a few numbers of measurements and higher numbers of measurements were used in CoSaMP algorithm.

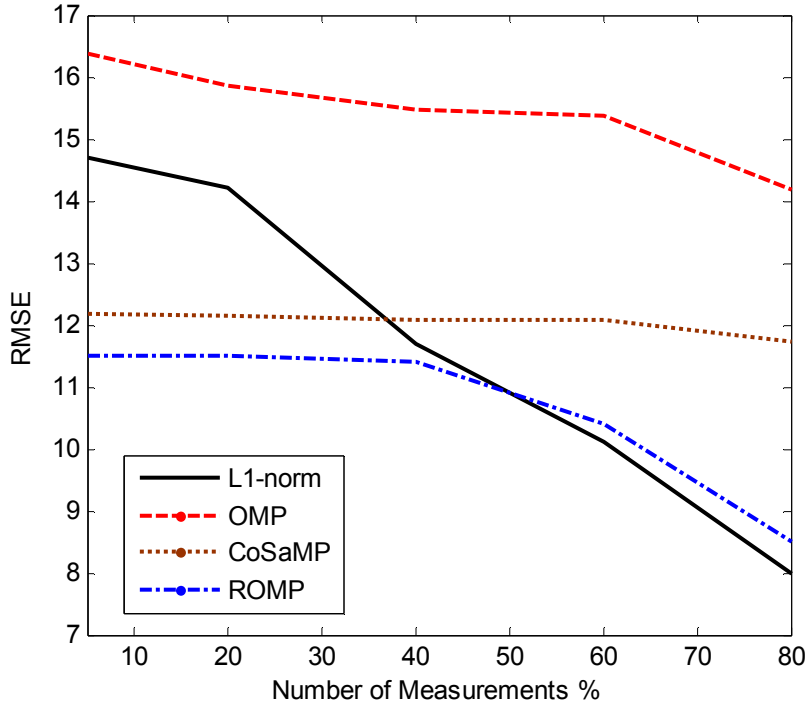


Figure 7-22. Number of measurements vs RMSE for different algorithms

Beside the time and RMSE also the quality of the reconstructed images was compared by comparing the PSNR from each reconstruction algorithm, the result shown in figure 7.23. From the figure the worst image quality was obtained when OMP used. For a few numbers of measurements (less than 30 %), regularized orthogonal matching pursuit give higher PSNR (best quality images), when higher numbers of measurements were used (higher than 40 %)  $\ell_1$ -norm gives the best results (higher PSNR). When the Doppler signal reconstructed via CoSaMP, the result shows that there is no significant difference when the Doppler signal reconstructed using a few numbers of measurements and higher number of measurements. The PSNR difference between the higher and lower numbers of measurements when CoSaMP used is 0.32 dB.  $\ell_1$ -norm and ROMP gives an image with same quality when the number of measurements used for the reconstructions are about 40 %. The quality of the reconstructed images increased by increasing the numbers of measurements and decreased by decreasing the numbers of measurements used for the reconstructions.

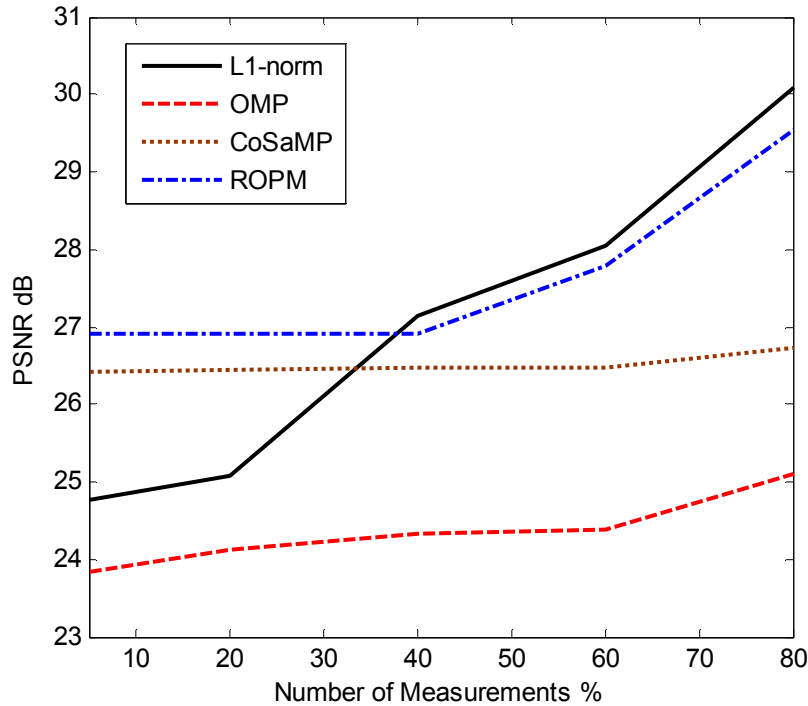


Figure 7-23. Number of measurements vs PSNR for different algorithms

## 7.2 Parallel Computing Results

Table 7.5 shows the reconstruction time for the Doppler ultrasound spectrogram by applying parallel algorithms. The reconstructions perform using different numbers of measurements and  $\ell_1$ -minimization ( $\ell_1$ -norm) reconstruction algorithm. As shown, using two cores leads to significant reduction in the reconstruction time per core, with speed up of about 3.25 for a few numbers of measurements and 2.55 for higher numbers of points. This leads us to expect that when more cores used for example four cores gives shortest reconstruction time.

Figure 7-24 shows the reconstruction time using serial parallel methods. The results show that the time reduced to less than half in all the numbers of measurements.

Table 7.5. The parallel reconstruction time and speed up for different number of measurements

Number of measurements %	5	20	40	60	80
Elapse time (s)	1.49	2.00	2.35	3.00	3.34
Speed up	3.25	2.80	2.76	2.45	2.55

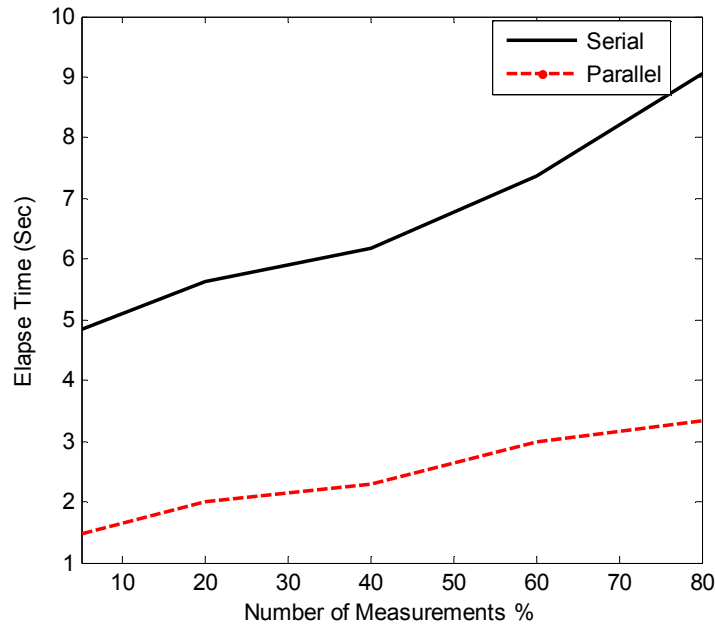


Figure 7-24. The reconstruction time with serial and parallel algorithms

## 7.3 Clutters Rejection Results

### 7.3.1 Simulation Results

In this section we want to describe the simulation result of our proposed clutter rejection filter based on ICA and PCA, beside the present cluttering algorithms. The Doppler IQ data consist of blood flow signal and clutter signal used. The clutter filter applied to this signal as described in chapter 6 so as to remove unwanted signal and remains the blood flow signal only. Our proposed clutter method applied to the Doppler IQ data. The result of the simulation shows that, when the proposed clutter with ICA and PCA used, the clutter suppressed from the Doppler signal effectively, the result signal

illustrated in figure 7-25 and 7-26 respectively, and we only display the first four signals for simplicity.

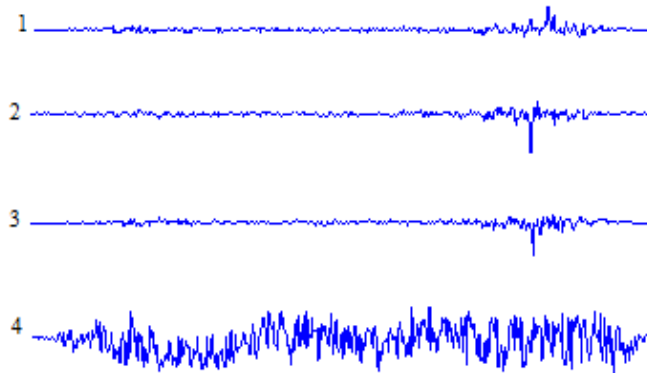


Figure 7-25. The filtered signal via ICA, in time domain.

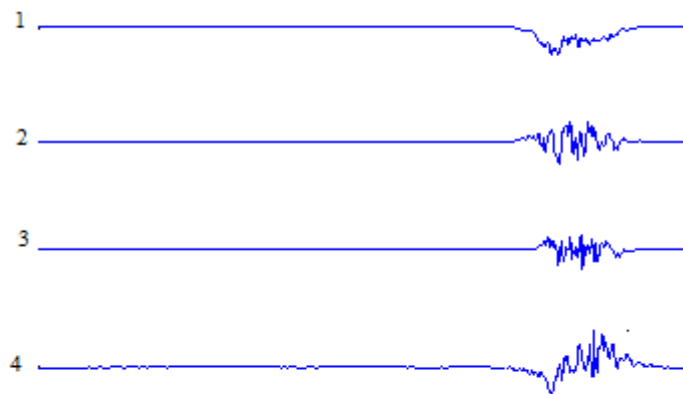


Figure 7-26. The filtered signal with PCA, in time domain.

The spectrum of the signal calculated from the filtered signal by using both ICA and PCA, the signal spectrum shown in figure 7-27 and 7-28 respectively.

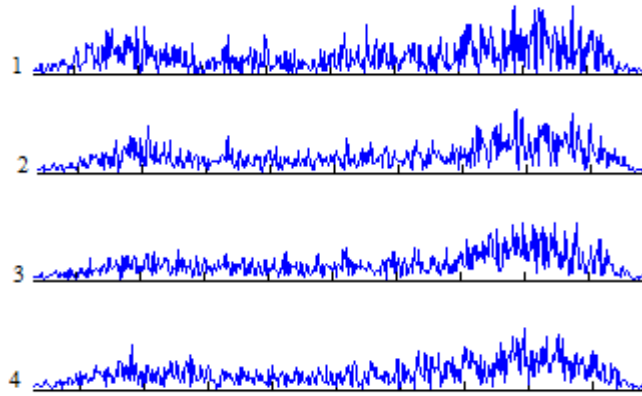


Figure 7-27. The spectrum of the signal filtered using ICA.

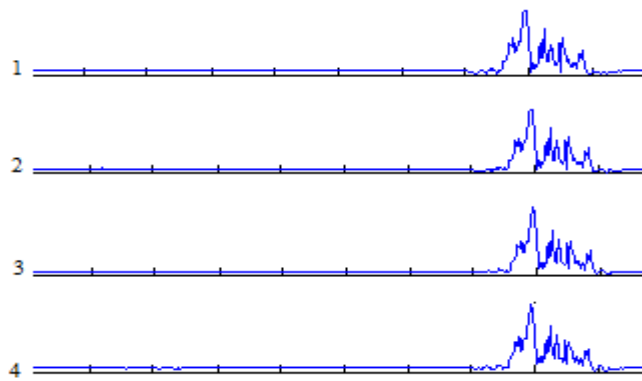


Figure 7-28. The spectrum of the signal filtered using PCA.

Beside our proposed method the Doppler IQ data filtered using present clutter rejection methods, FIR, IIR and PR filters. The result of present clutters illustrated in figures 7-29, 7-30 and 7-31 respectively. The result shows that all types of clutter filters are able to remove the clutter from the Doppler IQ data.

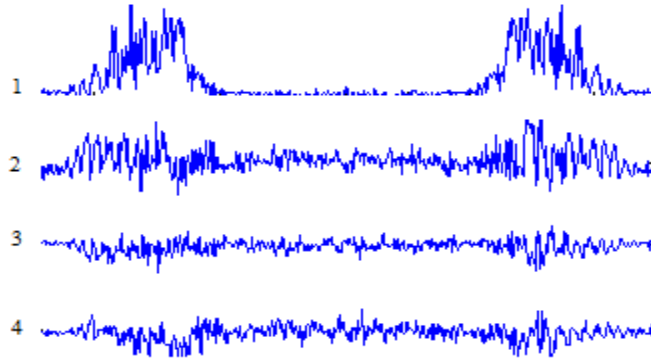


Figure 7-29. The filtered signal via FIR, in time domain

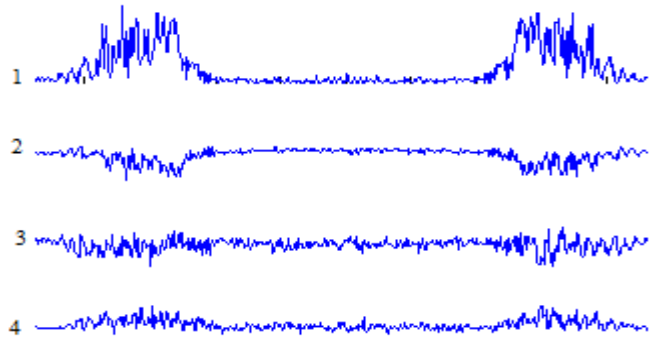


Figure 7-30. The filtered signal via IIR, in time domain

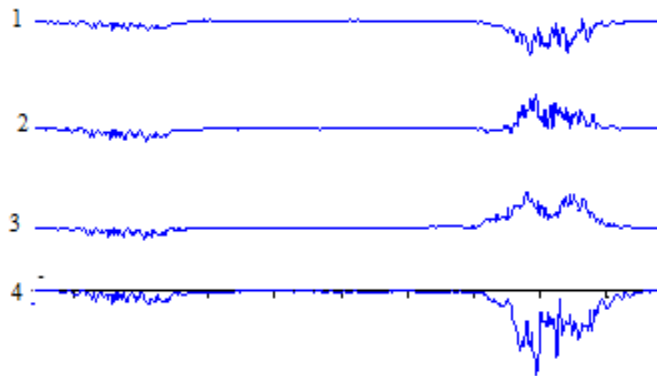


Figure 7-31. The filtered signal via PR, in time domain

The spectrum of the filtered signal was calculated from the output of the three types of filters, the result shown in figure 7-32, the result from FIR and PR only were shown.

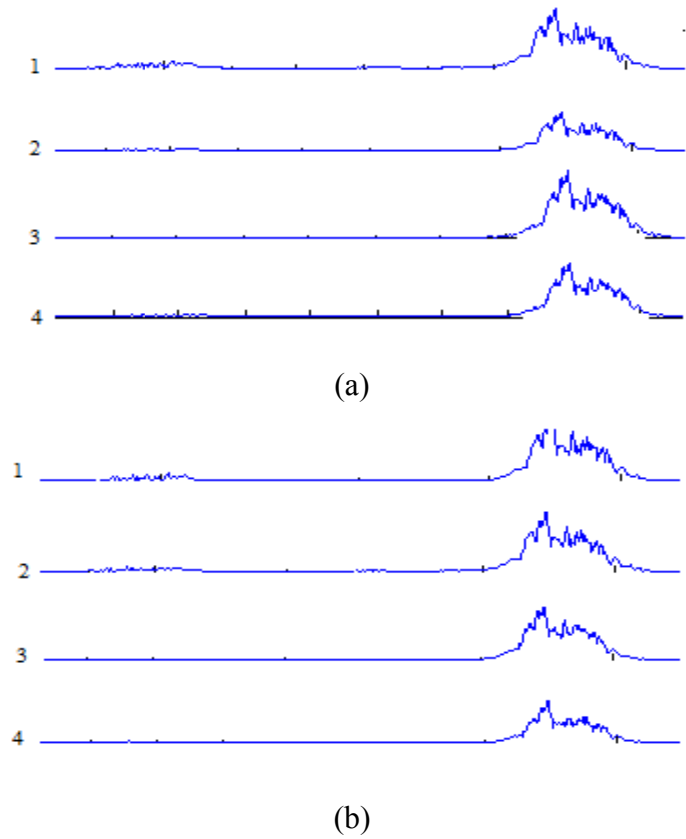


Figure 7-32. The spectrum of filtered signal (a) Using FIR and (b) using PR.

To make sure that the clutter signal was removed from our Doppler IQ data by using all five clutter rejection filters. The original Doppler IQ data was projected into the filter output data. The inner product results show the blood signal contaminated with clutter, the result shown in figure 7-33.

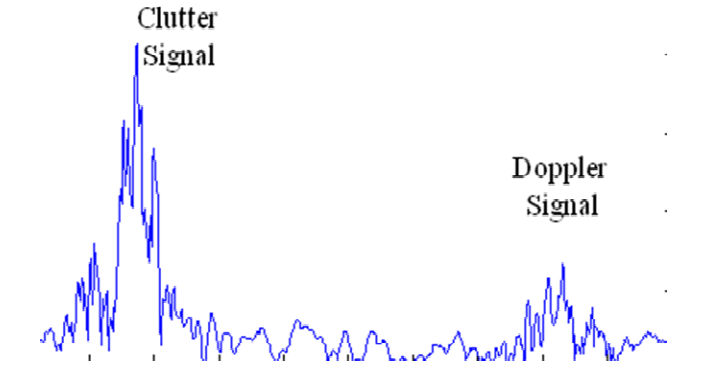


Figure 7-33. Doppler signal contaminated with clutter

To compare the propose clutter method using ICA and PCA with present clutter rejection methods, FIR, IIR and PR, root mean square deviation and error for each was computed. Since the clutter rejection characteristics differ from each other, performance of the clutter rejection methods also varies according to the clutter filter. The result shows that the proposed clutter based on ICA gives lower error values, while the proposed clutter based on PCA, gives error higher than that from ICA. The resulting error of PR using clutter space dimension given in table 6.2 is lower than FIR. FIR gives highest error value among all the clutters, the result of RMSE and error for different clutters illustrated in table 7.6. The table shows that there is an improvement on the error and the RMSE when the signal cluttered with the proposed clutter rejection filter. The performance categorized from 1 to 5, the clutter filter with highest performance has lower error and the clutter filter with lower performance has highest error value. Figure 7-34 shows the performance of the clutter filters, the better clutter rejection obtained by using ICA. PR clutter filter give the same performance as ICA when the filter designed with space dimension equal to 20, which is needed more calculations. When PCA used for filtering, the clutter was removed with performance lower than that obtained by using ICA. IIR give comparable clutter rejection. FIR gives a lower performance among all types of clutters. The propose clutter rejection method; suppress the clutter signal without altering the blood signal. The ICA and PCA give better performance when used for Doppler signal cluttering.

Table 7.6. The error and RMED for different types of clutters

Filter Types	FIR	IIR	PR	PCA	ICA
Error	$22.76 \times 10^8$	$10.5 \times 10^8$	$4.97 \times 10^8$	$7.91 \times 10^8$	$4.97 \times 10^8$
RMSD	80142.7	49578.5	32038	43684.1	32038
Categorization	1	3	5	4	5

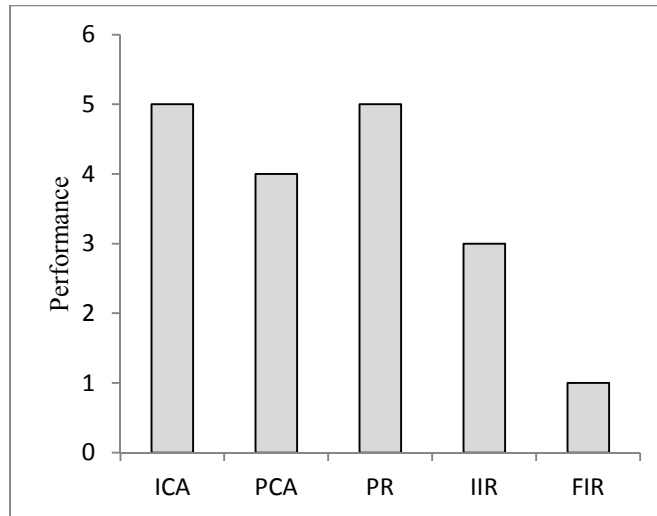
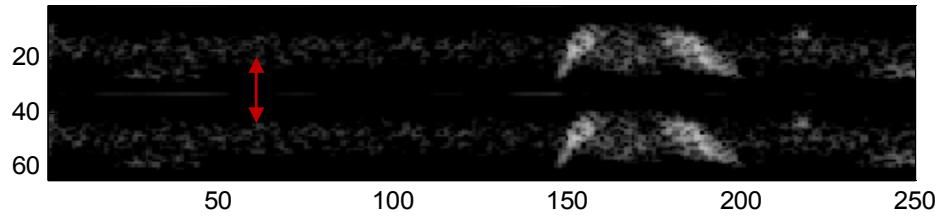


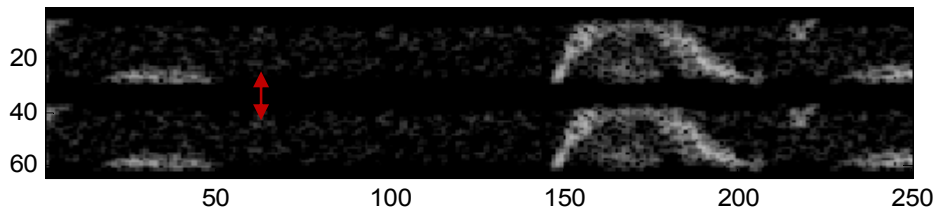
Figure 7-34. The performance of different clutter rejection

### 7.3.2 Real Doppler Data Results

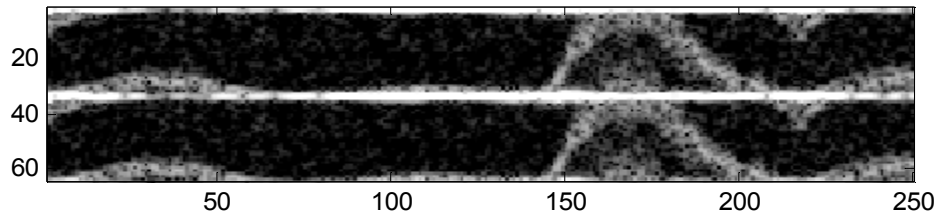
The experiments with the real Doppler data illustrated in figure 7-35. Figure 7-35 (a) demonstrates Doppler spectrogram image generated from Doppler data filtered by using minimum phase FIR filters. Wide clutter line presented down the center of resulting Doppler image, this indicates that FIR filter showed insufficient suppression of the clutter. Figure 7-35 (b) illustrates the Doppler spectrogram form data filtered via IIR filter where the clutter line is significantly reduced, this mean that the clutter removed with performance better than FIR. PCA gives an image with a clutter line down the center narrower than that from IIR filter; figure 7-35 (c) shows the result spectrogram image. When ICA and PR used for cluttering the result image illustrated in figure 7-35 (d, e), the resulting image has no clutter line around the image center. ICA, PR and PCA are able to eliminate all tissue motion clutter without significantly altering the blood flow estimation.



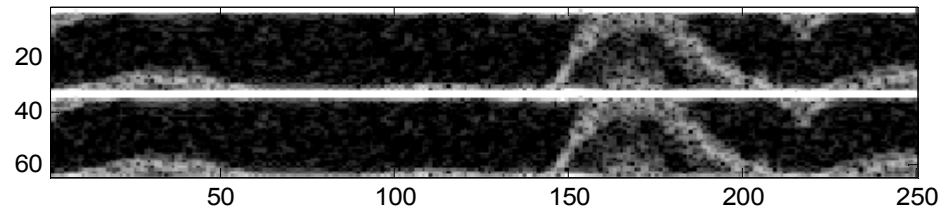
(a)



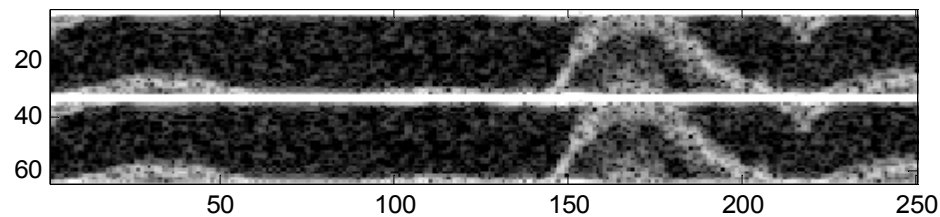
(b)



(c)



(d)



(e)

Figure 7-35. The resulting Doppler sonogram images of heart for different types of clutter rejection filters (a) The Doppler sonogram using FIR clutter (b) The Doppler sonogram using IIR clutter (c) The Doppler sonogram using PR clutter (d) The Doppler sonogram using PCA clutter (e) The Doppler sonogram using ICA clutter

We can conclude that the proposed clutter rejection method can remove the clutter originated from stationary and slowly moving tissue with a performance better than present clutter rejection filters, and gives the Doppler spectrum image without clutter line around the center. The proposed methods eliminate all the clutter without altering the flow signal.

Beside the PSNR and RMSE used for clutter evaluation, the process time for cluttering from each clutter was used. The cluttering time from each filter was calculated by running the program several times and calculates the average. The filtering time during cluttering the real Doppler data using current and proposed filters illustrated in table 7.7. The result shows that the proposed clutter based on PCA gives lower cluttering time, while the proposed clutter based on ICA gives process time higher than that from PCA. PR gives the highest cluttering time among all the clutters types and FIR gives lower time than PR. The IIR gives lower time among the present cluttering methods as shown in figure 7-36. We can conclude that our proposed cluttering methods give lower cluttering time.

Table 7.7 the process time filtering for different clutters

Filter types	IIR	FIR	PR	ICA	PCA
Process time (S)	0.114	0.329	0.465	0.069	0.025

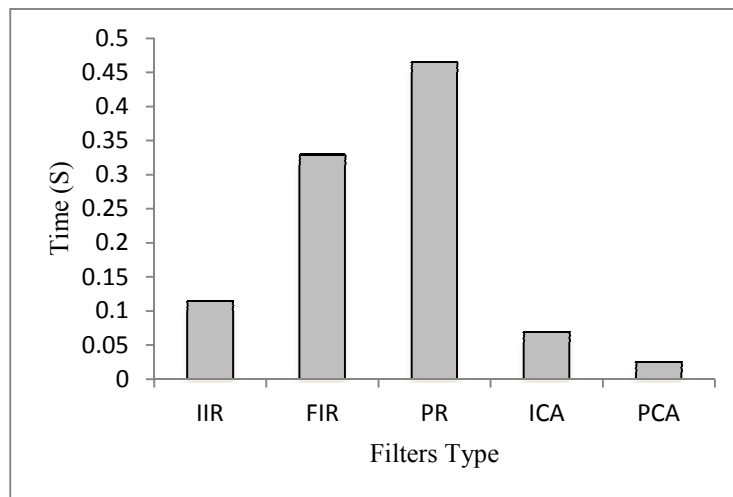


Figure 7-36. Cluttering time for different filter

# Chapter 8

## Conclusion and Recommendations for Future Work

### 8.1 Conclusion

Compressed sensing is a new sampling theory, states that it is possible to reconstruct signals and images using a few numbers of measurements. CS has been applied successfully in different fields such as medical image. The CS framework, used to reconstruct the Doppler ultrasound spectrogram, so as to overcome the current Doppler data acquisition limitation. The reconstruction performed using four different CS algorithms. It is shown that it is possible to use a very few number of measurements to reconstruct the signal keeping the diagnostic quality intact. This alleviates the major Doppler limitations by reducing the number of acquisitions and eliminating the sampling uniformity constraints. The quality and the reconstruction time form the algorithms compared with each.  $\ell_1$ - minimization gives higher reconstruction time and ROMP gives lower time. When a few numbers of measurements were used ROMP gives higher PSNR (best quality), for number of measurements more than 40 % were used,  $\ell_1$  minimization gives the best quality. Among all the reconstruction algorithms, OMP gives higher error in other words the worst quality of image obtains by using OMP algorithm. When the number of measurements about 35 % was used ROMP and  $\ell_1$ -norm gives same quality. We can conclude that the CS framework can recover Doppler signal with a few numbers of measurements, within a unique time and with a good quality. This overcomes the current Doppler data acquisition.

The recovered time can be reduced as illustrated from the result by combining the CS algorithms and parallel computation algorithms. From the result the process time was reduced to less than half by using duo-core system. When the more advance computer system used, the time will decrease and this enables us to achieve a very low reconstruction time and display the Doppler signal in real-time.

The frequency response of non-adaptive filters, FIR, IIR and PR compared. Three types of FIR filters were compared the results shows that minimum phase gives best frequency response among all types of FIR. A large performance can be obtained by using a minimum phase filter instead of linear phase filter and equiripple filter. All IIR filter types compared to select the best filter for cluttering. The comparison shows that Butterworth and Chebyshev filters give a better frequency response. We found the best frequency response for IIR filters is obtained when projection initialization is used. Within the class of regression filters, polynomial basis functions were shown to provide useful frequency responses. Projection initialization IIR filter and polynomial regression filter of the same design properties gives same frequency response. Among the three filter classes, polynomial regression and projection initialization IIR filters have the best frequency response. For equal stop bandwidth, the transition rejoin were narrower than for FIR filters.

The adaptive clutter filter technique, based on ICA and PAC has been demonstrated. The results show that the clutter filters reduce the clutter signal originate from stationary and slowly moving tissue. The methods were tested in a simulation Doppler IQ data and real Doppler heart data. The simulation result shows that the clutter filters are able to reduce the clutter signal from the echo signal. When the result of our proposed clutter rejection filter compared with other cluttering filter methods, the result shows that the proposed methods based on ICA gives error less than FIR and IIR and comparable result with PR. When proposed methods based on PCA used the results show that ICA gives better clutter rejection than the PCA. PCA removes the clutter with better performance than FIR and IIR filters. For the real Doppler data, the result Doppler image shows that the Doppler spectrogram image, changed adaptively depending on the type and characteristics of clutter. The result shows that the proposed clutter suppress the clutter more effectively than other clutter rejection algorithms. The resulting images from our proposed clutters are more accurate than that from other clutter algorithms. The proposed methods eliminate all the clutter originated from stationary and slowly moving tissue without altering the blood flow signal. Thus, it can be stated that the adaptive approach

for clutter rejection provided excellent performance in discriminating flow and clutter signal components even if the velocities were low and roughly the same. The cluttering time shows that the proposed clutters give lower time compared to the present cluttering methods.

## **8.2 Recommendations for Future Work**

Further work needed to be done in the application of CS to reconstruct Doppler ultrasound signal by considering different reconstruction algorithms and different Doppler data then compare the result with the reconstruction algorithms used in this work. More work needed for image enhancements to remove the noise within the reconstructed image.

Use quad core or higher central processing unit so as to reduce the reconstruction time for different reconstruction algorithms.

Proposed a new clutter filter to remove the clutter signal originated from stationary and slowly moving tissue to remove the clutter without altering the blood flow, and compare the result with the result given in this work. Use multiprocessor system for cluttering time reduction.

## References

- 1- D. Evans, and W. McDicken, Doppler ultrasound: physics, instrumentation and signal processing second ed. John Wiley & Sons Ltd., New York, 2000.
- 2- J. Jensen, Estimation of Blood flow velocities using ultrasound, Cambridge University Press, Cambridge, 1996.
- 3- A. Macpherson, S. Meldrum and D. Tunstall, Angioscan: a spectrum analyzer for use with ultrasonic Doppler velocimeters, J. Med. Eng. Technology, **5**, 84 - 89, 1981.
- 4- D. Cooley, and J. Tukey, An algorithm for the machine calculation of complex Fourier series, Math. Comp., **19**, 297 - 301, 1985.
- 5- D. Donoho, Compressed Sensing, IEEE Trans. Info. Theory, **52**, 1289 - 1306, 2006.
- 6- S. Bjaerum and H. Torp, Statistical Evaluation of Clutter Filters in Color Flow Imaging, Elsevier Ultrasonics, **38**, pp. 376 - 380, 2000.
- 7- S. Bjaerum, H. Torp and K. Kristoffersen, Clutter Filter Rejection for Ultrasound Color Flow Imaging, IEEE Transaction on Ultrasonic, Ferroelectrics and Frequency Control, **49** (2), pp. 204 - 216, 2002.
- 8- S. Bjaerum, H. Torp and K. Kristoffersen, Clutter Filter Adapted to Tissue Motion in Ultrasound Color Flow Imaging, IEEE Transaction on Ultrasonic, Ferroelectronics and Frequency Control, **49**, pp. 693 - 704, 2002.
- 9- Y. Yoo, R. Managuli, Y. Kim, Adaptive Clutter Filtering for Ultrasound Color Flow Imaging, Ultrasound in Med. & Bio., **29**, pp. 1311 - 1320, 2003.
- 10- H. Torp, Clutter Rejection Filter in Color Flow Imaging: A Theoretical Approach, IEEE Transaction on Ultrasonics, , Ferroelectronics and Frequency Control, **44**, pp. 417 - 424, 1997.
- 11- A. Kadi and T. Loupas, On the Performance of Regression Step-initialized IIR Clutter Filters for Color Doppler System in Diagnostic Medical Ultrasound, IEEE

- Transaction on Ultrasonics, , Ferroelectronics and Frequency Control, **42**, 927 - 937, 1995.
- 12-D. Zrnig, Ground Clutter Canceling with a Regression Filter, Journal of Atmospheric and Oceanic Technology, **16**, pp. 1364 - 1372, 1999.
- 13-Y. Liu, H. Jianxin and H. Yang, A Study of Ground Clutter Suppression with a Regression Filter, IEEE ICSP 2006 proceedings, **1**, 2006.
- 14-R. Peterson, L. Atlas and K. Beach, A Comparison of IIR initialization Techniques for Improved Color Doppler Wall Filter Performance, IEEE International Ultrasonics Symposium Proceedings, **3**, pp. 1705 - 1708, 1994.
- 15-E. Chornoboy, Initialization for Improved IIR Filter Performance, IEEE Transaction on Signal Processing, **40**, pp. 543 - 550, 1992.
- 16-J. Mick, An Initialization Technique for Improved MTI Performance in Phase Array Radar, IEEE Proceedings, **60** (12), 1551 - 1552, 1972.
- 17-F. Mauldin, D. Lin and J. Hossack, A Singular Value Filter for Rejection of Stationary Artifact in Medical Ultrasound, IEEE International Ultrasonics Symposium Proceedings, pp. 359 - 362, 2010.
- 18-A. Yu and L. Lovestakken, Eigen-Based Clutter Filter Design for Ultrasound Color Flow Imaging: A Review, IEEE Transaction on Ultrasonic, Ferroelectronics and Frequency Control, **57**, pp. 1096 - 1111, 2010.
- 19-I. Jolliffe, Principal Component Analysis, 2<sup>nd</sup> Edition, Springer, 2002.
- 20-A. Hyvarinen and E. Oja, Independent Component Analysis: Algorithms and Application neural network, **13**, pp. 411 - 430, 2000.
- 21-J. Sarela and H. Valpola, Denoising Source Separation, Journal of machine learning research, **6**, pp. 233 - 272, 2005.
- 22-S. Makeig, A. Bell, T. Jung and T. Sejnowski, Independent Component Analysis of electroencephalographic data, Advance in Neural Information Processing Systems, vol. **8**, pp. 145 - 151, 1996.
- 23-S. Makeig and T. Jung, Independent Component Analysis of Simulated ERP data, Technical report INC-9606, 1996.

- 24-R. Viviani, G. Gron and M. Spitzer, Functional Principal Component Analysis of FMRI Data, *Human Brain Mapping*, **24**, pp. 109 - 129, 2005.
- 25-C. Chen, Spatial and Temporal Independent Component Analysis of Micro-Doppler Feature, *IEEE international Radar Conference*, pp. 348 - 353, 2005.
- 26-A. Elnokrashy, A. Youssef and Y. Kadah, Nonparametric clutter rejection in Doppler ultrasound using principal component analysis, *Proc. SPIE Medical Imaging 2003*, San Diego Feb 2003.
- 27-H. Torp and L. Lovstakken, Short Course 6A: Estimation and Imaging of Blood Flow Velocity, *IEEE ultrasonics symposium 2009*.
- 28-D. Christensen, *Ultrasonic Bioinstrumentation*, University of Utah.
- 29-P. Hoskins, K. Martin and A. Thrush, *Diagnostic Ultrasound Physics and Equipment*, 2<sup>nd</sup> Edition, Cambridge University Press, 2010.
- 30-J. Baun, *Physical Principle of General and Vascular Sonography*, Chapter 10, the Doppler Effect, Available: [http://www.jimbaun.com/jimbaun\\_may\\_07\\_007.htm](http://www.jimbaun.com/jimbaun_may_07_007.htm).
- 31-L. Formaggia, A. Quarleroni and A. Veneziani, *Cardiovascular mathematics Modeling and Simulation of the Circularity System*, Springer-Verlag, 2009.
- 32-C. Deane, *Doppler Ultrasound: Principle and Practice*, Available, [http://www.centrus.com.br/DiplomaFMF/SeriesFMF/doppler/capitulos-html/chapter\\_01.htm](http://www.centrus.com.br/DiplomaFMF/SeriesFMF/doppler/capitulos-html/chapter_01.htm).
- 33-H. Torp, *Signal Processing in Real-time, two Dimensional Doppler Color Flow Mapping*, University of Trondheim, Norway, 1991.
- 34-M. Priestly, *Spectral Analysis and Time Series*, London, Academic Press, 1981.
- 35-G. Aldis and R. Thompson, Calculation of Doppler spectral power density functions, *IEEE Trans Biomed Eng*, **51**, pp. 182 - 191, 1992.
- 36-D. Maulik, *Spectral Doppler: Basic principles and instrumentation*, Chapter 3. Available: <https://woc.uc.pt/deec/getFile.do?tipo=2&id=7496>.
- 37-K. Ferrara and G. Deangelis, Color Flow Mapping, *Ultrasound in Med. & Biol.*, **23** (3), pp 321-345, 1997.

- 38-P. Macpherson, S. Meldrum and D. Tunstall, Angioscan: a spectrum analyzer for use with ultrasonic Doppler velocimeters, *J. Med. Eng. Technology*, **5**, pp. 84 - 89, 1981.
- 39-J. Cooley, and J. Tukey, "An algorithm for the machine calculation of complex Fourier series," *Math. Comp.*, **19**, pp. 297 - 301, 1985.
- 40-E. Candes, T. Tao, "Decoding by Linear Programming," *IEEE Trans. Inf. Theory*, **51**, pp. 4203 - 4212, 2005.
- 41-E. Candes, J. Romberg, T. Tao, "Stable Signal Recovery from Incomplete and Inaccurate measurements," *Comm. Pure and Appl. Math*, vol. **59**, pp. 1207 - 1223, 2005.
- 42-MATLAB, Parallel Computing Toolbox User Guide, R2011b, MathWorks, Inc. 2011.
- 43-W. Wigbbgers, V. Bakker, A. Kokkeler and G. Smit, Implementation the Conjugated Gradient Algorithm on Multi-core Systems, *IEEE Proceeding of International Symposium on system-on-Chip*, pp. 11 - 14, 2007.
- 44-H. Kim, J. Mullen and J. Kepner, Introduction to Parallel Programming and pMatlab v2.0, MIT Lincoln Laboratory.
- 45-C. Chang and J. Ji, Compressed Sensing MRI with Multichannel Data Using Multicore Processors, *Magnetic Resonance in Medicine*, **64**, 1135 - 1139, 2010.
- 46-A. Broghi, J. Darbon, S. Peyronnet, T. Chan and S. Osher, A Simple Compressive Sensing Algorithm for Parallel Many-Core Architecture, *CAM Report 8 - 64*, UCLA, 2008.
- 47-J. Cortial, C. Farhat, L. Guibas and M. Rajashekar, Compressed Sensing and Time-Parallel Reduced-Order Modeling for Structural Health Monitoring using a DDDAS, In proceeding of the international conference on computational science, pp. 1171 - 1179, 2007.
- 48-B. Liu, Y. Zou and L. Ying, Sparseness: Application of Compressed Sensing in Parallel MRI, *International Conference on ITAB*, pp. 127 - 130, 2008.

- 49-A. Hoeks, J. van-de-Vorst, A. Dabekaussen, P. Brands, and R. Reneman, An efficient algorithm to remove low frequency Doppler signals in digital Doppler systems, *Ultrason. Imaging*, **13** (2), pp. 135- 144, 1991.
- 50-L. Smith, A Tutorial on Principal Component Analysis, 2002, available, [http://www.sccg.sk/~haladova/principal\\_components.pdf](http://www.sccg.sk/~haladova/principal_components.pdf).
- 51-T. Zawistowski, P. Shah, An Introduction to Sampling Theory, <http://www2.egr.uh.edu/~glover/applets/Sampling/Sampling.html>.
- 52-C. Shannon, Communication in the Presence of Noise, *Proc. IRE*, **37**, pp. 10 - 21, 1949.
- 53-C. Shannon, Classic Paper: Communication in the Presence of Noise, *Proc. IEEE*, **86** (2), pp. 447 - 457, 1998.
- 54-E. Candes, T. Tao, Near-optimal Signal Recovery from Random Projections and Universal Encoding Strategies, *IEEE Trans. Infom. Theory*, **52** (12), pp. 5406 - 5425, 2006.
- 55-E. Candes, Compressive Sampling, International Congress of Mathematicians, Madrid, Spain, 2006.
- 56-M. Fornasier, H. Rauhut, Compressive Sensing, Hand book of Mathematical Methods in Imaging Chapter in part 2, Available: <http://dsp.rice.edu/cs>.
- 57-E. Candes, M. Wakin, An Introduction to Compressive Sampling, *IEEE Signal Processing Magazine*, **25**, pp. 21 - 30, 2008.
- 58-C. Chen, A Survey on Sub-Nyquist Sampling”, available: [www.seas.ucla.edu/~chienchi/.../survey\\_sub\\_nyquist\\_sampling.pdf](http://www.seas.ucla.edu/~chienchi/.../survey_sub_nyquist_sampling.pdf).
- 59-R. Baraniuk, M. Davenport, M. Duarte, C. Hegde, An Introduction to Compressed Sensing, 2011. Available: <http://cnx.org/content/col11133/1.5/>.
- 60-J. Pant, W. Lu, A. Antoniou, Reconstruction of Sparse Signal by Minimizing a Re-weighted Approximate  $\ell_0$ -Norm in Null Space of the Measurement Matrix, *IEEE International Midwest Symposium on Circuits-System*, pp. 430 - 433, 2010.
- 61-R. Gribonval, M. Nielsen, Sparse representation in unions of bases, *IEEE Trans. on Information Theory*, **49**, pp. 3320 - 3325, 2003.

- 62-J. Tropp, A. Gilbert, Signal recovery from random measurements via orthogonal matching pursuit, *IEEE Trans. Inform. Theory*, **53** (12), pp. 4655 - 4666, 2007.
- 63-R. Baraniuk, Compressive Sensing, *IEEE Signal Processing Magazine*, **24** (4), 118 - 121, 2007.
- 64-M. Elad, A. Bruckstein, A generalized uncertainty principle of sparse representation in pairs of  $\mathbb{R}^N$  bases, *IEEE Trans. on Information Theory*, **48**, pp. 2558 - 2567, 2002.
- 65-M. Davenport, M. Duarte, Y. Eldar, Introduction to compressive sensing, Chapter in *Compressed Sensing: Theory and Application*, Cambridge University Press, 2011. Available: <http://dsp.rice.edu/cs>.
- 66-R. Gribonval, M. Nielsen, Sparse signal representation in unions of bases, *IEEE Trans. Inform. Theory*, **49** (12), pp. 3320 - 3325, 2003.
- 67-D. Donoho, M. Elad, Optimally sparse representation in general (nonorthogonal) dictionaries via  $\ell_1$  minimization, *Proc. Natl. Acad. Sci.*, **100** (5), 2003.
- 68-E. Candes, J. Romberg, Sparsity and incoherence in compressive sampling, *Inverse Problem*, **23** (3), pp. 969 - 985, 2007.
- 69-M. Davenport, P. Poulounos, M. Wakin. R. Baraniuk, Signal Processing with Compressive Measurements, *IEEE Journal of Selected Topics in Signal Processing*, **4** (2), pp. 445 - 460, 2010.
- 70-E. Candes, J. Romberg, T. Tao, Robust Uncertainty Principles: Exact Signal Reconstruction from Highly Incomplete Frequency Information, *IEEE Trans. Info. Theory*, **52** (2), pp. 489 - 509, 2006.
- 71-R. Baraniuk, M. Davenport, R. DeVore, M. Wakin, A Simple Proof of the Restricted Isometry Property for random matrices, *Construction Approximation*, **28** (3), pp. 253 - 263, 2008.
- 72-R. Baraniuk, P. Steeghs, Compressive Radar Imaging, *IEEE Radar Conference*, Waltham, Massachusetts, pp. 128 - 133, 2007.
- 73-M. Davenport, Random observations on random observations: Sparse signal acquisition and processing, PhD thesis, Rice University, 2010.

- 74-F. Krahnert, R. Ward, New and Improved Johnson-Lindenstrauss Embeddings via the Restricted Isometry Property, Preprint, 2010.
- 75-Y. Zhang, Solution-Recovery in  $\ell_1$ -norm for non-square Linear System: Deterministic Condition and Open Questions, Technical Report, 2005. Available: [www.caam.rice.edu/~zhang/reports/index](http://www.caam.rice.edu/~zhang/reports/index).
- 76-D. Needell, J. Tropp, COSAMP: Iterative Signal Recovery from Incomplete and Inaccurate Samples, 2008. Available: <http://dsp.rice.edu/cs>.
- 77-J. Tropp, Signal Recovery from Random Measurements Via Orthogonal Matching Pursuit, IEEE Trans. Inf. Theory, **52** (12), pp. 4655 - 4666, 2007.
- 78-M. Figueiredo, R. Nowak, S. Wright, Gradient Projection for Spares Reconstruction: Application to Compressed Sensing and Other Inverse Problems, IEEE Selected Topic in Signal Processing, **1** (4), 586 - 597, 2007.
- 79-D. Needell, J. Tropp, R. Vershynin, Greedy Signal Recovery Review, 2008. Available: [www.acm.caltech.edu/~jtropp/conf/NTV08-greedy-signal-asilomar.pdf](http://www.acm.caltech.edu/~jtropp/conf/NTV08-greedy-signal-asilomar.pdf).
- 80-T. Tony, L. Wang, Orthogonal Matching Pursuit for Sparse Signal Recovery, available: [www.stat.wharton.upenn.edu/~tcai/paper/html/OMP.html](http://www.stat.wharton.upenn.edu/~tcai/paper/html/OMP.html).
- 81-R. Berinde, A. Gilbert, P. Indyk, H. Karloff, M. Strauss, Combining Geometry and Combinatorics: A unified Approach to Sparse Signal Recovery, IEEE Communication, Control, and computing, 46<sup>th</sup> Annual Allerton Conference, pp. 798 - 805, 2008.
- 82-S. Sra, J. Tropp, Row-Action Methods for Compressed Sensing, In Proc. 2006 IEEE Int. Conf. Acoustics, Speech, and Signal Processing (ICASSP), **3**, pp. 868 - 871, Toulouse, 2006.
- 83-P. Boufounos, R. Baraniuk, Reconstruction Sparse Signal from their Zero Crossing, in Proc. of IEEE International Conference on Acoustics, speech and signal processing, pp. 3361 - 3364, 2008.

- 84-M. Duarte, M. Davenport, M. Wakin, R. Baraniuk, Sparse Signal Detection from Incoherent Projection, In Proc. IEEE Int. Conf. Acoust., Speech, and Signal Processing (ICASSP), Toulouse, France, pp. III-872 - 875, 2006.
- 85-J. Haupt, R. Castro, R. Nowak, G. Fudge, A. Yeh, Compressive Sampling for Signal Classification, In Proc. Asilomar Conf. Signals, Systems, and Computers, Pacific Grove, CA, pp. 1430 - 1434, 2006.
- 86-J. Haupt, R. Nowak, Compressive Sampling for Signal Detection, In Proc. IEEE Int. Conf. Acoust., Speech, and Signal Processing (ICASSP), Honolulu, HI, **3**, pp. 1509 - 1512, 2007.
- 87-S. Chen, D. Donoho, M. Saunders, Atomic Decomposition by Basis Pursuit, SIAM J. Sci. Comp., **20** (1), pp. 33 - 61, 1998.
- 88-E. Candes, J. Romberg, Practical Signal Recovery from Random Projections, 2005. Available: <http://dsp.rice.edu/cs>.
- 89-S. Auethavekiat, "Introduction to implementation of compressive sensing," *AU J. T.*, **14** (1), pp. 39 - 46, 2010.
- 90-A. Carmi, P. Gurfil, Convex Feasibility Methods for Compressed Sensing, IEEE Journal of Selected Topics in Signal Processing, **1**, pp. 586 - 597, 2010.
- 91-M. Wakin, Compressed Sensing, available: <http://cnx.org/content/m18733/latest>.
- 92-J. Tropp, Greedy is Good: Algorithmic Results for Sparse Approximation, IEEE Trans. Info. Theory, **50** (10), pp. 2231 - 2242, 2004.
- 93-R. Berinde, P. Indyk, M. Ruzic, Practical Near-Optimal Sparse Recovery in the  $\ell_1$  norm, In Proc. Allerton Conf. Communication, Control, and Computing, Monticello, IL, pp. 198 - 205, 2008.
- 94-T. Blumensath, M. Davies, Gradient pursuits, IEEE Trans. Signal Processing, **56** (6), pp. 2370 - 2382, 2008.
- 95-W. Dai and O. Milenkovic, Subspace Pursuit for Compressive Sensing Signal Reconstruction, IEEE Trans. Inform. Theory, **55** (5), pp. 2230 - 2249, 2009.
- 96-D. Donoho, I. Drori, Y. Tsaig, J. Stark, Sparse Solution of Underdetermined Linear Equations by Stagewise Orthogonal Matching Pursuit, Preprint, 2006.

- 97-D. Donoho, Y. Tsaig, Fast Solution of  $\ell_1$  norm Minimization Problems when the Solution May be Sparse, IEEE Trans. Inform. Theory, **54** (11), pp. 4789 - 4812, 2008.
- 98-P. Indyk, M. Ruzic, "Near-Optimal Sparse Recovery in the  $\ell_1$ -norm", In Proc. 49<sup>th</sup> Annu. Symp. Found. Comp. Science (FOCS), pp. 199 - 207, 2008.
- 99-D. Needell, R. Vershynin, Signal Recovery from Incomplete and Inaccurate Measurements via Regularized Orthogonal Matching Pursuit, IEEE J. Select. Top. Signal Processing, **4** (2), pp. 310 - 316, 2010.
- 100- G. Gui, A. Mehbodniya, Q. Wam, Sparse Signal Recovery with OMP Algorithm using Sensing Measurement Matrix, IEEE Electronic Express, **8** (5), pp. 285 - 290, 2011.
- 101- M. Fazel, M. Meila, Greedy Recovery Algorithm, EE546/STAT593C Lecture 9, 2010.
- 102- D. Needell and R. Vershynin, Uniform Uncertainty Principle and Signal Recovery via Regularized Orthogonal Matching Pursuit, Found. Comput. Math., **9** (3), pp. 317 – 334, 2009.
- 103- N. Nguyen and T. Tran, The Stability of Regularized Orthogonal Matching Pursuit Algorithm, Available: [http://dsp.rice.edu/sites/dsp.rice.edu/files/cs/Stability\\_of\\_ROMP.pdf](http://dsp.rice.edu/sites/dsp.rice.edu/files/cs/Stability_of_ROMP.pdf).
- 104- R. Berinde, P. Indyk, Sequential Sparse Matching Pursuit, In Communication, Control and computing, IEEE 47<sup>th</sup> Annual Allerton Conference, pp. 36 - 43, 2009.
- 105- A. Gilbert, M. Strauss, J. Tropp, R. Vershynin, One Sketch for all: Fast Algorithms for Compressed Sensing, In Proceedings of the 39<sup>th</sup> annual ACM symposium on Theory of computing, ACM, pp. 237 - 246, 2007.
- 106- G. Cormode, S Muthukirshnen, Combinatorial Algorithms for CS, In proc. 40<sup>th</sup> Ann. conf. information science and systems, Princeton, pp. 198- 201, 2006.
- 107- L. Rudin, S. Osher, E. Fatemi, Nonlinear Total Variation Based Noise Removal Algorithm, Physica D, **60**, pp. 259 - 268, 1992.

- 108- C. Berger, Application of Compressive Sensing to Sparse Channel Estimation, IEEE communications magazine, **48**, pp. 164 - 174, 2010.
- 109- M. Duarte, M. Davenport, D. Takhar, J. Laska, T. Sun, K. Kelly, R. Baraniuk, Single-Pixel Imaging via Compressive Sampling, IEEE Signal Processing Magazine, **25** (2), pp. 83 - 91, 2008.
- 110- A. Skodras, C. Christopoulos, T. Ebrahimi, The JPEG2000 Still Image Compression Standard, IEEE Signal Processing Mag., **18**, pp. 36 - 58, 2001.
- 111- H. Yu, G. Wang, Compressed Sensing Based Interior Tomography, Physics in Medicine and Biology, **54**, 2791 - 2805, 2009.
- 112- M. Lusting, D. Donoho, J. Pauly, Sparse MR: The Application of Compressed Sensing For Rapid MR Imaging, Magnetic Resonance in Medicine, **58** (6), pp. 1182 - 1182, 2007.
- 113- S. Aviyente, Compressed Sensing Framework for EEG Compression, IEEE Statistical Signal Processing / SP 14<sup>th</sup> Workshop, pp. 181 - 184, 2007.
- 114- A. Achim, B. Buxton, G. Tzagkarakis, P. Tsakalids, Compressive Sensing for Ultrasound RF Echoes using  $\alpha$ -Stable Distribution, Engineering in Medicine and Biological Society, Annual International Conference of the IEEE, pp. 4303 - 4307, 2010.
- 115- M. Iwen, A Deterministic Sub-Linear Time Sparse Fourier Algorithm via Non- Adaptive Compressed Sensing Methods, in Proceedings of the Nineteenth Annual ACM-SIAM symposium on Discrete algorithms, Society for Industrial and Applied Mathematics Philadelphia, PA, USA, pp. 20 - 29, 2008.
- 116- M. Nishant, S. Ivana, S. Bahaa, T. Malvin, Compressed Sensing in Optical Coherence Tomography, Proceedings of the SPIE, **7570**, pp. 75700L - 75700L - 5, 2010.
- 117- S. Zobly, Y. Kadah, Compressed Sensing: Doppler Ultrasound Signal Recovery by Using Non-uniform Sampling & Random Sampling, Proc. 28<sup>th</sup> National Radio Science conference IEEE Catalog Number CFP11427-PRT, 2011.

- 118- S. Zobly, Y. Kadah, Novel Doppler Ultrasound Data Acquisition Framework Based on Compressed Sensing, International Conference on: Advance in Biomedical Engineering, Tripoli – Lebanon, 2011.
- 119- A. Krishnamurthy, S. Samsi and V. Gadepally, Parallel Matlab Techniques, Image Processing, 2009.
- 120- D. Smith, J. Gore, T. Yankeelov and E. Welch, Real-Time Compressive Sensing MRI Reconstruction using GPU Computing and Split Bregman Methods, International Journal of Biomedical Imaging, vol. 2012, 2012.
- 121- J. Kepner, Parallel Matlab for Multicore and Multinode Computers, Philadelphia: Society of Industry and Applied Mathematics, 2009.
- 122- H. Torp, Clutter Rejection Filters in Color Flow Imaging: A Theoretical Approach, IEEE Transaction on Ultrasonics, Ferroelectrics, and frequency control, **44** (2), 417 - 424, 1996.
- 123- W. Hedrick, D. Hykes and D. Starchman, Ultrasound Physics and Instrumentation, 3<sup>rd</sup> edition. St. Louis: Mosby, 1995.
- 124- M. Shariati, J. Dripps and W. McDicken, Deadbeat IIR Based MTI Filtering for Color Flow Imaging System, IEEE Ultrasonic Symposium, **2**, pp. 1059 -1063, 1993.
- 125- C. Kargel, G. Hobenreich, B. Trummer and M. Insana, Adaptive Clutter Rejection Filtering in Ultrasonic Strain-Flow Imaging, IEEE Transaction on Ultrasonics, Ferroelectrics, and frequency control, **50** (7), 824 - 835, 2003.
- 126- R. Losada, Digital Filters with MATLABS, The MathWork, Inc, 2008.
- 127- A. Johansson, Advance Filter Design, Reference Manual, 2004.
- 128- R. Mick, An Initialization Technique for Improved MTI Performance in Phased Array Radar, Proceedings of the IEEE, **60** (12), pp. 1551 - 1552, 1972.
- 129- S. Torres and D. Zrnica, Ground Clutter Cancelling with a Regression Filter, Journal of Atmospheric and Oceanic Technology, **16**, 1364 - 1372, 1999.
- 130- Y. Liu, H. Jianxin and H. Yang, A Study of Ground Clutter Suppression with Regression Filter, ICSP processing, **4**, 2006.

- 131- M. Richardson, Principal Component Analysis, 2009, available, <http://people.maths.ox.ac.uk/richardsonm/SignalProcPCA.pdf>.
- 132- L. Smith, A Tutorial on Principal Component Analysis, 2002, available, [http://www.sccg.sk/~haladova/principal\\_components.pdf](http://www.sccg.sk/~haladova/principal_components.pdf).
- 133- J. Shelns, A Tutorial on Principal Component Analysis, 2009, available, <http://www.snl.salk.edu/~shlens/pca.pdf>.
- 134- T. Kohonen, Self-Organizing Maps, New York, Springer-Verlag 1995.
- 135- A. Hyvarinen and E. Oja, Independent Component Analysis: Algorithms and Application, Neural Network, **13**, pp. 411 - 430, 2000.
- 136- S. Crucis, L. Castedo and H. Cichocki, Robust Blind Source Separation Methods using Cumulants, Elsevier Neurocomputing, **49**, pp. 87 - 118, 2002.
- 137- C. Jutten and J. Karhunen, Advance in Nonlinear Blind Source Separation, 4<sup>th</sup> International Symposium on Independent Component Analysis and Blind Signal Separation, (ICA 2003), Japan.
- 138- G. Clifford, Biomedical Signal and Image Processing chapter 15: Blind Source Separation: Principal & Independent Component Analysis, Springer 2008.
- 139- M. Bartlett, S. Makeig, A. Bell, T. Jung, and T. Sejnowski, Independent Component Analysis for EEG Data, Society for Neuroscience Abstracts, **21**: 437, 1995.
- 140- Y. Kadah, Spatio-temporal Analysis of Color Doppler Information using Independent Component Analysis, Proc. SPIE medical Imaging, **4687**, pp. 227 - 234, 2002.
- 141- A. Hyvarinen and E. Oja, A Fast Fixed-Point Algorithm for Independent Component Analysis, Neural Computation, **9**, 1483 - 1492, 1997.
- 142- A. Hyvarinen, J. Karhunen and E. Oja, Independent Component Analysis, John Wiley and Sons, New York, 2001.
- 143- S. Zobyly, A. Youssef and Y. Kadah, Doppler Ultrasound Image Reconstruction Based on Compressed Sensing, Submitted to SPIE.

- 144- S. Zobly and Y. Kadah, Orthogonal Matching Pursuit & Compressive Sampling Matching Pursuit for Doppler Ultrasound Signal Reconstruction, CIBEC December 2012.
- 145- S. Zobly and Y. Kadah, A New Clutter Rejection Technique for Doppler Ultrasound Signal Based on Principal and Independent Component Analysis, CIBEC December 2012.